JPRS L/8578

20 July 1979

USSR Report

ELECTRONICS AND ELECTRICAL ENGINEERING

(FOUO 1/79)

FBIS FOREIGN BROADCAST INFORMATION SERVICE

NOTE

JPRS publications contain information primarily from foreign newspapers, periodicals and books, but also from news agency transmissions and broadcasts. Materials from foreign-language sources are translated; those from English-language sources are transcribed or reprinted, with the original phrasing and other characteristics retained.

Headlines, editorial reports, and material enclosed in brackets [] are supplied by JPRS. Processing indicators such as [Text] or [Excerpt] in the first line of each item, or following the last line of a brief, indicate how the original information was processed. Where no processing indicator is given, the information was summarized or extracted.

Unfamiliar names rendered phonetically or transliterated are enclosed in parentheses. Words or names preceded by a question mark and enclosed in parentheses were not clear in the original but have been supplied as appropriate in context. Other unattributed parenthetical notes within the body of an item originate with the source. Times within items are as given by source.

The contents of this publication in no way represent the policies, views or attitudes of the U.S. Government.

For further information on report content call (703) 351-2938 (economic); 3468 (political, sociological, military); 2726 (life sciences); 2725 (physical sciences).

APPROVED FOR RELEASE: 2007/02/09: CIA-RDP82-00850R000100070023-8

JPRS L/8578

20 July 1979

USSR REPORT

ELECTRONICS AND ELECTRICAL ENGINEERING

(FOUO 1/79)

This serial publication contains articles, abstracts of articles and news items from USSR scientific and technical journals on the specific subjects reflected in the table of contents.

Photoduplications of foreign-language sources may be obtained from the Photoduplication Service, Library of Congress, Washington, D. C. 20540. Requests should provide adequate identification both as to the source and the individual article(s) desired.

CONTENTS PAGE

CONTENTS (Continued) Page

CIRCUIT THEORY

UDC: 621.396.96; 621.391.26

ANALYSIS OF BAYES AMPLITUDE ESTIMATES WITH 'INTERMITTENT' SIGNAL DISTORTIONS

Kiev IVUZ RADIOELEKTRONIKA in Russian No 4, Apr 79 pp 94-98

[Article by V. A. Vishnyakov and V. M. Katikov]

[Text] Received radio-frequency signals, in addition to fluctuation-type distortions, frequently experience brief ("intermittent") distortions which either substantially alter receiving conditions or make it totally impossible for the observer to extract the information contained in the signal. Optimal processing of signals under such conditions involves employment of statistical methods which are presently being developed for simultaneous testing of hypotheses and evaluation of the parameters characterizing these hypotheses [1-3, 4]. This article deals with analysis of an optimal algorithm for estimating the amplitude of a radio signal on a background of fluctuation interference under conditions of "intermittent" distortions of the signal disappearance type (hypothesis H_1) and its limitations in a receiving circuit as a consequence of a sharp intensity increase with intersystem pulse interference (hypothesis H_2).

The specific features of these disturbances boil down to the fact that hypotheses H_1 and H_2 presume total loss of transmitted information and observed realization, so that the best estimate under the condition of correctness of hypothesis H_1 or H_2 is a priori mean $\bar{\vartheta}$ of measured parameter ϑ. Consequently, the general expression for optimal Bayes estimate $\hat{\vartheta}_\Sigma$, obtained in [5, 6], under conditions of several mutually excluding hypotheses, can in this case be altered as follows:

$$\hat{\vartheta}_\Sigma(x) = P(H_0/x)\,\hat{\vartheta}_0(x) + [1 - P(H_0/x)]\,\bar{\vartheta}. \qquad (1)$$

where $P(H_0/x)$ -- a posteriori probability of acceptance of hypothesis H_0 on the absence of "intermittent" distortions in adopted realization x;
$\hat{\vartheta}_0(x)$ -- optimal Bayes estimate under the condition of correctness of hypothesis H_0, that is, with signal reception on a background of fluctuation interference alone.

Our task is investigation of the qualitative characteristics of estimate (1) in comparison with the known Bayes estimate of conditional mean $\hat{\vartheta}_0(x)$, as well as an estimate of maximum plausibility $\hat{\vartheta}_{MП}(x)$, which in this case lose their

optimality. We shall examine signal estimation in the assumption that the a priori density of probability $W(\vartheta)$ is uniform in interval $[\vartheta_1, \vartheta_2]$ and the signal/noise ratio is sufficiently large that one can utilize a Gaussian approximation of density of probability of selective values of the observed process in the absence of "intermittent" distortions (hypothesis H_0). We shall also stipulate that observed realization x shall mean n independent selective values x_i of a stationary random process, that is, the hypothesis on the character of interference does not change during the entire observation interval.

These assumptions enable us to write conditional densities of probability $W(x/\vartheta, H_1)$ of observed data for all hypothetical disturbances as follows:

$$W(x/\vartheta, H_0) = (2\pi\sigma^2)^{-\frac{n}{2}} \exp\left\{-\frac{\sum_{i=0}^{n}(x_i-\vartheta)^2}{2\sigma^2}\right\}, \quad (2)$$

$$W(x/H_1) = \prod_{i=1}^{n}\left[\frac{x_i}{\sigma^2}\exp\left(-\frac{x_i^2}{2\sigma^2}\right)\right], \quad (3)$$

$$W(x/H_2) = \prod_{i=1}^{n}\frac{1}{\sigma}\,\delta\left(\frac{x_i}{\sigma}-\frac{\vartheta_{rp}}{\sigma}\right), \quad (4)$$

where σ^2 -- standard deviation of observation noise; ϑ_{rp} -- receiving circuit clipping threshold; $\delta(\cdot)$ -- Dirac delta function. Density of probability (4) describes the determined character of observations in the case of correctness of hypothesis H_2, whereby in actual receiving devices quantity ϑ_{rp} is located beyond the limits of the range of possible signal fluctuations, that is, one can assume that

$$\vartheta_{rp} \geqslant \vartheta + 3\delta.$$

The latter circumstance enables us to ignore in numerical calculations the effect of cutting off of densities (2), (3), connected with signal clipping in the receiving circuit.

We shall find functions $P(H_0/x)$ and $\hat{\vartheta}_0(x)$ contained in (1) on the basis of the following known relations:

$$\hat{\vartheta}_0(x) = \int \vartheta W(\vartheta/x, H_0)\, d\vartheta, \quad (5)$$

$$P(H_0/x) = \frac{p_0 W(x/H_0)}{\sum_{i=0}^{2} p_i W(x/H_i)}, \quad (6)$$

where p_i -- a priori probabilities of hypotheses H_i for i=0, 1, 2;

$$W(x/H_i) = \int_{\theta} W(\theta/H_i)\, W(x/\theta, H_i)\, d\theta, \tag{7}$$

$$W(\theta/x, H_0) = W(\theta/H_0)\, W(x/\theta, H_0)/W(x/H_0) \tag{8}$$

and on assumption $\theta = [\theta_1, \theta_2]$,

$$W(\theta/H_i) = W(\theta) = \begin{cases} 1/(\theta_2 - \theta_1), & \text{if } \theta \in \theta, \\ 0 & \text{otherwise.} \end{cases} \tag{9}$$

Substituting in relations (5)-(8) initial probability densities (2)-(4), (9) and performing the necessary algebraic transformations and integration, we finally obtain:

$$P(H_0/x) = \frac{p_0}{\sqrt{n}(\theta_2-\theta_1)}\left[\Phi\left(\frac{\sqrt{n}(\theta_2-\hat{\theta}_{mn})}{\sigma}\right)-\Phi\left(\frac{\sqrt{n}(\theta_1-\hat{\theta}_{mn})}{\sigma}\right)\right]\times$$

$$\times\left\{\frac{p_0}{\sqrt{n}(\theta_2-\theta_1)}\left[\Phi\left(\frac{\sqrt{n}(\theta_2-\hat{\theta}_{mn})}{\sigma}\right)-\Phi\left(\frac{\sqrt{n}(\theta_1-\hat{\theta}_{mn})}{\sigma}\right)\right]-\right.$$

$$-\frac{p_1(\sqrt{2\pi})^{(n-1)}}{\sigma}\exp\left(-\frac{n\hat{\theta}_{mn}^2}{2\sigma^2}\right)\prod_{i=1}^{n}\frac{x_i}{\sigma}+\frac{p_2(\sqrt{2\pi})^{(n-1)}}{\sigma}\times$$

$$\left.\times\exp\left(\frac{\sum_{i=1}^{n}x_i^2-n\hat{\theta}_{mn}^2}{2\sigma^2}\right)\prod_{i=1}^{n}\delta\left(\frac{x_i-\theta_{np}}{\sigma}\right)\right\}^{-1}, \tag{10}$$

$$\hat{\theta}_0(x) = \hat{\theta}_{mn}-\frac{\sigma}{\sqrt{2\pi n}}\left\{\exp\left[-\frac{n}{2\sigma^2}(\theta_2-\hat{\theta}_{mn})^2\right]-\exp\left[-\frac{n}{2\sigma^2}(\theta_1-\hat{\theta}_{mn})^2\right]\right\}\times$$

$$\times\left[\Phi\left(\frac{\sqrt{n}(\theta_2-\hat{\theta}_{mn})}{\sigma}\right)-\Phi\left(\frac{\sqrt{n}(\theta_1-\hat{\theta}_{mn})}{\sigma}\right)\right]^{-1}, \tag{11}$$

where $\Phi(z) = \frac{1}{\sqrt{2\pi}}\int_{-\infty}^{z}\exp\left(-\frac{t^2}{2}\right)dt$ — integral of probabilities

$$\hat{\theta}_{mn}(x) = \frac{1}{n}\sum_{i=1}^{n}x_i \tag{12}$$

-- maximally plausible estimate, which in the given case is the estimate of a selective average. Expressions (10) and (11) together with (1) and considering $\bar{\theta} = (\theta_1+\theta_2)/2$ determine the algorithm of an optimal estimate, in the Bayes sense, of the signal envelope under conditions of "intermittent" interference.

We shall further examine the effectiveness of the obtained estimate in comparison with estimates $\bar{\theta}_0$ and $\bar{\theta}_{mn}$, which are simpler in practical

realization. For this we shall determine displacement and root-mean-square error of the examined estimates, that is:

$$\alpha_{(\cdot)} = E\{\hat{\vartheta}_{(\cdot)}(x) - \vartheta\} = \int_{\Theta}\int_{X} (\hat{\vartheta}_{(\cdot)}(x) - \vartheta) W(\vartheta) [p_0 W(x/\vartheta, H_0) + p_1 W(x/H_1) + p_2 W(x/H_2)] d\vartheta dx, \quad (13)$$

$$\beta_{(\cdot)} = E\{(\hat{\vartheta}_{(\cdot)} - \vartheta)^2\} = \int_{\Theta}\int_{X} (\hat{\vartheta}_{(\cdot)}(x) - \vartheta)^2 W(\vartheta) [p_0 W(x/\vartheta, H_0) + p_1 W(x/H_1) + p_2 W(x/H_2)] d\vartheta dx, \quad (14)$$

where X -- space of selective values $x=[x_1, x_2, \ldots, x_n]$. Analytical determination of these characteristics is difficult in the general case. Therefore we shall utilize simplifying assumptions:

$$\vartheta_1 \gg \sigma,\ \vartheta_2 - \vartheta_1 \gg \sigma \quad \text{and} \quad \vartheta_{rp} - \vartheta_1 \gg \sigma,$$

which make it possible to obtain approximate relations for illustration of the effectiveness of the examined estimates. Substituting in (13), (14) corresponding expressions for estimates $\hat{\vartheta}_{M\Pi}$, $\hat{\vartheta}_0$ or $\hat{\vartheta}_6$ and utilizing (2)-(4), (9), we obtain following integration:

for maximally probable estimate $\hat{\vartheta}_{M\Pi}$

$$\alpha_{M\Pi} \simeq p_1 \sqrt{\frac{\pi}{2}}\sigma + p_2\vartheta_{rp} - (1-p_0)\bar{\vartheta}, \quad (15)$$

$$\beta_{M\Pi} \simeq p_0\frac{\sigma^2}{n} + p_1\left[\frac{2\sigma^2}{n} + \frac{C_n^2\pi\sigma^2}{n^2} - \sqrt{2\pi}\bar{\vartheta}\sigma\right] + p_2[\vartheta_{rp}^2 - 2\vartheta_{rp}\bar{\vartheta}] + (p_1+p_2)\frac{\vartheta_1^2 + \vartheta_1\vartheta_2 + \vartheta_2^2}{3}; \quad (16)$$

for quasioptimal Bayes estimate $\hat{\vartheta}_0$

$$\alpha_0 \simeq p_1\vartheta_1 + p_2\vartheta_2 - (1-p_0)\bar{\vartheta}, \quad (17)$$

$$\beta_0 \simeq p_0\frac{\sigma^2}{n} + (p_1+p_2)\frac{(\vartheta_2-\vartheta_1)^2}{3}; \quad (18)$$

for optimal Bayes estimate

$$\alpha_6 = 0, \quad (19)$$

$$\beta_6 \simeq p_0\frac{\sigma^2}{n} + (p_1+p_2)\frac{(\vartheta_2-\vartheta_1)^2}{12}. \quad (20)$$

The results of numerical calculations with formulas (15)-(20) with n=1 are presented in Figure 1 in the form of standardized dependences $\alpha(\cdot)/\hat{\sigma}$ (Figure 1a) and $\beta(\cdot)/\sigma^2$ (Figure 1b) on parameters of interference p_1 and p_2.

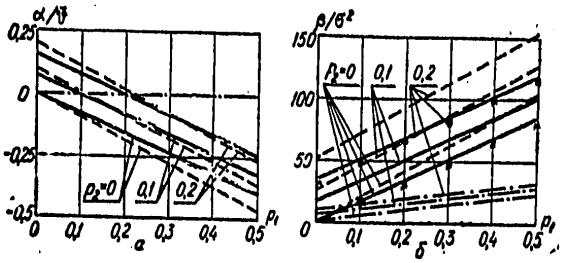

Figure 1.

The solid lines in Figure 1 correspond to estimate $\hat{\vartheta}_0$, the dashed lines -- to estimate $\hat{\vartheta}_{МП}$, and the dot-dash lines -- to optimal Bayes estimate $\hat{\vartheta}_б$. The following input data were adopted in our calculations:

$$\vartheta_1/\sigma=3, \quad \vartheta_2/\sigma=30, \quad \vartheta_{гр}/\sigma=33.$$

It is evident from the figure that the optimal Bayes estimate is distinguished from the other examined estimates by greater effectiveness and little dependence of errors on interference parameters. This is due to the selective action of the function of a posteriori probability of reception of an undistorted signal $P(H_0/x)$, contained in expression (1). In addition, an important advantage of estimate $\hat{\vartheta}_б$ is the absence of displacement, which with other quasioptimal estimates can reach significant values (see Figure 1a).

For illustration of the quality of the obtained approximate expressions, the asterisk in Figure 1b designates the results of calculations of effectiveness of estimate $\hat{\vartheta}_0$, obtained by means of numerical integration on a computer of expression (14) with utilization of (2)-(4) and (9)-(12). These results confirm the applicability of the obtained expressions for practical applications.

BIBLIOGRAPHY

1. Repin, V. G., and Tartakovskiy, G. P. "Statisticheskiy sintez pri apriornoy neopredelennosti i adaptatsiya informatsionnykh sistem" [Statistical Synthesis With A Priori Uncertainty and Adaptation of Information Systems], Moscow, Sovetskoye radio, 1977.

2. Levin, B. R. "Teoreticheskiye osnovy statisticheskoy radiotekhniki" [Theoretical Principles of Statistical Radio Engineering], Moscow, Sovetskoye radio, 1975, 2.

3. Grishin, Yu. P., and Katikov, V. M. "Combined Detection and Estimation of Random Signals (a Survey)," ZARUBEZHNAYA RADIOELEKTRONIKA, No 6, 1977, page 3.

4. Levin, B. R., and Shinakov, Yu. S. "Combined Optimal Algorithms of Signal Detection and Estimate of Their Parameters (a Survey)," RADIOTEKHNIKA I ELEKTRONIKA, 22, No 11, 1977, page 2239.

5. Shinakov, Yu. S. "Bayes Estimates of Parameters of a Signal Masked by Interference With Several Mutually Excluding Hypotheses on the Observed Process," RADIOTEKHNIKA, 26, No 4, 1971, page 12.

6. Fredriksen, A.; Middlton, D., and Vandelinde, D. "Simultaneous Signal Detection and Estimation Under Multiple Hypotheses," IEEE TRANS., IT-18, No 5, 1972, page 607.

Submitted 14 December 1977;
Revised and resubmitted 9 March 1978

3024
CSO: 1870

CIRCUIT THEORY

UDC: 621.391.1

POTENTIAL NOISE STABILITY OF RECEPTION OF SIGNALS WITH DISCRETE FREQUENCY MODULATION ON A NOISE AND STRUCTURAL INTERFERENCE BACKGROUND

Kiev IVUZ RADIOELEKTRONIKA in Russian No 4, Apr 79 pp 85-87

[Article by M. A. Sokolov, I. I. Chadovich, and R. F. Obukhovich]

[Text] The mutual influence of discrete information transmission systems operating simultaneously and independently in the same frequency band can be reduced by efficient selection of signal waveform. A phase-manipulated signal with discrete frequency modulation (DFM) appears promising in this regard. Noise is also a DFM signal, but with a different elementary pulse frequency sequence, that is, it is structural. One can demonstrate that resistance to structural noise will be the greatest if equal-probability selection of DFM signal elementary pulse frequencies is performed.
It is natural to assume that selection of elementary noise pulse frequencies is also equally probable, but independent of selection of frequencies in the signal. The potential noise stability of reception of such signals on a background of additive fluctuation interference is well known [1]. It is of interest to estimate the potential noise stability with simultaneous influence of noise and structural interference.

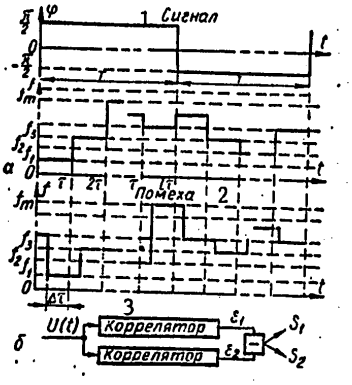

Figure 1.

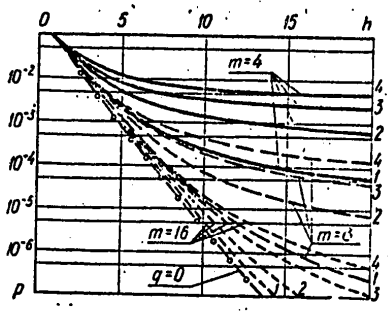

Figure 2.

Key to Figure 1 on preceding page:

1. Signal
2. Noise
3. Correlator

We shall assume that (Figure 1a): information is transmitted by binary code with equal symbol probability; transmission -- DFM signal of duration $T=L\tau$ (τ -- duration of elementary pulse; L -- their number); the elementary pulse frequency assumes with a probability of $p=\frac{1}{m}$ one of m values f_1, f_2, ... f_m; transmission phases differ by π (opposite signals); noise -- continuous sequence of elementary pulses of duration τ with frequencies f_1, f_2, ... f_m; relative overlap of signal and noise pulses

$$\gamma=\frac{\Delta\tau}{\tau}\ (0<\gamma<1)$$

is random and has a uniform distribution; the difference in noise and signal phases is random and has a uniform distribution in interval $[0,2\pi]$; in interval T the number of congruences of signal and noise frequencies is $k(0\leq k\leq L)$; the unknown signal parameter is the transmission phase.

Figure 1b shows the structure of an optimal coherent receiver. Let signal $S_1(t)$ be transmitted in time interval T, then $U(t)=S_1(t)+G(t)+n(t)$, where $G(t)$ is structural noise, while $n(t)$ is fluctuation noise, and

$$\varepsilon_1=\int_0^T S_1^2(t)\,dt+\int_0^T S_1(t)\,G(t)\,dt+\int_0^T S_1(t)\,n(t)\,dt,$$

$$\varepsilon_2=-\varepsilon_1.$$

If $\varepsilon_1-\varepsilon_2>0$, that is,

$$\int_0^T S_1(t)\,n(t)\,dt>-\int_0^T S_1^2(t)\,dt-\int_0^T S_1(t)\,G(t)\,dt,$$

a decision is made in favor of $S_1(t)$. During transmission of an opposite signal $S_2(t)=-S_1(t)$ $U(t)=-S_1(t)+G(t)+n(t)$ and a decision is made in favor of $S_2(t)$, if

$$\int_0^T S_1(t)\,n(t)\,dt<\int_0^T S_1^2(t)\,dt-\int_0^T S_1(t)\,G(t)\,dt. \qquad (2)$$

We shall write down 1 signal and noise pulses in the following form:

$$s_i(t)=a\cos(\omega_i t+\varphi_i),\quad (i-1)\tau\leq t<i\tau, \qquad (3)$$

$$g_i(t)=b\cos(\omega_n t+\psi_i),\quad i\tau-\Delta\tau\leq t<(i+1)\tau-\Delta\tau, \qquad (4)$$

where i and $n\in\overline{(1,m)}$, $S_1(t)=\sum_{i=1}^{L}s_i(t)$ and $G(t)=\sum_{i=1}^{L}g_i(t)$.

The left terms in (1) and (2) are random normally distributed quantities with zero mean and dispersion $\sigma^2=a^2NT/4$ (N -- spectral density of noise). Taking into consideration (3) and (4), we write the terms of the right sides of (1) and (2):

$$\int_0^T S_1^2(t)\,dt = \sum_{l=1}^{L} \int_{(l-1)\tau}^{l\tau} a^2 \cos^2(\omega_l t + \varphi_l)\,dt = \frac{a^2 T}{2}, \tag{5}$$

$$\int_0^T S_1(t)\,G(t)\,dt = \sum_{l=1}^{L} \int_{(l-1)\tau}^{l\tau} ab \cos(\omega_l t + \varphi_l)\cos(\omega_n t + \psi_l)\,dt \approx \frac{kab\Delta\tau}{2}\cos\delta. \tag{6}$$

Here, due to the orthogonality of oscillations with different frequencies, the terms of sum (6) differ from zero only at k intervals of $\Delta\tau$ congruence of signal and noise frequencies, while $\delta=\phi_1-\psi_1$.

Substituting (5) and (6) in (1) and (2), and dividing both sides of the inequalities by σ, we obtain:

$$\theta > -\sqrt{2h}\left(1+\gamma\frac{k}{L}\sqrt{q}\cos\delta\right), \tag{7}$$

$$\theta < \sqrt{2h}\left(1-\gamma\frac{k}{L}\sqrt{q}\cos\delta\right), \tag{8}$$

where θ -- normal random quantity with zero mean and single standard deviation; $h=a^2T/2N$ -- signal/noise energy ratio; $q=b^2/a^2$ -- structural noise and signal power ratio.

Since phase difference δ is equally-probable in interval $[0.2\pi]$, the factors in parentheses (7) and (8) change within identical limits. In determining mean probability of spurious reception, the result of averaging the right sides of (7) and (8) by δ is identical. Therefore we shall utilize only (7) below.

The probability of reception error with fixed γ, k and δ

$$P_y\left(\theta < -\sqrt{2h}\left(1+\gamma\frac{k}{L}\sqrt{q}\cos\delta\right)\Big|_{\gamma,k,\delta}\right) = 0{,}5 - F\left[\sqrt{2h}\left(1+\gamma\frac{k}{L}\sqrt{q}\cos\delta\right)\right], \tag{9}$$

where

$$F(x) = \frac{1}{\sqrt{2\pi}}\int_0^x e^{-\frac{z^2}{2}}\,dz.$$

To determine mean absolute probability of error it is necessary to average (9) by γ, k and δ. Selection of each signal and noise DFM elementary pulse frequency is independent, and therefore distribution W(k) of discrete random quantity κ is binomial

$$W(k) = p^k (1-p)^{L-k} C_L^k, \quad p = \frac{1}{m}.$$

Averaging (9) taking into account equal probability of symbol transmission, we obtain error probability

$$P = 0{,}5 - \frac{1}{2\pi} \sum_{k=0}^{L} p^k (1-p)^{L-k} C_L^k \int_0^{2\pi} \int_0^1 F\left[\sqrt{2h}\left(1 + \gamma \frac{k}{L} \sqrt{q} \cos\delta\right)\right] d\gamma d\delta. \quad (10)$$

Figure 2 shows dependences of P on h when m=L, calculated according to (10) with different q. The dashed curve corresponds to optimal coherent reception (q=0).

The obtained relations indicate the following. With large h probability of error is determined primarily by q and with fixed m and L is limited from below. With an increase in the dimension of the frequency-time matrix with given q and h, noise stability increases rapidly. For example, when q=2 and h=10 an increase of m=L from 4 to 16 decreases the probability of error by more than two orders of magnitude. When m=L=16 and with typical allowable values of probability of error in the order of 10^{-3}-10^{-4}, reception resistance to interference on a background of additive noise and structural interference is practically no different from the noise stability of optimal coherent reception on a noise interference background. Thus with a sufficiently large dimensionality of the frequency-time matrix, structural interference does not exert substantial influence on the quality of reception.

Expression (10) and the curves in Figure 2 make it possible in each concrete instance to estimate the quality of reception and reasonably to select appropriate parameters, in particular when frequency-division multiplexing.

BIBLIOGRAPHY

1. Kotel'nikov, V. A. "Teoriya potentsial'noy pomekhoustoychivosti" [Theory of Potential Noise Stability], Moscow, Gosenergoizdat, 1956.

Submitted 6 July 1978

3024
CSO: 1870

COMMUNICATIONS

UDC 621.39:629.78

DETERMINATION OF THE ZONE OF A GUARANTEED SIGNAL LEVEL IN A SATELLITE COMMUNICATION SYSTEM

Moscow RADIOTEKHNIKA in Russian No 4, Apr 79 pp 13-18

[Article by L. M. Mashbits, N. M. Zevelev, L. I. Smolich and Z. F. Patrusheva]

[Text] Introduction. One of the basic complexities in introducing satellite communication systems (SCS) is determining the actual limits of the zone of a guaranteed signal level (GSL). This problem must be solved to establish the degree to which specific realized systems correspond to design data, as well as for a general evaluation of the design methods and the feasibility of using special steps to correct the limits of the GSL zone. The problem came up almost at the start of using relay satellites to set up communication systems, but is now taking on particular urgency in connection with the introduction of systems for handling local traffic [Ref. 1] that are designed for comparatively simple receivers.

Formulation of the Problem. Determination of the GSL zone of an operating SCS can be broken down into two independent stages: first -- determination of the relay parameters that influence the location of the zone; second -- calculation of the limits of the zone from the known relay parameters.

We will not consider the second stage since it can be realized on the basis of methods that have already been developed for calculating zones [Ref. 2]. In realizing the first stage, it is necessary to meet two major conditions: first of all, one must not place excessively stiff requirements on the placement of ground-based control points (for instance a requirement to locate the control points at strictly predetermined geographic coordinates or beyond the planned limits of the GSL zone is unacceptable); secondly, if special working conditions of the transmitting complex of the relay unit are provided for making measurements, then there should not be any essential difference between the spectral power densities of the emitted signal during measurements and during operation of the system.

In solving the given problem, we can take the following as known (assigned): the working frequency of the transmitter f; the geographic coordinates of the

point beneath the satellite -- longitude μ_0 and latitude θ_0 -- of the planned aiming point of the axis of symmetry of the radiation pattern of the relay transmitting antenna (RPRTA) μ_t and θ_t, and of the control points μ_i and θ_i (i is the number of the point); the functional dependence of losses in the earth's atmosphere on the angle of elevation β and working frequency $L_\beta = F_1(f;\beta)$; the apex angles of the RPRTA along the major and minor axes 2η and 2λ respectively and the functional dependence of the relative gain over the RPRTA $S = F_2(\eta; \lambda; \xi; \gamma)$, where ξ is the angle between the axis of symmetry of the RPRTA and the direction of the radius vector from the point at which the relay is located to the investigated point of the earth's surface N (the angles of projection of this radius vector τ and δ), γ is the angle between the major aperture of the RPRTA and the plane passing through the axis of symmetry and the investigated point N (Fig. 1).

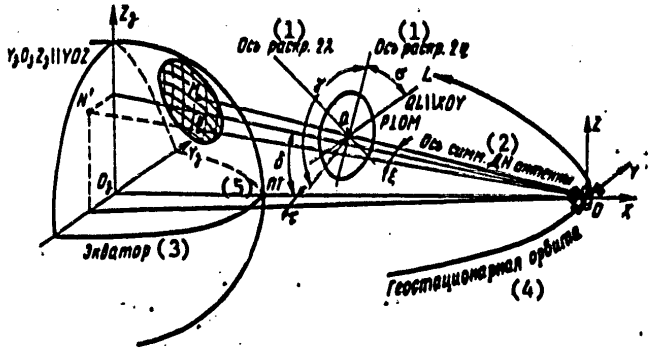

Fig. 1

KEY: 1--Aperture axis
2--Axis of symmetry of the antenna radiation pattern
3--Equator
4--Geostationary orbit
5--point beneath the satellite

Thus the problem portion of our task is to find a method and the mathematical tools that enable us (with consideration of the above-mentioned factors) to determine two characteristics of the relay -- the spatial position of the RPRTA and the equivalent isotropically emitted power (EIEP). In the remainder of this article we will examine four directions in the solution of this problem. For convenience of the exposition, these directions will be designated: DZC and DZSC -- determination of zones based on comparator measurements and satellite-borne calibration respectively; DZDA and DZDSC -- determination of zone with displacement of the relay antenna and spacecraft respectively.

Measurement of Primary Parameters and Formulation of the Criterion Functional. We divide the four directions of solution of the problem listed above into two

categories: in the first, absolute measurements (the comparator method) are used to get the primary parameters (parameters determined by control points), and it includes only DZC; in the second category, there parameters are determined by relative measurements DZSC, DZDA and DZDSC.

To get the primary parameters in DZC, the relay transmitter at a set time is put into the measurement mode, and each control station determines the absolute level of the signal at the input to the receiver complex by replacing the antenna-feeder channel with a control oscillator in which the output power level P_r is adjusted so that the readings of the output display of the receiver remain constant. The results of the measurements are then converted to field strength according to the formula [Ref. 3]

$$E = \sqrt{\frac{480\pi^2 P_r}{\lambda_p^2 G_{np}\eta_{\phi.np}}}, \qquad (1)$$

where E is the effective field strength; λ_p is wavelength; G_{np} is the gain of the receiving antenna (relative to an isotropic radiator); $\eta_{\phi.np}$ is the efficiency of the antenna-receiver feeder.

The values of E_i and the geographic coordinates of these points μ_i and θ_i are the input parameters for a computer program that determines the angles ψ_r, ψ_p and ψ_y (roll, pitch and yaw of the spacecraft [Ref. 2]) and the power P of the satellite-borne transmitter by optimizing (minimizing) the criterion functional

$$Z = \sqrt{\frac{1}{n}\sum_{i=1}^{n}\left(\frac{E_{\pi i}-E_i}{E_i}\right)}. \qquad (2)$$

where n is the number of control points, $E_{\pi i}$ is the "programmed" field strength at the i-th point that corresponds to instantaneous values of the varied parameters ψ_r, ψ_p, ψ_y and P. Since in implementing this procedure the gain of the relay transmitting antenna and the efficiency of the feeder from transmitter to the transmitting atnenna are taken as constant (equal to the rated values), the value of P found as a result of solution uniquely determines the EIEP.

In methods of the second category (DZSC, DZDA and DZDSC) the goal of measurements made by the control points is to determine the ratios of the field strength levels E_i (or the corresponding signal levels U_i at the linear output of the receiver) for two versions of the characteristic of the relay transmitting complex $a_i = U_{i2}/U_{i1}$. In doing this, the characteristic of the transmitting complex of the relay in the method of DZSC is changed by switching from the main antenna to an auxiliary ("calibration") weakly directional antenna for which the relative gain with respect to the radii vectores of all control points can be considered identical in the first approximation; in the DZDA procedure the change is made by altering one of the parameters that determine the position of the antenna relative to the spacecraft, ψ_e, ψ_s or σ (the angles of extension, side deflection and initial turn of the antenna respectively [Ref. 4]); in the method of DZDSC -- by changing one of the parameters that determine the spatial position of the spacecraft -- ψ_r, ψ_p or ψ_y.

For all methods that use relative measurements, the criterion functional is equal to

$$Z = \sqrt{\frac{1}{n}\sum_{i=1}^{n}\left(\frac{a_{ni}-a_i}{a_i}\right)^2}. \qquad (3)$$

where a_{ni} is the programmed value of the signal level ratio corresponding to the instantaneous value of the varied parameters that is determined by the computer program. The parameters that are varied are the angles ψ_r, ψ_p and ψ_y that correspond to the working position of the relay, and the parameter Δ that characterizes the amount of variation of the parameter that is used to change the working conditions of the transmitting complex of the relay in the accepted measurement method (the latter only in the case where exact data on the value of the parameter Δ cannot be obtained directly from the conditions of the experiment).

As compared with DZC, the methods that use relative measurements (DZSC, DZDA and DZDSC) have a considerable advantage -- the major sources of error inherent in DZC are eliminated from calculations -- lack of agreement between the nominal and true values of the gain of the antennas and the efficiency of the feeders of the control points, and also the error of homing and the errors of the control oscillators at the points. There is no need to use a special mode for measurements in the relay unit since they can be made on a "pseudo-working" signal (e. g. on a test pattern in television systems).

Since only parameters of the spatial orientation of the relay atnenna can be obtained from calculations in the case of relative measurements, the EIEP needed for calculating the GSL zone is determined in this instance from data of telemetry or by absolute measurements at any single ("leading") control point, which for this purpose is equipped with reference instruments.

The procedure for optimizing the criterion functional ((2) or (3) respectively) is realized on the basis of using methods of programming that are considered in detail in Ref. 5.

Computational Algorithm. The basic computational procedure can be represented by the following algorithm (as applied to DZC):

1. In accordance with formula (1) and data of measurements of the control points, we determine the E_i for each point, and determine β_i, d_i and $L_{\beta i}$ according to the formulas from Ref. 2 and 6.

2. We take as zero approximations

$$\psi_{r0} = \psi_{p0} = \psi_{y0} = 0, \quad P_0 = P_{nom}.$$

3. We determine the angles

$$t = \operatorname{arctg}\sqrt{\frac{P_0}{P_0}}; \quad \tau = \arccos\sqrt{\frac{P_i^2}{P_0 P_0}}. \qquad (4)$$

where

$$P_1 = C^2(LV-1) - B(TCV+LC+V) - (1-T)(C+B^2) + L(B+V) + T;$$
$$P_2 = (TC)^2 + (LB)^2 + 2(TC + LB + TCLB) + 1;$$
$$P_3 = C^2(1+L^2) + B^2(1+T^2) + T^2 + L^2 - 2(TC + LB + TCLB);$$
$$P_4 = C^2 + V^2 + (CV)^2 - 2(CBV - B^2 - BV - C) + 1;$$
$$T_l = \operatorname{tg}\tau_l = \frac{R\cos(\theta_l-\theta_0)\sin(\mu_l-\mu_0)}{H - R\cos(\theta_l-\theta_0)\cos(\mu_l-\mu_0)}; \quad C = -\frac{m_1}{m_3}; \quad B = -\frac{m_2}{m_3};$$
$$L_l = \operatorname{tg}\delta_l = \frac{R\sin(\theta_l-\theta_0)}{H - R\cos(\theta_l-\theta_0)\cos(\mu_l-\mu_0)}; \quad V = \frac{m_6(m_1-m_4)+m_3(m_5-m_6)}{m_1m_5 - m_4m_6};$$

$m_1, \ldots, m_6$ are functions of the angles ψ_r, ψ_p, ψ_y, μ_t, θ_t and σ [Ref. 2], R is the radius of the earth, H is the radius of the geostationary orbit.

4. We determine S_i from the given formula $S = F_2(\eta, \lambda, \xi, \gamma)$ [Ref. 2, 3].

5. We determine $E_{\Pi i}$ from the relation [Ref. 6]

$$E = \frac{S}{d}\sqrt{\frac{30PG\eta_\Phi}{L_\beta L_\Delta}},$$

where G is the gain of the relay transmitting antenna, L_Δ are additional losses [Ref. 6], η_Φ is the efficiency of the feeder between the transmitter and the relay transmitting antenna.

6. We determine the criterion functional Z from formula (2).

7. By going through points 3-6 in a cyclic procedure to minimize Z [Ref.5], we get the most probable values of the varied parameters ψ_r, ψ_p, ψ_y and P.

Presentation of Results and Evaluation of Errors. The values of ψ_r, ψ_p, ψ_y and P obtained as a result of measurements and subsequent calculations enable us to compute the boundary points of the GSL zone [Ref. 2], and after plotting this zone on a single map with the projected zone, to evaluate the degree of discrepancy between the projected and true state of the system. Such a technique for presenting the results of measurements is quite graphic, but it is cumbersome and gives only a qualitative estimate of discrepancy.

For operational evaluation it is desirable to use some generalized parameter that permits evaluation of the quantitative state of the system and does not need graphic constructions for determination. As such a parameter it is advisable to use the "coefficient of utilization of the nominal zone" -- $K_з$ defined (Fig. 2) as the ratio of the area of the overlapping part of contours 1 and 2 ($S_П$) to the area bounded by contour 1 (S_1),

$$K_з = \frac{S_П}{S_1}. \qquad (5)$$

where contours 1 and 2 are formed by the cross section that is made by the plane perpendicular to the projected axis of symmetry of the RPRTA in two conical surfaces -- the surface of relative gain with respect to a level of

-3 dB that corresponds to the projected position of the antenna (contour 1), and the surface of relative gain with respect to a level of -3 dB that corresponds to the true position of the antenna found from the results of measurements (contour 2). Of course $K_э$ is not an exhaustive characteristic of discrepancy of the projected and actual GSL zones; however, it is a quantitative characteristic, which is quite important for solving the question of the need for taking corrective steps.

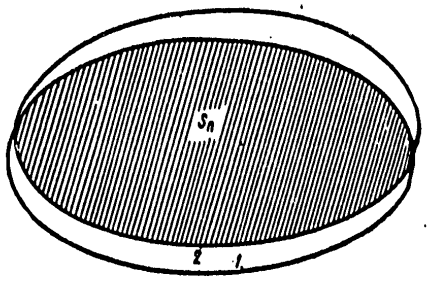

Fig. 2

The error of the initial value of $K_э$ is determined chiefly by the error of measurements of the initial parameters coming from the control points (E_1 or α_1). With application to a specific system with predetermined location of control points we can calculate the dependence

$$\delta_{2max} = F_э(\delta_1), \qquad (6)$$

beforehand, where δ_1 is the calculated relative error of measurements of the initial parameters, δ_2 is the calculated relative error of determination of $K_э$. Using a graph of function (6) [for one of the investigated systems (Fig. 3)], we can also solve the inverse problem -- determining the admissible relative error of measurements of the initial parameters δ_1 for which the maximum calculated error of determination of $K_э$ will not exceed the predetermined value δ_{2max}.

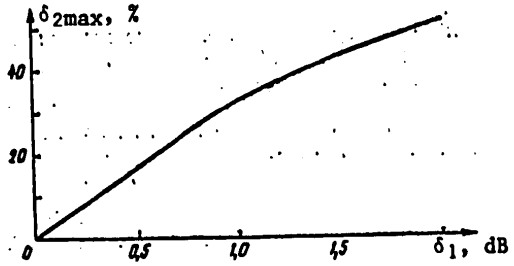

Fig. 3

Example. Given: working frequency $f = 12$ GHz; coordinates of the point beneath the satellite $\mu_0 = 50°$, $\vartheta_0 = 0$; power of the satellite-borne transmitter $P_{nom} = 1200$ W; gain of the relay transmitting antenna $G = 3600$; efficiency of the feeder between the transmitter and the relay transmitting antenna $\eta_\phi = 0.63$; additional losses $L_д = 0$ dB; normative level of field strength $E_n = 122.5$ V/m; angles of initial setting of the antenna $\psi_e = 6.87°$, $\psi_в = 1.78°$ and $\sigma = -6.5°$; angles of the aperture of the RPRTA $2\eta = 3.6°$ and $2\lambda = 2°$.

The gain of the antennas of the control points $G_{rec} = 10{,}000$; efficiency of the antenna-receiver feeder $\eta_{ф.пр} = 0.8$.

The results of measurements made by the control points are given in the table. At the instant of the measurements the coordinates of the point beneath the satellite were: $\mu_0 = 50.1°$ and $\vartheta_0 = -0.1°$. The functions F_1 and F_2 are given in Ref. 2.

It is required to determine the values of the parameters ψ_r, ψ_p, ψ_y, P and $K_э$, to calculate the boundary points of the GSL zone and to construct this zone on a map.

Solution. As a result of calculation we get: $\psi_r = 0.1999°$, $\psi_p = 0.2006°$, $\psi_y = 1.004°$, P = 1200 W, $K_э = 0.8565$. By the technique of Ref. 2 we determine the boundary points and plot the zone on a map. The result of execution of

i	μ_i	ϑ_i	P_{ri}
1	59,5°	38,0°	—107,3 дБВт*
2	77,0°	43,0°	—106,0 дБВт*
3	72,0°	50,5°	—104,0 дБВт*
4	60,0°	53,0°	—105,0 дБВт*

*дБВт = dBW

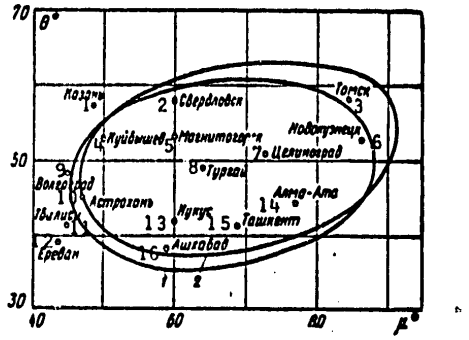

Fig. 4

KEY:
1--*Казань--Kazan'*
2--*Свердловск--Sverdlovsk*
3--*Томск--Tomsk*
4--*Куйбышев--Kuybyshev*
5--*Магнитогорск--Magnitogorsk*
6--*Новокузнецк--Novokuznetsk*
7--*Целиноград--Tselinograd*
8--*Тургай--Turgay*
9--*Волгоград--Volgograd*
10--*Астрахань--Astrakhan'*
11--*Тбилиси--Tbilisi*
12--*Ереван--Yerevan*
13--*Нукус--Nukus*
14--*Алма-Ата--Alma-Ata*
15--*Ташкент--Tashkent*
16--*Ашхабад--Ashkhabad*

the last part of the problem is graphically shown in Fig. 4 (contour 2); also given for comparison is the GSL zone calculated from known parameters $\psi_r = \psi_p = \psi_y = 0$, $P = P_{nom}$ (contour 1).

Conclusion. In the already rather extensive Soviet and non-Soviet technical literature dealing with different aspects of development of SCS, the problem of determining the zones of operating systems has in essence remained unexamined, which makes it difficult to introduce and operate these systems. This is apparently due to the lack of an analog (prototype) of the given problem in communication systems of other types, in virtue of which there are necessarily stages in the search for fundamental paths to solution of the problem, and very cumbersome checks on their technical realizability and effectiveness.

The directions that we have considered enable utilization of the simplest and most accessible solutions from the standpoint of the equipment used (ground-based and satellite-borne) and mathematical tools. Moreover, these directions do not exhaust all possible variants of solutions, which will change and improve as experience is accumulated and the satellite communication systems themselves are perfected.

REFERENCES

1. S. V. Borodich, ELEKTROSVYAZ', No 9, 1975.

2. L. M. Mashbits, RADIOTEKHNIKA, Vol 33, No 12, 1977.

3. G. Z. Ayzenberg, "Antenny ul'trakorotkikh voln" [Ultrashort-Wave Antennas], Moscow, Svyaz'izdat, 1957.

4. L. M. Mashbits, ELEKTROSVYAZ', No 11, 1976.

5. D. Khimmel'blau, "Prikladnoye nelineynoye programmirovaniye" [Applied Nonlinear Programming], Moscow, Mir, 1976.

6. A. D. Fortushenko, G. B. Askinazi, V. L. Bykov, L. Ya. Kantor, O. S. Kropotin, "Osnovy tekhnicheskogo proyektirovaniya sistem svyazi cherez ISZ" [Principles of Technical Design of Satellite Communication Systems], Moscow, Svyaz', 1970.

6610
CSO: 1870

OSCILLATORS AND MODULATORS

UDC: 621.373.5

MILLIMETER-WAVE SOLID-STATE OSCILLATORS

Kiev IZVESTIYA VUZ RADIOELEKTRONIKA in Russian Vol 21 No 10, 1978 pp 4-23

[Article by V. P. Taranenko, B. A. Kotserzhinskiy, and Ye. A. Machusskiy]

[Text] In this review, compiled from materials in Soviet and foreign publications, we shall examine active elements, basic types of designs, electrical characteristics and methods of modeling solid-state oscillators in the 30-300 GHz band.

Promising areas of application of millimeter waves have been specified [1-3]: waveguide communication links; short-range radars for detecting small objects; long-range airborne radars for mapping; intersatellite radio communications; short-range concealed communications.

Solid-state millimeter band oscillators form the basis of radio-frequency devices operating in these areas.

The authors of this survey have set for themselves the objective of synthesizing the latest data appearing in Soviet and foreign scientific and technical literature dealing with development, research and modeling of millimeter band solid-state oscillators.

Millimeter-Band Active Elements

Avalanche diodes and diodes based on intervalley electron transfer (Gunn diodes). Advances in the area of development of high-quality semiconductor materials as well as processing technology and assembling have made it possible substantially to improve their characteristics in recent years.

Figure 1 shows the outputs generated by avalanche and Gunn diodes at various frequencies in the millimeter band, obtained under laboratory conditions.

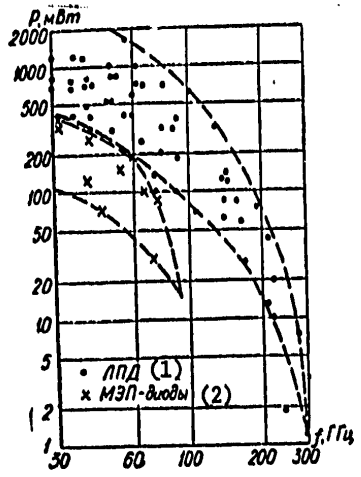

Figure 1.

Key:

1. Avalanche diode
2. Gunn diodes

At frequencies of 30-60 GHz power (P) generated by an avalanche diode in continuous mode reaches (1.2-1.6) watts, while efficiency (η) is (10-16)% [4-8]; at frequencies of (60-100) GHz P=(200-760) mw, and η=(8-12.5)% [4, 9-12]; at frequencies of (100-200) GHz P=(50-150) mw and η=(2-4)% [13-16]; at higher frequencies P<50 mw and η<2% [17, 18].

Maximum electronic efficiency of Gunn diodes does not exceed (5-7)% [19, 20], and generated power -- (200-450) mw at (30-60)GHz and (20-100) mw at frequencies to 90 GHz [20, 21]. Maximum power of commercially-manufactured devices is approximately 3-5 times below record levels [22]; Operating frequencies of commercially-manufactured avalanche diode o s c i l l a t o r s are limited to (75-100) GHz, and Gunn diode oscillators -- (40-70) GHz.

Figure 2 shows the design of millimeter-band diodes. An enclosed package (Figure 2a) [23] is employed in the longer-wave portion of the band. An open case (Figure 2b) [30] or caseless (frequently passivated) structure (Figure 2c) is employed [28] at higher frequencies. Any housing design introduces into the circuit of a millimeter band device additional losses and reactive elements, in the simplest case the series inductance of the connecting wire and capacitance parallel to the semiconductor structure. While in some instances housing inductance can play a positive role [23], housing capacitance is always undesirable, and an effort is made to minimize it. Minimum inductance and

capacitance values are in the range of hundreds of nanohenries and picofarads respectively. The influence of housing elements is particularly significant when designing wideband devices.

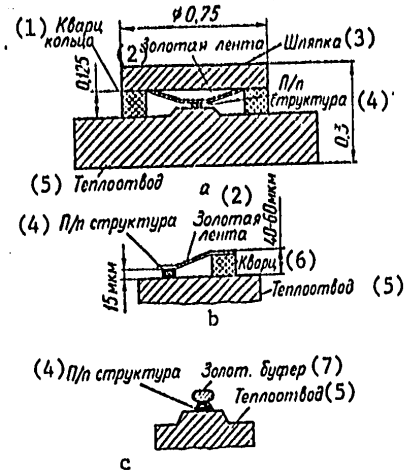

Figure 2.

Key:

1. Quartz ring
2. Gold strip
3. Cap
4. Semiconductor structure
5. Heat sink
6. Quartz
7. Gold buffer

Diode operation is determined in large measure by the quality of heat removal, which limits maximum dissipation. Usually a semiconductor is mounted on a copper or silver heat sink, and on diamond in especially critical applications.

Oscillator Design and Parameters

Waveguide oscillators appear to be the most preferable in the millimeter band. Their advantages include the following: practically complete shielding of millimeter band fields, small losses in the electrodynamic system, simplicity of mechanical frequency tuning, and simplicity of diode and heat sink mounting devices.

Development of millimeter-band coaxial oscillators encounters considerable technical difficulties. The condition of nonpropagation of higher types of waves limits the resonator diameter to a value of λ/π, which at a

frequency of 30 GHz is approximately 3.2 mm. Adjustment and mechanical tuning of oscillator frequency are difficult.

Difficulties arise in constructing microstrip systems connected with the imperfection of the base material (high dielectric losses, high levels of extraneous radiation of millimeter band energy). Mechanical frequency tuning is difficult. Microstrip oscillators are promising in the longer-wave portion of the millimeter band with integral technology and mass production.

Solid-state oscillators can be subdivided into two basic groups: fixed-frequency oscillators, and tunable oscillators.

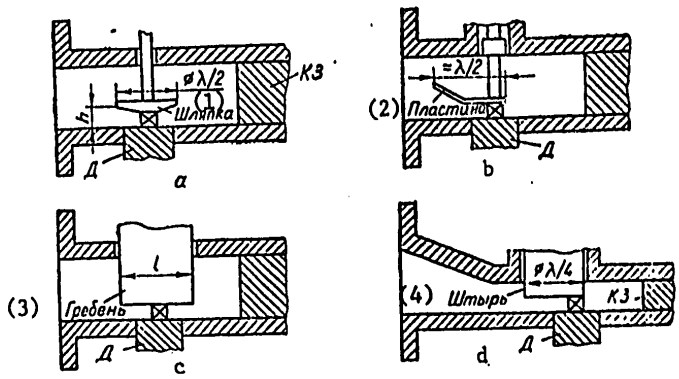

Figure 3.

Key:
1. Cap
2. Plate
3. Ridge guide
4. post

Fixed-frequency oscillators are employed as heterodynes in radars of various function, active FAR [expansion unknown] modules, and parametric amplifier pumping sources. At the specified fixed frequency they make it possible to obtain a comparatively high level of output power and efficiency.

Oscillators with an in-waveguide resonator. The most common design of a millimeter-band oscillator with fixed tuning [24] is shown schematically in Figure 3a. The active element is mounted in the middle of a wide waveguide wall of standard section under a cap-type structure which is attached to the end of a current-feeding diode power circuit filter post. The cap (its diameter is approximately equal to one half wavelength λ) makes it possible to match the low impedance of the diode (a few ohms to tens of ohms)

with the high (hundreds of ohms) impedance of the standard waveguide. A movable shorting device (KZ) provides additional fine tuning. A load-matching device is usually provided at the oscillator output (for example, an E-H transformer). The fine tuning range of the shorting device in this design does not exceed several percent. A power output of 1.6 watts at a frequency of 55.5 GHz is obtained with utilization of a special power circuit filter design, which makes it possible to eliminate avalance diode low-frequency instability [6, 7].

In the oscillator depicted in Figure 3b, the in-waveguide resonator is formed by a bent paddle (length $\lambda/2$) and the lower wall of the waveguide. Such oscillators based on Gunn diodes in the range (58-65) GHz have a power output of (35-62) mw with $\eta=(1.22-2.21)\%$ [25].

In the design depicted in Figure 3c an active diode is placed under a narrow vertical ridge guide of length l, which simultaneously performs the function of contact conductor. Oscillation frequency is determined primarily by the length of the ridge guide and is weakly dependent on the position of the shorting device. Power output of an avalanche diode oscillator is 380 mw at a frequency of 30 GHz with an efficiency of up to 8% [26].

Oscillators for the shorter-wave portion of the millimeter band have been developed on the basis of a reduced height waveguide, with a "fat" (diameter up to $\lambda/4$) post (Figure 3d). At frequencies of 136-170 GHz the power output of such an avalanche diode oscillator is 30-80 mw. Silicon double-transit (DT) diodes are employed. When the shorting device is displaced the frequency can be tuned within a small range, up to 3% [27].

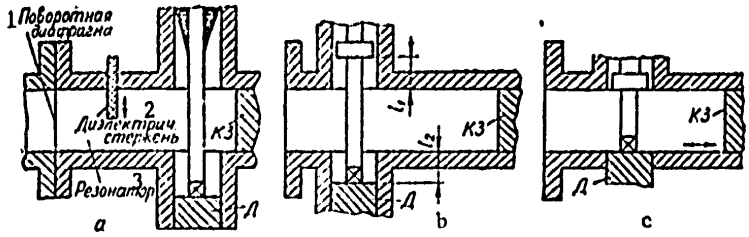

Figure 4.

Key:
1. Revolving diaphragm
2. Dielectric rod
3. Resonator

When utilizing a standard section waveguide and a "fat" post, one obtains generation of millimeter band oscillations up to the submillimeter band.

At frequencies of (202-214) GHz the output power of oscillators with single transit silicon avalanche diodes reaches (44-50) mw with an efficiency of (1.2-1.3)%. At a frequency of f=301 GHz, power output is 1.2 mw [17].

The parameters of oscillators with in-waveguide resonators are listed in Table 1.

Table 1. Characteristics of Oscillators With In-Waveguide Resonators

(1) Рабочая частота, ГГц	(2) Выходная мощность, мВт	(3) К. п. д., %	(4) Тип диода	(5) Тип конструкции	(6) Литер. источник
29,5—34,8	390—680	12,4—16	ОП GaAs ЛПД	(7) рис. 3, *а*	[8]
29,6—39,9	500—700	8,45—10,9	ОП Si ЛПД	»	[28]
26—42	200—400	4—8	ДП Si ЛПД	»	[29]
30	380	8	GaAs ЛПД	рис. 3, *в*	[26]
36	1200	7,5	ДП Si ЛПД	рис. 3, *а*	[12]
50	530	10,3	ОП Si ЛПД	»	[11]
50	1000	14,2	ДП Si ЛПД	»	[11]
50	304	4,6	Ш GaAs ЛПД	»	[30]
52—60	600	8,7	ОП Si ЛПД	»	[31]
55,5	1600	11,5	ДП Si ЛПД	»	[7]
58—65	35—62	1,22—2,21	GaAs МЭП	рис. 3, *б*	[25]
62	760	5,9	ДП Si ЛПД	рис. 3, *а*	[12]
66—71	30—40	0,9—1	GaAs МЭП	»	[20]
74	100	2,5	Ш GaAs ЛПД	»	[30]
78,3—90,1	170—314	4,7—12,5	ДП Si ЛПД	»	[15]
92	180	7,4	ДП Si ЛПД	»	[11]
101	620	7,7	ДП Si ЛПД	»	[12]
106—111	37—74	2—3,2	ОП Si ЛПД	»	[32]
135—142	80—140	2—3	ОП Si ЛПД	»	[13]
136—170	30—80	—	ДП Si ЛПД	рис. 3, *г*	[27]
142	120	4	ДП Si ЛПД	рис. 3, *а*	[14]
161	85	—	ОП Si ЛПД	рис. 3, *г*	[101]
187	82	2,5	ОП Si ЛПД	»	[18]
202—214	44—50	1,2—1,3	ОП Si ЛПД	»	[17]
207	23	—	ДП Si ЛПД	»	[103]
214	12,7	0,7	ОП Si ЛПД	»	[101]
230	10	—	ДП Si ЛПД	»	[103]
250	1,9	—	ДП Si ЛПД	»	[103]
285	7,5	0,35	ОП Si ЛПД	»	[18]
300	0,3	0,025	ОП Si ЛПД	»	[101]
330	0,7	—	ОП Si ЛПД	»	[18]
361	0,2	—	ОП Si ЛПД	»	[18]
394	—	—	ОП Si ЛПД	»	[18]
423	0,008	—	ОП Si ЛПД	»	[101]

Key:

1. Operating frequency, GHz
2. Power output, mw
3. Efficiency, %
4. Type of diode
5. Type of design
6. Bibliographic source
7. Figure

Note: Ш -- diode with Schottky barrier; ОП -- single-transit; ДП -- double-transit; ЛПД -- avalanche diode; МЭП -- Gunn diode

Waveguide-coaxial and waveguide-post designs. In the longer-wave portion of the millimeter band the design schematically depicted in Figure 4a is extensively employed. A coaxial line, at one end of which an active element is placed and at the other -- a matched dissipative load, is perpendicular to the wide walls of any waveguide resonator formed by a shorting device and a revolving diaphragm on the oscillator output flange. The dielectric rod is used to fine-tune the waveguide resonator. Extraneous oscillations outside its passband are effectively suppressed by a low-ohm antiparasitic millimeter band resistor, while at the operating frequency the bulk of the oscillation power passes through the waveguide resonator into the useful load. The efficiency of the electrodynamic system of such an oscillator is (85-95)% [33, 34]. Sometimes a quarter-wave inductor is placed on the central conductor of the coaxial line to increase it.

Placing two avalanche diodes in parallel results in a power output of 518 mw at a frequency of 32.3 GHz [35] and 750 mw at a frequency of 34 GHz [34]. The dielectric rod oscillator frequency fine tuning range is 3.3% at a frequency of 40 GHz, with a power output change from 140 to 200 mw [29].

The design of a waveguide-coaxial oscillator is illustrated in Figure 4b. The diode is placed under the central conductor of a coaxial line millimeter band short-circuited at the opposite end. A waveguide resonator is formed between the shorting device and the axis of the coaxial line. The power output of such an oscillator is 1.2 w at a frequency of 38 GHz (η=10%) when utilizing double-transit silicon avalanche diodes [5]. In avalanche diode oscillators with single-transit passivated diodes power output is 100 mw at a frequency of 67 GHz and efficiency of 1% [36].

With a decrease in length of coaxial segments l_1 and l_2 to zero, a waveguide coaxial system degenerates to a waveguide-post system (Figure 4c). An avalanche diode oscillator of such a design has a power output of 320-370 mw with an efficiency of (6-7)% at frequencies of (36.5-39) GHz [37].

Characteristics of waveguide-coaxial and waveguide-post oscillators with fixed frequency are summarized in Table 2.

Microstrip oscillators. Millimeter-wave oscillators have been developed with a microstrip electrodynamic system. System topology is shown in Figure 5a [38]. The active element is connected to the cavity with the aid of a metal angle bracket; coupling between resonator cavity and microstrip transmission line is capacitive; the diode power circuit filter is on the same dielectric base. With utilization of double-transit silicon avalanche diodes, a power output of 320 mw is obtained at a frequency of 30 GHz, η=5.2%; power output is 270 mw at a frequency of 55 GHz and an efficiency of 5.2%; at a frequency of 108 GHz power output is 25 mw and efficiency is 1.6% [39, 40].

Table 2. Characteristics of Waveguide-Coaxial and Waveguide-Post Oscillators

Рабочая частота, ГГц (1)	Выходная мощность, мВт (2)	К. п. д., % (3)	Тип диода (4)	Тип конструкции (5)	Литер. источник (6)
30,6	518	8,5	2 шт. Ш GaAs ЛПД	рис. 4, а (7)	[35]
32—34,5	435—192	9,6—11,7	Ш GaAs ЛПД	»	[35]
34	750	5	2 шт. ОП GaAs ЛПД	»	[34]
34	680	10	ОП GaAs ЛПД	»	[34]
30,5—39	370—320	6—7	ОП Si ЛПД	рис. 4, в	[37]
38	1200	10	ДП Si ЛПД	рис. 4, б	[5]
44—59	100—250	5—8	ОП GaAs ЛПД	рис. 4, а	[34]
49—57	100—140	5,2—7,2	Ш GaAs ЛПД	»	[33]
62	100	1	ОП ЛПД	рис. 4,	[36]
75	60	3,2	Ш GaAs ЛПД	рис. 4, а	[33]

Key (see key to Table 1)

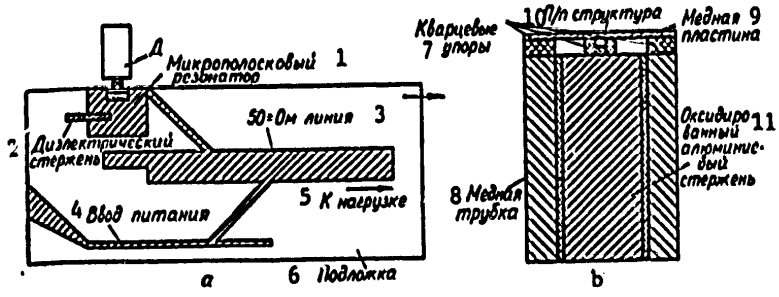

Figure 5.

Key:

1. Microstrip resonator
2. Dielectric rod
3. 50-ohm line
4. Power input
5. To load
6. Base
7. Quartz supports
8. Copper tube
9. Copper plate
10. Semiconductor structure
11. Oxidized aluminum rod

A microstrip oscillator with a lowered-Q resonant system, designed for use in external synchronization mode, is investigated in [41]. The resonator, formed by avalanche diode mounting elements (a copper strip and quartz supports, Figure 5b), is capacitance-coupled with a microstrip line. A resonator of this design makes it possible to reduce the Q of the oscillator by reducing the energy stored in a "quasiconcentrated" circuit in comparison with a

resonator based on a segment of a millimeter band transmission line. Oscillator power output is 120 mw at a frequency of 30.6 GHz. The oscillator locking band extends to 1300 MHz.

Oscillators with an external stabilizing resonator. Millimeter-band stabilized oscillators have a reduced noise level and are extensively employed as heterodynes and driving oscillators in radar and communication systems.

Parametric methods of stabilization prove to be most preferable in most cases, methods which make it possible to realize the principal advantages of a solid-state oscillator -- small size, light weight, and high reliability. A widespread method of parametric frequency stabilization involves external high-Q and high-calibration resonator cavities [42]. Figure 6 contains three basic stabilizing resonator arrangements.

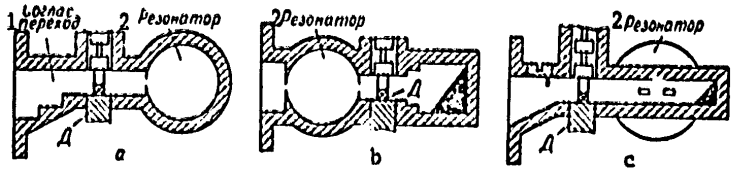

Figure 6.

Key:
1. Matched transition
2. Cavity

Oscillators with a reflecting resonator (Figure 6a) ensure high stabilization factors with comparatively small power output losses [43, 47]; an arrangement with a transmission cavity (Figure 6b) realizes maximum stabilization factors, but with increased power losses [48, 49]; the principal advantage of an oscillator with a band-reflecting stabilizing system (Figure 6c) is a one-frequency operating mode [7, 43, 50].

Table 3 contains the parameters of millimeter-wave stabilized oscillators.

Tunable oscillators are employed as heterodynes and driving oscillators for radars and communication lines, and in measuring equipment. They must meet demands of wide-band frequency tuning with minimal power output drop.

In order to obtain wide-band tuning it is necessary carefully to design placement arrangements of diodes, power supply filters, and matching circuits. The resonances of diode case reactive elements and wiring diagrams can lead to disturbances in frequency tuning characteristics or oscillator operation at untuned frequencies. The best results are obtained when utilizing unpackaged and miniature diodes [10, 51-53].

Table 3. Characteristics of Oscillators Stabilized by External Cavities

1 Рабочая частота, ГГц	2 Выходная мощность, мВт	Темпер. нестаб. и нестаб. по режиму питания 3	Тип диода 4	Тип конструкции 5	Литер. источник 6
26—31	200	$2 \cdot 10^{-6}$ 1/°K —	GaAs МЭП	7 рис. 6, *а*	[45]
26—33	50	$4 \cdot 10^{-6}$ 1/°K 2 МГц/В	GaAs МЭП	»	[45]
30	20	$6 \cdot 10^{-7}$ 1/°K 0,7 МГц/В	GaAs МЭП	»	[46]
52	1000	— 0,015 МГц/мА	ДП Si ЛПД	рис. 6, *в*	[7]
79	16	$2 \cdot 10^{-6}$ 1/°K 0,16 МГц/мА	ОП Si ЛПД	рис. 6,	[48]
80	65	$2{,}5 \cdot 10^{-6}$ 1/°K 0,05 МГц/мА	ОП Si ЛПД	рис. 6, *а*	[47]

Key:
1. Operating frequency, GHz
2. Power output, mw
3. Temperature instability and power feed condition instability
4. Type of diode
5. Type of design
6. Bibliographic source
7. Figure

Oscillators with mechanical frequency tuning. The waveguide-post design mechanically tuned generator is the most common (Figure 4c). Frequency tuning range amounts to (20-30)%. Reduced-height waveguides are employed to increase "saturation" frequency [53].

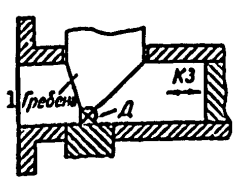

Figure 7.

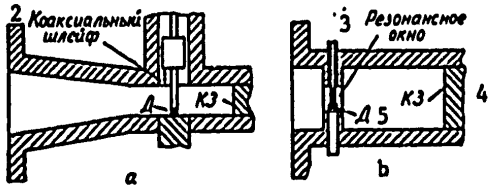

Figure 8.

Key:
1. Ridge guide
2. Coaxial stub
3. Resonance window
4. Shorting device
5. Diodes

When utilizing a waveguide design with a nonresonant ridge guide (Figure 7), Gunn diode oscillator tuning has been obtained in a waveguide operating band of (26.5-40) GHz [52].

During displacement of a dielectric rod (DR) in a waveguide oscillator cavity with an antiparasitic resistor (Figure 4a), one obtains $\Delta f_M/f_{cp}=(10-19)\%$ (f_{cp} -- mean band frequency) [10].

Table 4 contains parameters of millimeter-band oscillators with mechanical frequency tuning.

Table 4. Characteristics of Oscillators With Mechanical Frequency Tuning

1 Средняя частота диапазона, ГГц	2 Диапазон перестройки частоты, 3 ГГц	3 %	4 Выходная мощность, мВт	5 Перепад выходной мощности, дБ	6 Тип констр.	7 Элем. перестройки	8 Тип диода	9 Лит ист.
27,8	2,5	9	85—100	0,7	рис. 8, а (10)	ДС	ЛПД	[39]
28,4—33,3	8,2—13,5	29—41	50—330	2,5—7,4	рис. 7	КЗ	МЭП	[52]
28,8—35	7,5—10	26—29	25—75	4,8	рис 4, в	КЗ	МЭП	[52]
31,5—63	5—8	11—19	200	—	рис. 4, а	ДС	ЛПД	[10]
34	8	24	—	—	Коакс. (11)	КЗ	МЭП	[53]
45	5,7	13	40—70	2,4	Коакс.	ДС	МЭП	[20]
55—68,5	6,4—13	10—19	50—250	3—4,1	Волнов. (12)	КЗ	ЛПД	[54]
60,5	17	28	—	—	Волнов.	КЗ	ЛПД	[51]
63,5—79	8—10	10—14	100	—	рис. 4, а	ДС	ЛПД	[10]
94	6	6,4	27—50	2,7	Волнов.	КЗ	ЛПД	[54]
230	14	6,1	0,7—4,3	7,8	рис. 3, в	КЗ	ЛПД	[103]

Key:

1. Mean band frequency, GHz
2. Frequency tuning range
3. GHz
4. Power output, mw
5. Power output drop, db
6. Type of design
7. Tuning element
8. Type of diode
9. Bibliographic source
10. Figure
11. Coax
12. Waveguide

Note: ДС -- dielectric rod; КЗ -- shorting device; ЛПД -- avalanche diode

---

Oscillators with electronic frequency tuning. The main areas of application of electrically tunable oscillators are the following: communication links with frequency modulation, measuring equipment, electronic countermeasures systems. Oscillators with frequency tuning by active diode feed current, YIG-spheres, and varactors are employed in the millimeter band.

The capability of wide-band frequency tuning of avalanche diode oscillators by supply current is demonstrated in [55]. These oscillators are waveguide-coaxial in design (Figure 8a). The coaxial segment is formed in the power supply filter circuit, running through the wide wall of a reduced-height waveguide. Transition to a standard waveguide section is smooth. Single-transit silicon avalanche diodes with an open case are used. Ten different oscillators cover the frequency band from 19 to 92.5 GHz. The power output drop is extraordinarily great, reaching (20-30) db. The range of frequency tuning with a drop $\Delta P_{вых}$=3 db does not exceed (10-15)%. By selecting a shorting device position, one can equalize power output in the band to 20%. The oscillator noise level is high. In another waveguide oscillator design (Figure 8b), with a single-transit silicon avalanche diode, mounted in a resonance window under an inductive post, an avalanche diode supply current frequency tuning of (53-63) GHz was obtained with a change in power output from 1 to 45 mw [56].

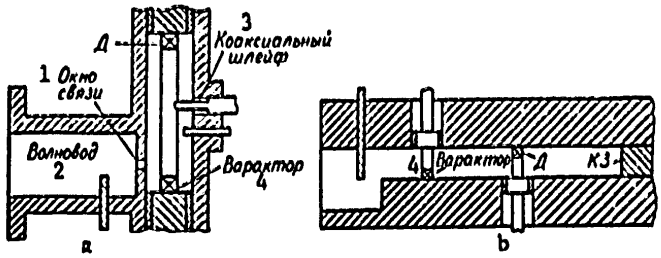

Figure 9.

Key:
1. Connecting window
2. Waveguide
3. Coaxial stub
4. Varactor

A 25-43 GHz waveguide oscillator with YIG sphere frequency tuning has been developed [57]. The tuning band reaches 50% with a power output up to 11 mw with a drop to 12 db. Tuning characteristics show very high linearity -- ±0.1%. With a power output drop of 3 db $\Delta f_э/f_{ср}$ reaches (22-33%). Requisite control magnetic field induction is as much as 1.5 T. Frequency control circuit power is approximately 5 w. Oscillators with YIG tuning contain a substantial deficiency -- slow tuning rate. The necessity of providing very high magnetic field strengths makes employment of oscillators with YIG elements in the shorter-wave portion of the millimeter band unpromising.

A considerable modulation frequency (tens to hundreds of megahertz) can be obtained by oscillators with varactor tuning. Following are additional advantages of utilizing varactors: low frequency control circuit power (less than 1 mw), small size, weight and cost of oscillators and power supplies. Principal drawbacks: reduced resonant system Q and nonlinearity of the electrical frequency tuning characteristic curve [58].

The design of a millimeter-band coaxial oscillator with varactor frequency tuning is illustrated in Figure 9a. A Gunn diode and varactor in miniature cases are mounted at the ends of the coaxial cavity under the central conductor. The power supply circuit filters are capacitance filters. The electrical frequency tuning range of such an oscillator is 3.05 GHz with a mean frequency of 39.5 GHz, with power output ranging from 10 to 12 mw [59].

Coaxial systems are not promising at frequencies above (40-60) GHz due to considerable technological complexity, difficulty of tuning and adjustment. Employment of waveguide designs employing diodes in miniature cases and caseless diodes is promising.

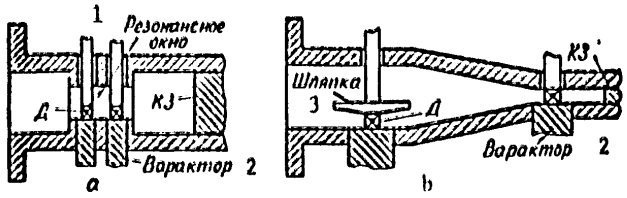

Figure 10.

Key:
1. Resonance window
2. Varactor
3. Cap

An oscillator based on a reduced-height waveguide (Figure 9b) has an electrical tuning range of 1.2 GHz, mean frequency of 37.6 GHz, and power output of 70-80 mw (Gunn diode and varactor in miniature cases) [59, 60].

In the design illustrated in Figure 10a unpackaged avalanche diodes and varactor are positioned in the waveguide diaphragm windows under inductive pins. Frequency tuning amounts to 2.5 GHz at a mean frequency of 56.5 GHz, and power output is (4.2-2.7) mw. Capability of sine wave varactor capacitance modulation with a frequency of 500 MHz has been demonstrated [56].

An oscillator with an open in-waveguide cavity (Figure 10b) tunes in a 300 MHz range (mean frequency 50.6 GHz). The shunting effect of the local resonator limits the tuning range [61].

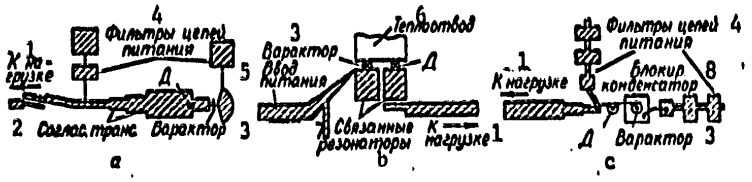

Figure 11.

Key:

1. To load
2. Matched transmission line
3. Varactor
4. Supply circuit filter
5. Supply input
6. Heat sink
7. Coupled cavities
8. Blocking capacitor

Oscillators with microstrip electrodynamic systems have been developed. 1.6 GHz tuning at a mean frequency of 35.3 GHz has been obtained utilizing an unpackaged varactor and a Gunn diode in a standard package (Figure 11a). Power output varies from 0.5 to 13 mw. The 3 db tuning range is 900 MHz [62].

In Figure 11b a double-transit silicon avalanche diode and varactor (avalanche diode in preconduction mode) are mounted in open cases on a common heat sink. Oscillator tuning is 1.6 GHz (mean frequency 59.3 GHz), and power output ranges from 125 to 95 mw. Sine-wave varactor modulation frequency reaches 50 MHz [63].

Figure 11c shows a 26-40 GHz microstrip oscillator with a resonant circuit containing "quasi-concentrated" components [64]. The capacitances of the semiconductor structures of the varactor and avalanche diode and the inductances of the connecting conductors are employed as reactive elements of the resonant circuit. Oscillator tuning range is (6-8) GHz with a power output of up to 36 mw.

A stabilized oscillator with varactor frequency fine tuning within a small range (up to 0.3%) is described in [45] (Figure 12). The oscillator consists of a segment of reduced-height waveguide with a Gunn diode mounted in the middle of the wide wall, a stabilizing cylindrical reflection type cavity and connected waveguide varactor section.

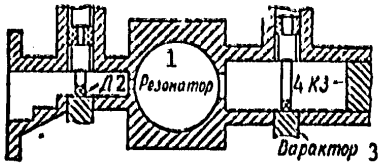

Figure 12.

Key:
1. Cavity
2. Diode
3. Varactor
4. Short circuiting device

Frequency tuning is 95 MHz at a mean frequency of 30.5 GHz, power output 30 mw, $\Delta P_{вых}$=±1.5 db, frequency temperature stability $-5 \cdot 10^{-6}$/°K. Compensation for tuning characteristic curve nonlinearity is possible in this design with selection of short circuiting device position.

Table 5 contains the parameters of millimeter-band solid-state oscillators with electronic frequency tuning.

Table 5. Characteristics of Oscillators With Electronic Frequency Tuning

1 Средняя частота диапазона, ГГц	2 Диапазон перестройки частоты		4 Выходная мощность, мВт	5 Перепад выходной мощности, дБ	6 Тип констр.	7 Элем. перестройки	8 Тип диода	9 Лит. ист.
	3 ГГц	%			(10)	(11)	(14)	
22,4—86	6,7—20,3	15—45	20	22—32	рис. 8, а	Ток п.	ЛПД	[55]
28—35,5	6—8	20—28,5	3—36	2,5—9,5	рис. 11, в	Вар.	ЛПД	[64]
30,5	0,095	0,3	30	3	рис. 12	(12) Вар.	МЭП	[45]
31—34,8	12—17	39—50	11	12	Волнов.(13)	ИГ	(15)	[57]
35,3	1,6	4,5	0,5—13	14	рис. 11, а	Вар.	МЭП	[62]
37,6	1,2	3,2	70—80	0,6	рис. 9, б	Вар.	МЭП	[59]
39,5	3,05	7,7	10—12	0,8	рис. 9, а	Вар.	МЭП	[59]
50,6	0,3	0,6	10—11	0,4	рис. 10, в	Вар.	ЛПД	[61]
56,5	2,5	4,4	2,7—4,2	1,9	рис. 10,	Вар.	ЛПД	[56]
58	10	17,2	1—45	16,5	рис. 8, б	Ток п	ЛПД	[56]
59,3	1,6	2,7	95—125	1,2	рис. 11, б	Вар.	ЛПД	[63]
208,5	7	3,4	0,2—4	13	рис. 3, г	Ток п.	ЛПД	[103]

Key:
1. Mean band frequency, GHz
2. Frequency tuning range
3. GHz
4. Power output, mw
5. Power output drop, db
6. Type of design
7. Tuning element
8. Type of diode
9. Bibliographic source
10. Figure
11. Supply current
12. Varactor
13. YIG
14. Avalanche diode
15. Gunn diode

Pulse mode. The power output of avalanche and Gunn diode oscillators in pulse mode can be increased by approximately one order of magnitude in comparison with continuous oscillation mode. Pulse duration usually does not exceed fractions of a microsecond to a few microseconds [4, 23, 65]. Achieved avalanche diode oscillator pulse power output levels are as follows: 11 watts at a frequency of 39 GHz, 2 watts at 98 GHz, 720 mw at 140 GHz and 520 mw at 214 GHz [4, 66, 102].

A power of 400 mw [21] was obtained at a frequency of 50 GHz and 137 mw at 64 GHz [25] with pulse amplitude modulation of Gunn diode millimeter-band oscillators.

External synchronization. Avalanche diode and Gunn diode oscillators are easily synchronized by an external signal [2]. The level of the applied signal can be almost 40 db below the oscillator power output level [67], and a 30 GHz avalanche diode oscillator synchronization band reaches 1300 MHz [41]. External synchronization mode can be used for frequency tuning and multiplication [68, 69].

Noise generation. Silicon avalanche diodes are employed in a noise generator [70] in a low-ohm rectangular waveguide with a ridge guide matched on both sides for broadening the operating band of frequencies. In the range (26.5-40) GHz the magnitude of excess noise varies within limits of 25-10 db. The conclusion has been drawn that it is possible to replace gas-discharge tubes with avalanche diode noise generators.

Frequency and power stability. Frequency temperature drift of unstable millimeter-band oscillators ranges from 0.5 to 1.5 x 10^{-4} 1/°K [2, 33].

Frequency drift caused by instability of oscillator power supply conditions amounts to (10-20) MHz/V for Gunn diode oscillators and (5-10) MHz/ma for avalanche diode oscillators. Power output temperature instability is 0.01-0.03 db/°K [29, 33].

Connection of external high-Q thermally compensated cavities makes it possible to improve oscillator stability characteristics by 1-2 orders of magnitude (Table 3).

Noise characteristics. The noise level of Gunn diode oscillators is approximately the same as that of reflex klystrons; AM noise of an avalanche diode oscillator is 10-20 and FM noise 20-30 db greater than that of reflex klystrons [2, 71].

AM noise of millimeter-band avalanche diode oscillators comprises (120-140) db/Hz when detuning Δf=(1-2) kHz from the carrier frequency and (150-160) db/Hz when detuning (1-2) MHz [8, 27, 28, 72-74]; Avalanche diode oscillator noise is (60-30) Hz/$Hz^{1/2}$ [73].

Oscillator frequency stabilization with exterior cavities makes it possible to reduce FM noise level by (20-30) db [45].

Oscillator Modeling and Calculation

Up to the present time the design of electrodynamic systems of solid-state millimeter-band devices has been in large measure of an empirical and to some extent intuitive character, and only in some particular instances is it possible to perform a sufficiently complete theoretical analysis.

Methods of numerical calculation of electrodynamic systems with complex boundary conditions developed in recent years potentially make it possible to solve a considerable portion of practical problems, but their application is held back by large expenditures of computer time.

The design substitution method with utilization of combined modeling (some design elements are determined theoretically, and some experimentally) has come into widespread use in designing millimeter-band oscillators.

It is convenient to perform high-frequency circuit modeling with conditional designation of three basic electrodynamic system components: packaged active element; diode mounting device in millimeter-band system; millimeter-band cavity or transmission line proper.

Substitution of millimeter-band diodes by the equivalent circuit shown in Figure 13a is a generally-accepted technique, where G_d, C_d and R_d -- negative conductance, capacitance and resistance of diode losses; L_k and C_k -- case inductance and capacitance. It is usually assumed that only G_d and C_d are dependent on amplitude and frequency of millimeter-band oscillations and diode power supply conditions. Parameters G_d and C_d are obtained experimentally [74-77] or by computation [61]. Representation of diode case parameters with concentrated frequency-independent components L_k and C_k is permissible if the case diameter is less than $\lambda/4$ [78]. Otherwise it is necessary either to modify the equivalent circuit (C' in Figure 13a) [79] or to prepare a formal diagram describing the actual behavior of impedance investigated experimentally [77] or with the aid of electrodynamic analysis.

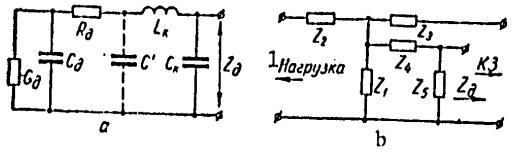

Figure 13.

Key:
1. Load

Basic difficulties arise when modeling a diode mounting device, which can have a varied configuration. The problem is complicated by the fact that in the

millimeter band the mounting device frequently performs functions of a matching circuit and in large measure determines oscillator characteristics. In recent years there have been published a great many studies dealing with a theoretical description of the most common designs: an inductive post in a waveguide has been investigated in detail in studies [80-86]; studies [85-88] deal with determination of the characteristics of a two-post structure of millimeter-band component holders; diodes in reduced-height millimeter-band systems are examined in [78, 89]; waveguide-coaxial structures are analyzed in [90-92].

Utilization of elaborated theoretical models has made it possible to raise to a higher level the method of analysis and optimization of solid-state devices of the centimeter and lower-frequency portion of the millimeter band. Existing models contain deficiencies which show up when transitioning to higher frequencies: active losses in millimeter-band systems are not considered, post diameter does not exceed 0.25 waveguide width, post gap width does not exceed 0.25 waveguide height, and the influence of higher types of waves caused by close-by discontinuities (for example, short-circuiting device) is not taken into account. An attempt to correct some of these deficiencies was made in [51], but the adequacy of the proposed model requires additional experimental verification.

At the present time there are no theoretical elaborations which make it possible sufficiently fully to consider the basic parameters of many other mounting arrangements for millimeter-band diodes. One possible approach is the utilization of a generalized equivalent circuit (Figure 13b), the parameters of which are determined experimentally across a broad range of frequencies and dimensions of electrodynamic system elements. Two configurations of millimeter-band systems -- with an in-waveguide open cavity (Figure 3a) and a resonance window with post (Figure 8b), have been examined with this method in [93-94].

Theory of resonant cavities and millimeter-band transmission lines has been most fully developed, and their modeling does not present any particular difficulties. In designing millimeter-band oscillators (particularly in the higher-frequency portion) it is desirable to consider transmission-line losses. Difficulties akin to those described above occur during theoretical description of cavity coupling elements and matching devices.

Solid-state oscillator equivalent circuits. Modeling does not present any particular difficulties in designing narrow-band oscillators, and simplified equivalent circuits can be employed.

Simplified oscillator circuits have been proposed, with an in-waveguide open cavity (Figure 14a) and a waveguide-coaxial oscillator with an antiparasitic resistor (Figure 14b). In the circuit shown in Figure 14a components G_d, C_d, and L_d have been obtained from an avalanche diode weak-signal analysis, equivalent parameters of in-waveguide cavity L_c, C_c, G_c -- from measurements of the external Q of a resonant system by the phase synchronization method; $\underline{l}$ -- distance from the short-circuiting piston to the axis of the contact post [61].

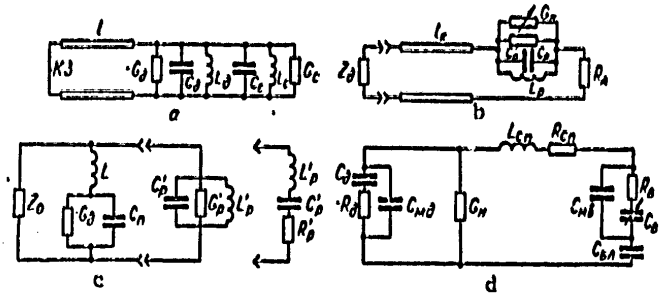

Figure 14.

In the circuit in Figure 14b G_H -- useful load conductivity; L_p, C_p, G_p -- equivalent parameters of waveguide cavity; R_a -- resistance of antiparasitic resistor; l_k -- length of coaxial segment in which is mounted a diode with impedance Z_d [33].

In oscillators with a stabilizing cavity, with line length $n\lambda_B/2$ (λ_B -- wavelength in waveguide; n -- integer) simplification of the equivalent circuit is possible (Figure 14c) [46-49]. Depending on n, the cavity is represented by a series or parallel circuit.

The described circuits in a narrow range of frequencies make it possible to perform qualitative analysis of oscillator operation, and to obtain quantitative estimates in experimental refinement of component values.

Theoretical analysis of a microstrip oscillator with wide-band varactor frequency tuning (Figure 11c) was performed with the aid of the equivalent circuit in Figure 14d. In view of the fact that unpackaged diodes were employed, and the assembly diagram comprises a concentrated circuit, modeling is simplified. C_{md} and C_{mb} -- avalanche diode and varactor mounting capacitances; $C_{бл}$ -- blocking capacitor; L_{cn} and R_{cn} -- inductance and resistance of coupling conductor losses. Discrepancy between results of calculation and experimental data does not exceed 10% [64].

When designing oscillators with a relatively large mechanical tuning range or electrically tuned oscillators, it becomes essential to put together extensive equivalent circuits (Figure 15).

An equivalent circuit (Figure 15a) of a Gunn diode millimeter-band waveguide-coaxial oscillator has been proposed [91]. Coaxial cavity recesses in the upper and lower walls of the waveguide are substituted with segments of short-circuited lines l_k and l_2. Line l_T replaces the diode case; $h_ш$ -- coaxial transformer taking into account the effect of the diode cap. Components

C_{ck1}, C_1, C_{ck2}, and C_2 take into account the higher types of waves excited at points of waveguide and coaxial line intersection; jx_0 -- reactance of the central rod; $Z_в$ and Z_d -- waveguide and diode impedance respectively. Refinement of equivalent circuit components has been performed experimentally.

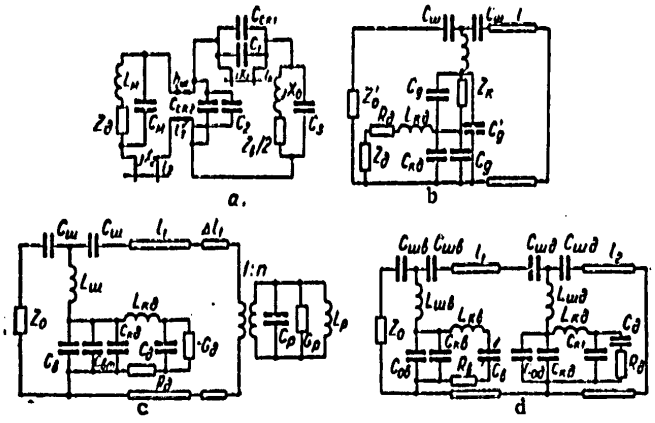

Figure 15.

In [51] there is performed a theoretical calculation of components of an equivalent circuit (Figure 15b) of the waveguide-coaxial oscillator in Figure 8a. The authors examine a thick (diameter greater than one fourth waveguide width) inductive post and take into account the influence of the close-by short-circuiting device; $C_ш$ and $L_ш$ are post parameters. The input impedance of the coaxial segment is substituted by element Z_k. C_g and C'_g -- reactive elements taking into account the post gap and the boundary capacitance of the waveguide-coaxial transition. The developed equivalent circuit was successfully utilized in calculating the frequency characteristics of a (50-70) GHz oscillator and amplifier.

Figure 15c contains an equivalent circuit of a waveguide avalanche diode oscillator with an external reflection type cavity [44]. Elements $C_ш$, $L_ш$, $C_в$ and $C_{вт}$ describe the post in the waveguide; they are obtained by calculation. The avalanche diode is represented by elements G_d, C_d, L_{kd}, R_d, and C_{kd}, the values of which are determined experimentally [76]. C_p, L_p, and G_p characterize a stabilizing cavity. The degree of coupling between cavity and waveguide 1:n and correction to waveguide cavity length Δl_1 were determined experimentally. Oscillator parameter calculation error doe.. not exceed (15-20)%.

An equivalent circuit of a Gunn diode oscillator with varactor tuning is contained in Figure 15d [95].

The equivalent circuits contained in Figure 15 make it possible to consider many features of oscillator operation -- frequency "saturation" [53, 96, 97] and abrupt changes in frequency and power [82, 96, 98, 99]. Analytical expressions for such circuits turn out very unwieldy and lose one of the main advantages -- the possibility of reaching conclusions on oscillator operating features without performing computations. Attempts to obtain clearer analytical expressions by idealizing circuits lead in many cases to loss of adequacy of the model and, as a consequence, to erroneous conclusions. Therefore extensive employment of computers is essential in calculating and optimizing oscillator characteristics [100], with utilization of analytical methods for determining the most general laws governing oscillator operation.

Conclusions

1. At the present time the following are achievable in practical terms: avalanche diode oscillators with a power output of (200-400)mw at a frequency of 30 GHz, (50-100) mw at frequencies to 100 GHz; Gunn diode oscillators with a power output of (50-100) mw at a frequency of 30 GHz, and (20-40) mw at frequencies to 60 GHz.

2. Waveguide oscillators are most preferable in the millimeter band. With integral technology and mass production, microstrip designs are promising in the lower-frequency portion of the band.

3. To obtain maximum output power and efficiency at a fixed frequency, oscillator designs involving open in-waveguide cavities appear to be the best.

4. Employment of external high-Q and high-standard resonator cavities makes it possible to improve the stability characteristics of oscillators by 1-2 orders of magnitude.

5. A broad oscillator mechanical tuning frequency range to (30-40)% is provided by a waveguide-post and waveguide with nonresonant ridge guide electrodynamic system design.

6. Avalanche diode oscillator frequency tuning can be performed by active element supply current in a range (20-40)% with a large power output loss and low oscillator noise characteristics.

7. With moderate demands on electronic tuning range (several percent), it is preferable to employ varactors. Wide-band (more than 10%) varactor frequency tuning for millimeter-band oscillators is achieved with an integral technology of oscillator manufacture with utilization of unpackaged diodes and quasi-concentrated resonant systems.

8. Power output of solid-state oscillators in pulse mode can be increased by approximately an order of magnitude in comparison with continuous oscillation modes.

9. Up to the present time designing of electrodynamic systems of solid-state millimeter-band devices has been in many respect empirical in nature; methods of theoretical calculation and optimization have not experienced proper development.

10. The most appropriate methods in analyzing oscillators are combined methods of modeling with utilization of equivalent circuits, some of the components of which are determined theoretically and some experimentally.

11. In oscillator calculation and optimization it is essential extensively to employ electronic computers with utilization of analytical methods for determining the most general patterns of oscillator operations.

BIBLIOGRAPHY

1. Vikulov, I. K. "Millimetrovyye volny za rubezhom. Obzory po elektronnoy tekhnike" [The Millimeter Band Abroad. Electronic Equipment Surveys], Series I, Millimeter Band Electronics, TsNII Elektronika, 1977, Issue 11, (481).

2. Andreyev, V. S. "Solid-State Millimeter-Band Oscillation Sources in Communications Systems," ELEKTROSVYAZ', No 11, 1974.

3. Dance, M. "Microwave Components and Instruments," ELECTRONICS INDUSTRY, No 11, 1976.

4. "Sovremennoye sostoyaniye proizvodstva generatorov i usiliteley na LPD" [Present State of Manufacture of Avalanche Diode Oscillators and Amplifiers] "Elektronnaya tekhnika" [Electronic Equipment], Series I, Elektronika, 1977, Issue 9.

5. Li; Ying; and Dzhamba. "K_a-Band Double-Transit Diodes Produced by Ion Implantation," TIIER, 62, No 7, 1974.

6. Hirachi, Y.; Toyama, Y.; Fukukawa, Y.; and Tokumitsu, Y. "A High Power 50 GHz DDR IMPATT Oscillator With Low Sideband Noise," IEEE S-MTT Int. Microwave Symp. "The Bicent. Symp.", Cherry Hill, New Jersey, 1976.

7. Hirachi, Y.; Nakagami, T.; Toyama, Y.; and Fukukawa, Y. "High Power 50 GHz Double-Drift-Region IMPATT Oscillators With Improved Bias Circuits for Eliminating Low-Frequency Instabilities," IEEE TRANS., MTT-24, No 11, 1976.

8. Weller, K. P.; Dreeben, A. B.; Davis, H. L.; and Anderson, W. M. "Fabrication and Performance of GaAs pin Junction and Schottky Barrier Millimeter IMPATTs," IEEE TRANS., ED-21, No 1, 1974.

9. Gokgor, H. S.; Howard, A. M.; and Purcell, J. J. "Millimetre-Wave Silicon IMPATT and PIN Diodes," International Conference on Millimetric Waveguide Systems, London, 1976.

10. Hulsh, P. W.; Groves, I. S.; and Lewis, D. E. "Millimetre-Wave Oscillators for Waveguide Communication Systems," International Conference on Millimetric Waveguide Systems, London, 1976.

11. Zeydel; Devis; and Iglesias. "Double-Transit Millimeter-Band IMPATT Diodes Manufactured by the Ion Implantation Method," TIIER, 59, No 8, 1971.

12. English, D. L.; Nakaji, E. M.; and Ying, R. S. "Improved Performance of Millimeter-Wave IMPATT Diodes on Type-IIa Diamond Heat Sinks," ELECT. LETT., 12, No 25, 1976.

13. Li and Yin. "Complementary D-Band IMPATT Diodes Manufactured by the Ion Implantation Method," TIIER, 62, No 9, 1974.

14. Ino, M.; Makimura, T.; and Jamasaki, H. ELECT. COMMUN. LAB. TECH. J., 25, No 9, 1976.

15. Ino, M.; Makimura, T.; and Yamasaki, H. "80 GHz Band Si DDR Diodes," REV. ELECT. COMMUN. LAB., 25, No 7-8, 1977.

16. Okamoto and Ikeda. "Comparative Investigation of the Noise Properties of Silicon IMPATT Diodes With an Operating Frequency of 80 GHz," TIIER, 64, No 3, 1976.

17. Ishibashi, T., and Ohmori, M. "200 GHz 50 mw CW Oscillation With Silicon SDR IMPATT Diodes," IEEE TRANS., MTT-24, No 11, 1976.

18. Ino, M.; Ishibashi, T.; and Ohmori, M. "Submillimeter Wave Si p^+-p-n^+ IMPATT Diodes," JAP. J. APPL. PHYS., 16, 89, 1977.

19. Prokhorov, E. D.; Arendar', V. N.; Beletskiy, N. I.; and Dyadchenko, A. "Influence of Temperature on the Generating Efficiency of Gunn Diodes in a Frequency Band," RADIOTEKHNIKA I ELEKTRONIKA, 21, No 11, 1976.

20. Ruttan, T. G. "High-Frequency Gunn Oscillators," IEEE TRANS., MTT-22, No 2, 1974.

21. Stertser. "Electron Transfer Effect Oscillators and Amplifiers," TIIER, 59, No 8, 1971.

22. "Sovremennoye sostoyaniye tverdotel'noy tekhniki mm-diapazona voln" [Current Status of Solid-State Millimeter-Band Equipment], "Elektronnaya tekhnika" [Electronic Equipment], Millimeter Band Electronics Series, 1975, Issue 6.

23. Kramer, N. B. "Millimeter-Wave Semiconductor Devices," IEEE TRANS., MTT-24 No 11, 1976.

24. Misawa, T., and Kenyon, N. D. "An Oscillator Circuit With Car Structures for Millimeter-Wave IMPATT Diodes," IEEE TRANS., MTT-18, No 11, 1970.

25. Barrera, J. S. "GaAs LSA V-Band Oscillators," IEEE TRANS., ED-18, No 10, 1971.

26. Mizuishi, K.; Miyazaki, M.; Sato, H.; and Migitaka, M. "Plate Type Oscillator Using Micropill Type GaAs AMPATT Diodes for 30 GHz Band," TRANS. INST. ELECTRON. COMMUN. ENG. JAP., B-58, No 10, 1975.

27. Weller, K. P.; Ying, R. S.; and Lee, D. H. "Millimeter IMPATT Sources for the 130-170 GHz Range," IEEE TRANS., MTT-24, No 11, 1976.

28. Swartz, G. A.; Chiang, Y.; Wen, C. P.; and Gonzales, A. "Performance of p-Type Epitaxial Silicon Millimeter-Wave IMPATT Diodes," IEEE TRANS., ED-21, No 2, 1974.

29. Bouvet, J. V.; Duchemin, J. P.; Funk, R.; Obregon, J.; and Gibeau, P. "Double Drift Silicon Avalanche Diodes for Millimetric Applications (26-42 GHz)," International Conference on Millimetric Waveguide Systems, London, 1976.

30. Nawata, K; Ikeda, M; and Ishii, Y. "Millimeter-Wave GaAs Schottky Barrier IMPATT Diodes," IEEE TRANS., ED-21, No 1, 1974.

31. Khirati; Nisi; Sinoda; and Fukukava. "Millimeter-Band IMPATT Diodes With Increased Efficiency, Utilizing Ohmic Contact Produced by Ion Implantation," TIIER, 63, No 9, 1975.

32. Misava and Marinachcho. "Continuous-Action Silicon Avalanche Diodes for 100 GHz," ZARUBEZHNAYA RADIOELEKTRONIKA, No 7, 1972.

33. Gibbons, G.; Purcell, J. J.; Wickens, P. R.; and Gokgor, H. S. "50 GHz Gallium-Arsenide IMPATT Oscillator," ELECT. LETT., 8, No 21, 1972.

34. O'Hara, S.; Speight, J. D.; Leigh, P.; McIntyre, N.; Cooper, K.; and O'Sullivan, P. "Solid State Techniques for Millimetric Waveguide Systems," International Conference on Millimetric Waveguide Systems, London, 1976.

35. Groves, I. S.; Speight, J. D.; Leigh, P; McIntyre, N.; O'Hara, S.; and Hemment, P. "Proton Isolated GaAs IMPATT Diodes," Fourth European Microwave Conference, Microwave-74, Montreux, Switzerland, 1974.

36. Li, D. Kh.; Yeller, K. P.; and Troyer, U. F.. "Millimeter-Wave Passivated Silicon IMPATT Diodes Produced With the Aid of Ion Implanatation," TIIER, 65, No 2, 1977.

37. Sven; Misava; and Briker. "Generation of Millimeter-Band Continuous Oscillations by Silicon Avalanche Diodes," TIIER, 55, No 10, 1967.

38. Davis, R. T. "Microstrip mm Wave Source Achieves Quarter Watt Output at 30 and 60 GHz," MICROWAVES, 13, No 8, 1974.

39. Glance, B. S., and Schneider, M. V. "Millimeter-Wave Microstrip Oscillators," IEE S-MTT Int. Microwave Symp., Atlanta, Georgia, 1974.

40. Glance, B. S., and Schneider, M. V. "Millimeter-Wave Microstrip Oscillators," IEEE TRANS., MTT-22, No 12, 1974.

41. Glans. "30-GHz IMPATT-Oscillator on a Low-Q Asymmetric Microstrip Line," TIIER, 60, No 9, 1972.

42. Taranenko, V. P.; Kotserzhinskiy, B. A.; Machusskiy, Ye. A.; and Tkachenko, L. A. "Temperature Stabilization of Solid-State Millimeter-Band Oscillators by External Resonator Cavities," IZV. VUZOV -- RADIOELEKTRONIKA, 18, No 10, 1975, page 4.

43. Vyrovoy, S. I.; Gumennyy, S. N.; and Tsvirko, Yu. A. "Comparison of Single-Circuit Oscillator Stabilization Employing Active Two-Terminal Networks," ELEKTRONNAYA TEKHNIKA, Series I. ELEKTRONIKA SVCH, No 3, 1976.

44. Kotserzhinskiy, B. A.; Machusskiy, Ye. A.; and Tkachenko, L. A. "Analysis of a Waveguide Avalanche Diode Oscillator With an External Reflecting Type Cavity," IZV. VUZOV -- RADIOELEKTRONIKA, No 7, 20, 1977, page 11.

45. Haga, I.; Tamura, R.; Sakamoto, K.; Aihara, S.; and Igata, M. "A Reflection Type Cavity Controlled Oscillator and a Cavity Controlled Frequency Modulator," NEC RESEARCH AND DEVELOPMENT, No 36, 1975.

46. Nagano, S., and Ohnaka, S. "A Highly Stabilized Ka-Band Gunn Oscillator," IEEE TRANS., MTT-20, No 2, 1972.

47. Nagano, S., and Ohnaka, S. "Highly-Stabilized IMPATT Oscillators at Millimeter Wavelengths," IEEE TRANS., MTT-21, No 7, 1973.

48. Nagano, S., and Ohnaka, S. "A Low-Noise 80-GHz Silicon IMPATT Oscillator Highly Stabilized With a Transmission Cavity," IEEE TRANS., MTT-22, No 12, 1974.

49. Nagano, S.; Ohnaka, S.; Sekido, K.; and Ayaki, K. "A Low-Noise 80-GHz Silicon IMPATT Oscillator Highly Stabilized With a Transmission Cavity," IEEE S-MTT Int. Microwave Symp., Atlanta, Georgia, 1974.

50. Gumennyy, S. N.; Kislyakovskiy, V. A.; Tsirko, Yu. A.; and Yasinskiy, V. K. "Waveband Characteristics of a Gunn Oscillator With Elevated Temperature Stability," IZV. VUZOV -- RADIOELEKTRONIKA, no 10, 19, 1976.

51. Fong, T. T.; Weller, K. P.; and English, D. L. "Circuit Characterization of V-Band IMPATT Oscillators and Amplifiers," IEEE TRANS., MTT-24, No 11, 1976.

52. Taylor, B. C., and Howes, M. J. "LSA Operation of GaAs Layers in Large Scale Tunable Microwave Circuits," IEEE TRANS., ED-16, N 11, 1969.

53. Taylor, B. C.; Fray, S. J.; and Gibbs, S. Ye. "Frequency Saturation Effects in Transferred Electron Oscillators," IEEE TRANS., MTT-18, 1970.

54. Weller, K. P.; English, D. L.; and Kuno, H. J. "Tunable Millimeter-Wave Packaged IMPATT Diode Oscillators," IEEE S-MTT Int. Microwave Symp., Atlanta, Georgia, 1974.

55. Akaike, M.; Kato, H.; and Yuki, S. "Oscillation Characteristics of Millimeter-Wave IMPATT Diodes Mounted in Low-Impedance Waveguide Mounts," IEEE TRANS., MTT-24, No 3, 1976.

56. Lee, T. P., and Standley, R. D. "Frequency Modulation of a Millimeter Wave IMPATT Diode Oscillator and Related Harmonic Generation Effect," BSTJ, No 1, 48, 1969.

57. Zublin, K. Ye.; Wilser, W. T.; and Green, W. R. "Ka-Band YIG-Tuned GaAs Oscillator," MICROWAVE J., No 9, 1975.

58. Taranenko, V. P.; Kotserzhinskiy, B. A.; "Electronic Solid-State Millimeter-Wave Oscillator Varactor Tuning," IZV. VUZOV -- RADIOELEKTRONIKA, No 10, 19, 1976.

59. Downing, B. J., and Myers, F. A. "Q-Band (38 GHz) Varactor-Tuned Gunn Oscillators," ELECT. LETT., No 11, 9, 1973.

60. Bullimore, E. D.; Downing, B. J.; and Myers, F. A. "Electronic Tuning and Stabilization of Gunn Effect Oscillators," European Microwave Conference, Brussels, 1973.

61. Lee, T. P.; Standley, R. D.; and Misawa, T. "A 50 GHz Silicon IMPATT Diode Oscillator Amplifier," IEEE TRANS., No 10, ED-15, 1968.

62. Rubin, D. "Varactor-Tuned Millimeter-Wave MIC Oscillator," IEEE TRANS., No 11, MTT-24, 1976.

63. Glance, B. S. "Microstrip Varactor-Tuned Millimeter-Wave Transmitter," IEEE Trans., MTT-24, No 3, 1976.

64. Denlinger, E. J.; Rosen, J.; Mykietyn, E.; and McDermott. "Microstrip Varactor-Tuned Millimeter-Wave IMPATT Diode Oscillator," IEEE TRANS., MTT-23, No 12, 1975.

65. Bowman, L. S., and Burris, C. A. "Pulse-Driven Silicon p-n-junction Avalanche Oscillators for the 0.9 to 20 mm Band," IEEE TRANS., ED-14, No 8, 1967.

66. Ying, S. R.; English, D. L.; Weller, K. P.; Nakaji, E. M.; and Bernick, R. L. "Millimeter Wave Pulsed IMPATT-Diode Oscillators," IEEE J. SOL.-ST. CIRC., No 2, 11, 1976.

67. Lazarus M.; Novak, S.; and Chzhun', K. "Controlling A Millimeter-Band Oscillator by External Synchronization With the Aid of Automatic Frequency Control," TIIER, No 8, 64, 1976.

68. Zubovich, N. A. "Synchronization of a Gunn Oscillator on the Oscillation Frequency Subharmonic," ELEKTRONNAYA TEKHNIKA, Series I, ELEKTRONIKA SVCH, 1977, Issue 1.

69. Rolland, P.; Vaterkowski, J. L.; Constant, E.; and Salmer, G. "New Modes of Operation for Avalanche Diodes: Frequency Multiplication and Upconversion," IEEE TRANS., MTT-24, No 11, 1976.

70. Keen, N. J. "Avalanche Diode Noise Sources at Short Centimeter and Millimeter Wavelengths," IEEE TRANS., MTT-24, No 3, 1976.

71. Kolosov, M. V., and Peregonov, S. A. "SVCH generatory i usiliteli na poluprovodnikovykh priborakh" [Solid-State Millimeter-Band Oscillators and Amplifiers], Moscow, Sovetskoye radio, 1974.

72. Weller, K. P. "A Study of Millimeter-Wave GaAs IMPATT Oscillator and Amplifier Noise," IEEE TRANS., ED-20, No 6, 1973.

73. Bugayev, A. V., and Rybalka, V. V. "Experimental Investigation of Millimeter-Band Avalanche Diode Oscillator Noise," "Elektronnaya tekhnika," Series I. "Elektronika SVCH," Issue 11, 1973.

74. Kuno, H. J., and Pusateri, P. H. "Use of Solid-State Components for Millimeter-Wave Measurements," MICROWAVE JOURNAL, No 8, 17, 1974.

75. Kuno, H. J.; Fong, T. T.; and English, D. L. "Characterization of IMPATT Diodes at Millimeter-Wave Frequencies," IEEE TRANS., ED-19, No 6, 1972.

76. Kotserzhinskiy, B. A.; Machusskiy, Ye. A.; and Tkachenko, L. A. "Measuring Avalanche Diode Impedance in the Millimeter Waveband," IZV. VUZOV -- RADIOELEKTRONIKA, No 10, 19, 1976, page 33.

77. Bayuk, F. J., and Raue, J. E. "Improved Characterization and Precision De-Embedding of Packaged Ka-Band IMPATT Diodes," 26th Electron. Components Conf., San Francisco, California, 1976.

78. Gecsinger, W. J. "The Packaged and Mounted Diode as a Microwave Circuit," IEEE TRANS., MTT-14, No 2, 1966.

79. Downing, B. J., and Robson, P. N. "Microwave-Package Measurement at the Q-Band," ELECT. LETT., No 11, 9, 1973.

80. Eisenhart, R. L., and Khan, P. J. "Theoretical and Experimental Analysis of a Waveguide Mounting Structure," IEEE TRANS, MTT-19, No 8, 1971.

81. Bradshaw, J. A. "Scattering from a Round Metal Post and Gap," IEEE TRANS., MTT-21, No 5, 1973.

82. Joshi, J. S., and Cornick, J. A. F. "Analysis of Waveguide Mounting Configuration for Electronically Tuned Transferred Electron Device Oscillators and Its Circuit Applications," IEEE TRANS., MTT-24, No 9, 1976.

83. Eisenhart, R. L. "Discussion of a 2-Gap Waveguide Mount," IEEE TRANS., MTT-24, No 12, 1976.

84. White, J. F. "Simplified Theory for Post Coupling Gunn Diodes to Waveguide," IEEE TRANS., MTT-20, No 6, 1972.

85. Joshi, J. S., and Cornick, J. A.F "Analysis of Waveguide Post Configurations: Part I -- Gap Immitance Matrices," IEEE TRANS., MTT-25, No 3, 1977.

86. Joshi, J. S., and Cornick, J. A. F. "Analysis of Waveguide Post Configurations: Part II -- Dual Gap Cases," IEEE TRANS., MTT-25, No 3, 1977.

87. El Sayyd, O. L. "Impedance Characterization of a Two-Post Mounting Structure for Varactor-Tuned Gunn Oscillators," IEEE TRANS., MTT-22, No 8, 1974.

88. El-Saued, O. L. "Generalized Analysis of Parallel Two-Post Mounting Structures in Waveguide," IEEE TRANS., MTT-25, No 1, 1977.

89. Yamashita, and Bayard. "Theory of Tunnel-Diode Oscillator in Millimeter-Band Element," TIIER, No 4, 54, 1966.

90. Hanson, D. C., and Rowe, J. E. "Microwave Circuit Characteristics of Bulk GaAs Oscillators," IEEE TRANS, ED-14, No 9, 1967.

91. Murav'yev, V. V., and Savel'yev, V. Ya. "Some Questions of Theory and Calculation of Gunn Diode Oscillators," "Elektronnaya tekhnika," Series I, "Elektronika SVCH," Issue 12, 1972.

92. Bugayev, V. Ya., and Rapoport, G. N. "Equivalent Circuit of a Waveguide-Coaxial T-Coupling," IZV. VUZOV -- RADIOELEKTRONIKA, No 2, 20, 1977, page 95.

93. Kasatkin, L. V., and Loshitskiy, P. P. "Equivalent Circuit of a High-Frequency Avalanche Diode Oscillator Circuit With in-Waveguide Open Cavity," "Elektronnaya tekhnika," Series I, "Elektronika SVCH," Issue 6, 1974.

94. Kasatkin, L. V., and Loshitskiy, P. P. "Equivalent Circuit of a High-Frequency Solid-State 'Resonance Window with Post' Oscillator," "Elektronnaya tekhnika," Series I, "Elektronika SVCH," Issue 7, 1973.

95. Templin, A. S., and Gunshor, R. L. "Analytic Model for Varactor Tuning Waveguide Gunn Oscillators," IEEE TRANS., MTT-22, No 5, 1974.

96. Eisenhart, R. L., and Khan, P. J. "Some Tuning Characteristics and Oscillation Conditions of a Waveguide-Mounted Transferred Electron Diode Oscillator," IEEE TRANS., ED-19, No 9, 1972.

97. Tsai, W. C.; Rosenbaum, F. J.; amd Mackenzie, L. A. "Circuit Analysis of Waveguide-Cavity Gunn Effect Oscillator," IEEE TRANS., MTT-18, No 11, 1970.

98. Karasek, M. "Nonlinear Behavior of the BARITT Diode Oscillator," PROC. IEEE, No 10, 65, 1977.

99. Stroganova, Ye. P., and Tsarapkin, D. P. "Influence of Parameters of Waveguide Design of a Gunn Oscillator on Tuning Range," RADIOTEKHNIKA I ELEKTRONIKA, No 4, 23, 1978.

100. Eaton, R. M., and Joshi, J. S. "Design VCOs Accurately With Computer Analysis," MICROWAVES, No 6, 1977.

101. Ohmori, M.; Ishibashi, T.; and Ono, S. "Dependency of Highest Harmonic Oscillation Frequency on Junction Diameter of IMPATT DIODES," IEEE TRANS., ED-24, No 12, 1977.

102. Chao, S.; Bernick, R. L.; Ying, R. S.; Weller, K. P.; Lee, D. H.; and Nakaji, E. M. "Pulsed IMPATT Diode Oscillators Above 200 GHz," IEEE Int. Solid-State Circ. Conf., Philadelphia, Pennsylvania, 1977.

103. Chao, C.; Bernick, R. L.; Nakaji, E. M.; Ying, R. S.; Weller, K. P.; and Lee, D. H. "Y-Band (170-260 GHz) Tunable CW IMPATT Diode Oscillators," IEEE TRANS., MTT-25, No 12, 1977.

Submitted 10 April 1978

3024
CSO: 8144/1368

OSCILLATORS AND MODULATORS

UDC 621.373

THE FILTERING CAPABILITY OF DIGITAL FREQUENCY SYNTHESIZERS

Kiev IZVESTIYA VUZ RADIOELEKTRONIKA in Russian Vol 21 No 11, 1978 pp 41-49

[Article by O. Gubernatorov, manuscript received 19 Apr 77, following revision 10 May 78]

[Text] Equations are derived for the transfer functions of a digital frequency synthesizer when interference acts at the input to the low pass filter and directly on the controlled oscillator of the synthesizer. Expressions are determined and analyzed for the parasitic frequency deviation of the controlled oscillator as a function of the frequency of the interference. Equations are derived for the calculation of the noise bandwidth of a digital synthesizer with the action of fluctuating interference.

The signal spectrum at the output of digital frequency synthesizers (TsSCh) has a complex structure. At frequencies 10 - 200 Hz offset from the carrier, it can have raised places, so-called "wings", the level of which is 30 - 50 dB below the primary signal level [1].

The finite spectral width of the synthesizer signal is due to the action of natural (internal noise) and harmonic interference. The latter arises by virtue of the conversion of the master oscillator (OG) and controlled oscillator signals into pulse processes, the imperfections in the filtering circuits, vibrational perturbations and a number of other factors.

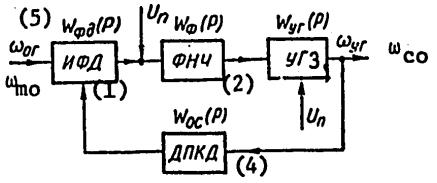

Figure 1.

Key: 1. Integrating phase detector;
2. Low pass filter;
3. Controlled oscillator;
4. DPKD [variable scaler type feedback loop frequency divider];
5. $W_{фд}(p)$ [phase detector transmission factor];

$W_{уп}(p)$ = controlled oscillator transfer function.

This paper is devoted to a determination of the level of the parasitic frequency deviation of a digital frequency synthesizer signal with the action of fluctuating and harmonic noise at the input to the low frequency filter (FNCh) as well as directly on the controlled oscillator.

An overall block diagram of a digital frequency synthesizer is shown in Figure 1. We shall determine and investigate its transfer function. For the case of an open feedback (OS) loop and the action of interference at the low pass filter input, the frequency deviation of the controlled oscillator is written as follows in operator form:

$$\Delta\omega_{\text{п}}(p) = S_{\text{уг}} U_{\text{п}}(p)\, W_{\phi}(p) = \Delta\omega'_{\text{п}}(p)\, W_{\phi}(p), \tag{1}$$

where $S_{\text{уг}}$ is the slope of the control characteristic of the controlled oscillator (rad/SV); $W_{\phi}(p)$ is the transmission factor of the low pass filter; $U_{\text{п}}(p)$ is the interference voltage tranform; $\Delta\omega'_{\text{п}}$ is the frequency deviation of the controlled oscillator when the interference acts directly on the controlled oscillator.

When a feedback loop is inserted, the overall frequency deviation of the controlled oscillator is

$$\Delta\omega_{\text{пол}}(p) = \Delta\omega_{\text{п}}(p) + \Delta\omega_{\text{ос}}(p). \tag{2}$$

Here, $\Delta\omega_{\text{ОС}}(p)$ is the frequency deviation of the controlled oscillator due to the action of the feedback loop. The frequency deviation caused by the feedback is:

$$\Delta\omega_{\text{ос}}(p) = \Delta\omega_{\text{пол}}(p)\, W_{\text{ос}}(p)\, W_{\text{пк}}(p), \tag{3}$$

where $W_{\text{ОС}}(p)$ is the transfer function of the feedback loop; $W_{\text{пк}}(p) = W_{\phi}(p) = W_{\phi}(p)N_{\phi\text{д}}(p)W_{\text{уг}}(p)$ is the transmission factor of the forward channel.

Substituting (1) and (3) in (2) and solving the obtained result for $\Delta\omega_{\text{пол}}(p)$, we obtain:

$$\Delta\omega_{\text{пол}}(p) = \frac{S_{\text{уг}} U_{\text{п}}(p)\, W_{\phi}(p)}{1 + W_{\text{ос}}(p) W_{\text{пк}}(p)}. \tag{4}$$

Expression (4) is the equation for the transfer function of the digital frequency synthesizer.

According to [2]:

$$W_{\text{ос}}(p)\, W_{\text{пк}}(p) = K_{\text{сз}} \frac{W_{\phi}(p)}{p}, \tag{5}$$

where $K_{сэ} = K_c/K$ is the static gain of the system; $K_c = K_ф \cdot S_{уг} S_{фд}$ is the static gain of the forward channel (the holding bandwidth); K is the division factor of the dividers in the feedback loop; $S_{фд}$ is the slope of the phase detector characteristic, ФД; $K_ф$ is the transition factor of the low pass filter at $\omega = 0$.

In the case of an integrating filter, ИФ, with a transmission factor of:

$$W_ф(p) = \frac{1}{1 + pt_1} \tag{6}$$

and the action of harmonic interference:

$$U_n(p) = \frac{U_{mn}\omega}{p^2 + \omega^2}, \tag{7}$$

expression (4) assumes the form:

$$\Delta\omega_{пол}(p) = \Delta\omega_{mn} \frac{p\omega}{(p^2 + \omega^2)(p^2 t_1 + p + K_{сэ})}. \tag{8}$$

In equations (6), (7) and (8), $t_1 = RC$ is the time constant of the low pass filter; $\Delta\omega_{mn} = S_{уг} U_{mn}$ is the maximum frequency deviation of the controlled oscillator; U_{mn} is the amplitude of the interference voltage.

By integrating (8) and isolating the forced component of the transient process, we obtain equations which describe the frequency and phase characteristics digital frequency synthesizers in the steadystate mode:

$$y(\omega) = \frac{\Delta\omega_{пол}(\omega)}{\Delta\omega_{mn}} = \frac{\omega}{\sqrt{(K_{сэ} - \omega^2 t_1)^2 + \omega^2}}; \tag{9}$$

$$\operatorname{tg}\varphi = \frac{\omega}{K_{сэ} - \omega^2 t_1}. \tag{10}$$

An extremum of function (9) occurs at a frequency of:

$$\omega_0^2 = \frac{K_{сэ}}{t_1} = \frac{K_{сэ}^2}{\tau_1}, \tag{11}$$

where ω_0 is the resonant frequency of the system; $\tau_1 = t_1 K_{сэ}$ is the normalized time constant of the digital frequency synthesizer.

By introducing the relative frequency coordinate:

$$\gamma = \frac{\omega}{\omega_0}, \tag{12}$$

into (9), we reduce the latter to the form:

$$y(\gamma) = \sqrt{\frac{\gamma^2}{\tau_1 (1 - \gamma^2)^2 + \gamma^2}}. \tag{13}$$

The calculation of the selectivity characteristic (13) and the noise bandwidth is simplified substantially if we go over from expression (13) to an equation equivalent to it, assuming that:

$$x^2 = \frac{(1-\gamma^2)^2}{\gamma^2} \tag{14}$$

is the square of the generalized frequency difference, we write (13) thus:

$$y(x) = \frac{1}{\sqrt{1+\tau_1 x^2}}. \tag{15}$$

Equation (15) is the equivalent of expression (13). If (13) is an asymmetrical function with respect to $\gamma = 1$ and is defined only in the range of positive frequencies, then y(x) is symmetrical with respect to $x = 0$, and is defined for both positive and negative frequencies. It follows from (14) that with a change in γ within a range of $0 \div +\infty$, x takes on a value in the range $-\infty \div +\infty$, where $\gamma = 1$ and $x = 0$.

At a specified attenuation, σ, the abscissas of the function y(x) are equal to:

$$x_{\sigma 1,2} = \pm \sqrt{\frac{\sigma^2-1}{\tau_1}}. \tag{16}$$

Solving (14) and (16) simultaneously, we find that for the same σ, the coordinates of function (13) are determined by the equations:

$$\gamma_{\sigma 1,2} = \sqrt{\frac{\sigma^2-1}{4\tau_1}}\left(\sqrt{1+\frac{4\tau_1}{\sigma^2-1}} \pm 1\right), \tag{17}$$

by means of which the relative passband of the system is found:

$$\Delta\gamma_\sigma = \gamma_{\sigma_1} - \gamma_{\sigma_2} = \sqrt{\frac{\sigma^2-1}{\tau_1}}. \tag{18}$$

and with the substitution of (12), the absolute value of the passband at the level of the σ readout is:

$$\Delta\omega\sigma = \omega_0 \sqrt{\frac{\sigma^2-1}{\tau_1}}. \tag{19}$$

For $\sigma = \sqrt{2}$, we obtain the following from (19) taking (11) into account:

$$\Delta\omega_{0,7} = \frac{\omega_0}{\sqrt{\tau_1}} = \frac{K_{cs}}{\tau_1} = \frac{1}{l_1}. \tag{20}$$

We determine the noise bandwidth by means of integrating the absolute value of the square of the equivalent characteristic y(x) with the subsequent transition from the x coordinate to the γ coordinate.

The noise bandwidth of a system with the equivalent characteristic is

$$\Pi_{ш э} = \int_{-\infty}^{\infty} |u(x)|^2 dx = \frac{1}{\tau_1} \int_{-\infty}^{\infty} \frac{dx}{\left(\frac{1}{\sqrt{\tau_1}}\right)^2 + x^2} = \frac{\pi}{\sqrt{\tau_1}}. \quad (21)$$

The values of the abscissas which define the equivalent noise bandwidth, because of the symmetrical nature of the characteristic $|y(x)|^2$ are:

$$x_{ш1,2} = \pm \frac{\pi}{2 \cdot \sqrt{\tau_1}}. \quad (22)$$

Solving (14) and (22) simultaneously, we find

$$\gamma_{ш1,2} = \frac{\pi}{4\sqrt{\tau_1}} \left(\sqrt{1 + \frac{16\tau_1}{\pi^2}} \mp 1 \right). \quad (23)$$

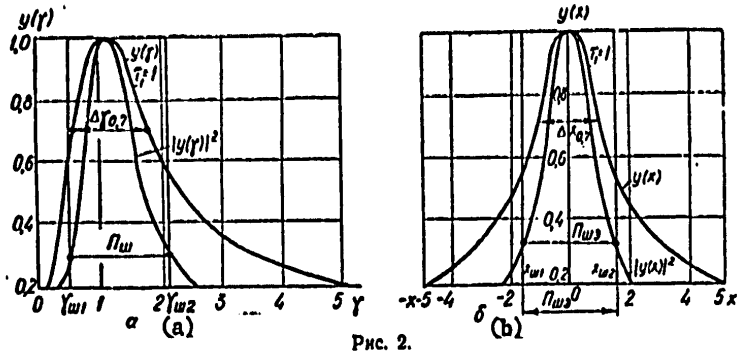

Рис. 2.

Figure 2.

The absolute value of the noise bandwidth of a digital frequency synthesizer, taking (20) into account, is equal to

$$\Pi_{ш} = \frac{f_0}{\sqrt{\tau_1}} \frac{\pi}{2} = \Delta f_{0,7} \frac{\pi}{2}.$$

Calculated data for the selectivity characteristic of a digital frequency synthesizer, y(γ) and the y(x) characteristic equivalent to it at $\tau_1 = 1$ are given in Table 1. The calculation was performed using expressions (16), (17) and (18). Also given here are the data for the noise indicators derived from equations (22), (23) and (18). Based on the calculated data, depicted in Figures 2a and 2b is the selectivity characteristic and the function y(x) equivalent to it.

TABLE 1

$\tau_1 = 1$

1/σ	σ²	x_1	x_2	γ_1	γ_2	$\gamma_2-\gamma_1$	$\sqrt{\frac{\sigma^2-1}{\tau_1}}$	Шумовые показатели (1)
0,9	1,25	+0,5	−0,5	0,82	1,31	0,49	0,5	$x_{m1,2} = \pm 1,57$
0,8	1,55	+0,77	−0,77	0,7	1,45	0,75	0,74	$\gamma_{m1} = 0,49$
0,7	2	+1	−1	0,62	0,62	1	1	
0,58	3	+1,41	−1,41	0,51	1,43	1,42	1,41	$\gamma_{m2} = 2,06$
0,5	4	+1,73	−1,73	0,46	2,2	1,74	1,73	$\Delta\gamma_m = 1,57$
0,25	16	+3,9	−3,9	0,25	4,15	3,9	3,87	$\frac{\Delta\gamma_m}{\Delta\gamma_{m.}} = 1,57$
0,168	36	+5,8	−5,8	0,177	6,1	5,8	5,9	

Key: 1. Noise indicators.

The selectivity properties of a digital frequency synthesizer depend on both the position of the resonant frequency ω_0 and on the transmittance bandwidth $\Delta\omega_{0,7}$. The position of ω_0 and the bandwidth $\Delta\omega_{0,7}$ are determined by the quantity τ_1, changing that so with an increase in τ_1, ω_0 shifts towards the lower frequencies, while $\Delta\omega_{0,7}$ is narrowed. In this case, the rate of change in the side slopes of the selectivity characteristic $y(\gamma)$ also increases at the same time.

This shape of the $y(\gamma)$ and $y(x)$ curves is explained, on one hand, by the influence of the low pass filter, and on the other, by the action of the control system which in the low frequency range compensates for the parasitic deviation. If the quantity $K_{C\Im}$ is clamped, and t_1 is increased, then not only is the action of the interference on the controlled oscillator attenuated, but the controlling effect fed to the phase detector from the feedback loop is also reduced. An analogous situation will arise if when τ_1 is clamped, the frequency of the interference voltage at the input to the low pass filter is increased. Control effectiveness is reduced if at a constant value of K_c and t_1, the division factor of the dividers inserted in the feedback network, is increased. This can be explained by working from the following arguments:

—In the first place, increasing K is equivalent to reducing the static gain of the entire system, $K_{C\Im}$;

—In the second place, in treating adigital frequency synthesizer as a feedback system in which a parasitic deviation arises in the controlled oscillator, we can write:

$$\Delta\omega_{psv} = \Delta\omega_p/(1 + \beta K_c),$$

where $\Delta\omega_{pgv}$ is the frequency deviation of the controlled oscillator due to the interference, where feedback is present; $\Delta\omega_p$ is the same deviation in the absence of feedback; β is the feedback gain.

But $\beta = 1/K$, and falls off with an increase in K, tending to zero when $K \to \infty$.

The passage of modulated pulse processes through digital frequency dividers was treated in [3]. An informational factor for the modulated pulse process $K_u = K/\mu$ was introduced in this paper to estimate the filtering of the modulating function, where K is the division factor of the divider; μ is the pulse repetition factor, and it was demonstrated that when $K_u \geq 1$, when one or fewer pulses arrives over a modulation frequency period, there is suppression of the modulating function, and when $K_u \leq 0.5$, the modulating function is transmitted practically without distortion. These conclusions are completely in agreement with Kotel'nikov's theorem.

The quantity τ_1 influences not only the selective properties, but also the dynamics of the transient processes in a digital frequency synthesizer. In this case, increasing τ_1 leads to a prolongation of the settling time for the oscillations and appearance of periodic frequency overshoots in the period of retuning from one frequency to another. For this reason, it is hardly possible to give any general recommendations for the selection of digital frequency synthesizer parameters.

However, based on many years of practice in digital frequency synthesizer design, we shall advance a few considerations which are in agreement with the theoretical analysis developed here.

The basis of harmonic noise in a digital frequency synthesizer is to be considered the comparison frequency voltage ω_{cp} and its harmonic, which are fed to the input of the low pass filter from the phase detector. A high degree of filtration of such interference can be assured by means of shifting the frequency ω_0 to the left, in the direction of the lower frequencies, and increasing the slope of the sides of the $y(\gamma)$ characteristic, i.e.:

$$\left.\begin{array}{l}\omega_{cp} \gg \omega_0 \\ \sigma_{cp} \gg 1\end{array}\right\}. \qquad (24)$$

When ω_{cp} = const, conditions (24) are met by increasing τ_1. But increasing τ_1 washes out the spectrum close to the carrier by virtue of the action of fluctuating interference, the reduction of the dynamic qualities and the lowering of the short term frequency stability of the output signal of the digital frequency synthesizer.

One frequently runs up against this contradiction in selecting synthesizer parameters. Sometimes, the contradiction is successfully resolved by means of using comb rejection filters, nonlinear integrating filters and DPKD's [variable scalers] with a fractional division factor in digital frequency synthesizers. These units are frequently used together.

The digital frequency synthesizer - the exciter and local oscillator of the "Reyd" radio set, which was demonstrated at the "Svyaz'" ["Communications"] Exhibition in 1975, can serve as an example here. A high level of filtration of ω_{cp} is assured in it by means of a nonlinear integrating filter and a DKPD with a fractional division coefficient, while good dynamic properties are assured by means of introducing a supplemental AFC loop. Tests have shown that in such a digital frequency synthesizer, the suppression of ω_{cp} is more than 100 dB. The "wings" are located at a frequency of 30-50 Hz and are suppressed by 40-50 dB relative to the carrier level (200 mv).

In contrast to the FAPCh [phase locked loop, PLL] systems of radio receiving devices, in which the carrier of the received signal is used as the reference signal, and the primary noise source is internal noise and antenna noise, which act directly on the PLL input, the role f a reference signal in a digital frequency synthesizer is played by the signal voltage of the internal high stability crystal oscillator.

The master oscillator signal, present at the input of the phase detector, has a high level (on the order of volts) and is characterized by a narrow amplitude and phase spectrum (units or tens of Hertz at a level of 80-90 dB).

Under these conditions, the major source of fluctuating perturbations is to be considered the low frequency natural and keying noise of the assemblies which are included both in the complement of the forward channel and in the feedback loop. The following are to be included among them: the phase detector, direct current amplifers, drivers, frequency dividers, the controlled oscillator, etc.

High spectral purity close to the carrier is achieved by means of optimum utilization of the control system, i.e., by shifting ω_0 to the right (in the direction of the higher frequency) by means of lowering τ_1. It is expedient to shift ω_0 by increasing K_c.

The transfer function of a digital frequency synthesizer, when interference acts on the controlled oscillator, follows directly from relationships (1), (4) and (5). If $W_\phi(p) = 1$ and (5) is used in (1) and (4), then we obtain

$$W_{пол}(p) = \Delta\omega_г^{\cdot}(p)\frac{p}{p + K_{c3}W_\phi(p)}. \qquad (25)$$

Assuming that the interference is an harmonic of (7), and using a proportional integrating filter (PIF) with a transmission factor*, we obtain

$$W_\phi(p) = \frac{1 + pt_2}{1 + pt_1},$$

where $\left.\begin{aligned} t_1 &= (R_1 + R_2)C \\ t_2 &= R_2C \end{aligned}\right\}$ are the time constants of the filter networks.

Following some simple transformations, we reduce expression (25) to the form

$$\Delta\omega_{non}(p) = \Delta\omega_{mn}\frac{p(1 + pt_1)\omega}{(p^2 + \omega^2)[p^2t_1 + (1 + K_{c3}t_2)p + K_{c3}]}. \qquad (26)$$

Integrating equation (26), we obtain the original of the function $\Delta\omega_{non}(p)$. The solution has two components:

The free component:

$$\Delta\omega_{non1}(t) = \Delta\omega_{mn}\frac{\omega t_1}{d^4 2a^2b^2}\left[b(d^2 - 2a^2)\left(\operatorname{sh}\alpha t + \frac{1-a}{b}\operatorname{ch}\alpha t\right) - a(d^2 - 2b^2)\left(\operatorname{ch}\alpha t + \frac{1-a}{b}\operatorname{sh}\alpha t\right)\right]e^{-\frac{\alpha t}{t_1}};$$

The forced component

$$\Delta\omega_{non2}(t) = \Delta\omega_{mn}\sqrt{\frac{\omega^2(1 + \omega^2t_1^2)}{\omega^4t_1 + (4a^2 - 2K_{c3}t_1)\omega^2 + K_{c3}^2}}\sin(\omega t + \varphi).$$

Here $d^2 = a^2 + b^2 + \omega^2t_1^2$ is the equivalent time constant, a = $= (1 + \tau_2)/2$ and $b = a^2 - \tau_1$ are coefficients; $\tau_1 = K_{c3}t_1$ and $\tau_2 = K_{c3}t_2$ are the normalized time constants of the filter; and $\alpha = b/t_1$ is the transient process frequency.

The free component decays with time, tending to zero. The amplitude of the forced component does not depend on time, and being only a function of frequency, can be treated as a model of the frequency characteristic of the system. By introducing (11) and (12), we reduce it to the form:

$$y(\gamma) = \frac{\Delta\omega_{non}(\gamma)}{\Delta\omega_{mn}} = \sqrt{\frac{\gamma^2(1 + \tau_1\gamma^2)}{\tau_1(\gamma^2 - 1)^2 + 4a^2\gamma^2}}. \qquad (27)$$

* Despite the fact that because of the finite attenuation in the RF range, proportional integrating filters are practically not used in digital frequency synthesizers, it was brought into consideration with the intent that theresults obtained will be useful to specialists engaged in the application of PLL's in other fields of engineering. The expressions obtained below are also extended to the case of an integrating filter, for which it is sufficient to set a = 0.5 in them.

The shape of (27) in the function γ differs substantially from the change in the characteristic (13). Moving away from zero, (27) passes through unity at a frequency corresponding to:

$$\gamma_1 = \sqrt{\frac{\tau_1}{\tau_э}}, \tag{28}$$

thereafter, when $\gamma = 1$, it reaches a level of:

$$y(\gamma)|_{\text{при } \gamma=1} = \frac{\sqrt{1+\tau_1}}{2a}.$$

further, upon passing through the extremum, which occurs at γ_{max},

$$\gamma^2_{max} = \frac{\tau_1}{\tau_э}\left(1 + \sqrt{1 + \frac{\tau_э}{\tau_1^2}}\right), \tag{29}$$

the characteristic slowly tends to unity.

In expressions (28) and (29), the quantity $\tau_э = 1 + 2\tau_1 - 4a$ is the normalized time constant of a system with a PIF. The selectivity characteristics are depicted in Figure 3 for an integrating filter for three values of τ_1. As follows from the derived expressions and the graphs, a digital frequency synthesizer, with the action of interference on the controlled oscillator, is characterized by poor selectivity. Compensation for the parasitic deviation actually occurs in an extremely narrow range, $0 < \omega < \omega_0\sqrt{\tau_1/\tau_э}$. Outside the bounds of the frequency equal to $\omega_1 = \omega_0\sqrt{\tau_1/\tau_э}$, the parasitic deviation is transmitted without attenuation, and regeneration even takes place.

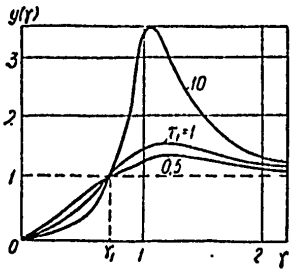

Figure 3.

It follows from the results obtained that, in the first place, a digital frequency synthesizer should either be powered from batteries or from rectifiers supplied by a high frequency current, and secondly, it is necessary to take structural design and technological steps to avoid the action of vibration and acoustic perturbations on the controlled oscillator, as well as that of the currents induced by the electromagnetic fields in the conducting structural components of the controlled oscillator. Finally, an effort is to be made to increase the Q of the oscillatory system of the controlled oscillator and reduce its coupling to the active element and the varicaps.

We shall find the level of the parasitic deviation due to the action of fluctuating interference on the controlled oscillator by determining the noise bandwidth. The solution cannot be derived in finite form for this problem, since the integral of the square of the absolute value of function (27) diverges.

To find a practically acceptable result, we write the square of the absolute value of (27) thus:

$$|y(\gamma)|^2 = y_1(\gamma)\, y_2(\gamma),$$

where

$$\left.\begin{aligned} y_1(\gamma) &= \frac{\gamma^2}{\tau_1(\gamma^2-1)^2 + 4a^2\gamma^2} \\ y_2(\gamma) &= 1 + \tau_1\gamma^2 \end{aligned}\right\},$$

$y_1(\gamma)$ and $y_2(\gamma)$ are the first and second components of the system characteristic.

The first is described by an equation similar to expression (13), and the second is a parabola. By making use of the mean value theorem [4], which states that for an integral of the product of two functions $y_1(\gamma)$ and $y_2(\gamma)$ where $y_1(\gamma)$ is a continuous function but does not change its sign in a range of $\gamma_1 - \gamma_2$, there is within this range at least one such number γ_Σ that:

$$\int_{\gamma_0}^{\gamma_2} y_1(\gamma)\, y_2(\gamma) = y_1(\gamma_\Sigma) \int_{\gamma_1}^{\gamma_2} y_2(\gamma)\, d\gamma, \tag{30}$$

where

$$\gamma_\Sigma = \frac{\gamma_1 + \gamma_2}{2}.$$

Assuming the range equal to the width of the noise bandwidth of the function $y_1(\gamma)$, and having determined $\gamma_{ш1}$, $\gamma_{ш2}$ and $\gamma_{ш\Sigma}$, we integrate (30). Since the function $y_1(\gamma)$ is similar to the function (13), then by employing expressions (14), (15), (16), (21) and (23), we obtain:

$$\left.\begin{aligned} \gamma_{ш1,2} &= \frac{a\pi}{2\sqrt{\tau_1}}\left(\sqrt{1 + \frac{4\tau_1}{a^2\pi^2}} \pm 1\right) \\ \gamma_{ш\Sigma} &= \frac{a\pi}{2\sqrt{\tau_1}}\sqrt{1 + \frac{4\tau_1}{a^2 + \pi^2}} \\ y_1(\gamma_{ш\Sigma}) &= \frac{\gamma_{ш\Sigma}^2}{\tau_1(\gamma_{ш\Sigma}^2 - 1)^2 + 4a^2\gamma_{ш\Sigma}^2} \end{aligned}\right\}.$$

By integrating (30) and substituting the limits $\gamma_{ш1}$ and $\gamma_{ш2}$, taking (18) into account, we have:

$$\Delta\gamma_ш = y(\gamma_{шΣ})\frac{a\pi}{\sqrt{\tau_1}}\left[1 + (\gamma_{ш1}^2 + \gamma_{ш2}^2 + \gamma_{ш1}\gamma_{ш2})\frac{\tau_1}{3}\right].$$

The absolute value of the noise bandwidth is:

$$П_ш = \Delta f_{0,7}^1 a\pi y(\gamma_{шΣ})\left[1 + (\gamma_{ш1}^2 + \gamma_{ш2}^2 + \gamma_{ш1}\gamma_{ш2})\frac{\tau_1}{3}\right],$$

where $\Delta f_{0,7}^1$ is the 0.7 level bandwidth of the function $y_1(\gamma)$.

The results obtained attest to the fact that when using digital frequency synthesizers as systems for generating and stabilizing a set of high stability signals, all steps which preclude the action of harmonic and fluctuating perturbations directly on the controlled oscillator should be taken. Filtering outside the limits of the frequency $\omega_1 = \omega_0\sqrt{\tau_x/\tau_э}$ can be accomplished either by virtue of the selectivity of the oscillatory system of the controlled oscillator or by the use of supplemental filters at the controlled oscillator output (high Q automatically tunable filters of supplemental PLL systems and other similar devices).

BIBLIOGRAPHY

1. "Apparatura dlya chastotnykh i vremennykh izmereniy" ["Equipment for Frequency and Time Measurements"], edited by A.P. Gorshkov, Moscow, Sovetskoye Radio Publishers, 1971.

2. Gubernatorov O.I., "Uravneniye dvizheniya tsifrovogo sintezatora chastot, kharakter i vremya Ustanovleniya kolebaniy pri skachke raznosti chastot signalov na vykhode fazovogo detektora" ["The Equations of Motion for a Digital Frequency Synthesizer; The Nature and Settling Time of the Oscillations with a Jump in the Frequency Difference of the Signals at the Phase Detector Output"], in the collection, "Radiotekhnika", Khar'kov, Khar'kov State University, 1974, No 29, p 3.

3. Gubernatorov O.I., "O parazitnom vremennom sdvige fronta impul'sov na vykhode formiruyushchego ustroystva pri deystvii flyuktuatsionnoy pomekhi i osobennostyakh preobrazovaniya modulirovannykh impul'snykh protsessov v delitele s peremennym koeffitsientom deleniya" ["On the Parasitic Time Shift in the Leading Edge of the Pulses at the Output of a Driver with the Action of Fluctuating Noise, and the Special Features of the Conversion of Modulated Pulse Processes in a Divider with a Variable Division Factor"], in the collection, "Radiotekhnika", Khar'kov, Khar'kov State University, 1976, No 39, p 8.

4. Bronshteyn I.N., Semendyayev K.A., "Spravochnik po matematike" ["Mathematics Handbook"], Moscow, Nauka Publishers, 1965.

8225
CSO:8144/1363

PHOTOELECTRIC EFFECT

UDC: 621.376.4

NOISE STABILITY OF DETECTION OF RELATIVE PHASE TELEGRAPHY SIGNALS IN OPTICAL DATA TRANSMISSION LINES

Kiev IVUZ RADIOELEKTRONIKA in Russian No 4, Apr 79 pp 68-73

[Article by E. V. Borisov]

[Text] Relations are obtained for estimating the potential noise stability of optical signals with modulation based on intensity of subcarrier oscillations, which in turn are modulated according to the relative phase telegraphy principle. The author examines the influence of atmospheric turbulence and reference generator frequency instability. The author derives formulas for estimating mean probability of error.

One method of transmitting information in the optical waveband is based on utilizing discrete modulation of subcarrier oscillations, which in turn intensity-modulate the optical carrier. In the literature individual problems pertaining to utilization of such a method are examined. In particular, in [1, 2, 3] the authors analyze the noise stability of signal detection with discrete modulation of subcarrier oscillations by frequency FM-IM, phase PM-IM and amplitude AM-IM.

In this article we shall examine the noise stability of detection of signals with discrete modulation of subcarrier oscillations employing the relative phase telegraphy method (RPT-IM). In addition to estimating the potential noise stability of detection of such signals, we present below an analysis of the influence of some of the most characteristic factors which diminish reliability of information transmission, such as fluctuations in the intensity of optical radiation in the atmosphere.

The photoelectron flux at the photodetector output in receiving RPT-IM signals constitutes a transient Poisson flux with density n(t). The mathematical expectation of density varies in conformity with the law of intensity modulation: $n_i(t)=n_c b(t)+n_ш$, where i is the hypothesis index; n_c, $n_ш$ -- mathematical expectation of a flux of signal and background emissions; b(t) -- modulating function.

For the examined method of modulation the value of the transmitted symbol is determined by the sequence of two elements in interval (0, T) [4].

Corresponding to the symbol "1" is modulating function

$$b_1(t) = \cos(\omega t + \varphi), \quad 0 \leqslant t \leqslant T,$$

and to the symbol "0"

$$b_0(t) = \begin{cases} \cos(\omega t + \varphi), & 0 \leqslant t < \frac{T}{2}, \\ -\cos(\omega t + \varphi), & \frac{T}{2} \leqslant t \leqslant T, \end{cases}$$

where ϕ -- in the general case the initial phase, which is not known during detection; ω -- subcarrier oscillation frequency. In conformity with this, in an interval of duration T in a binary channel with hypotheses Γ_1 and Γ_0 we have flux densities to which their mathematical expectations correspond:

$$\bar{n}_1(t) = \bar{n}_0 [1 + m_0 \cos(\omega t + \bar{\varphi})],$$

$$\bar{n}_0(t) = \begin{cases} \bar{n}_0 [1 + m_0 \cos(\omega t + \bar{\varphi})], & 0 \leqslant t < \frac{T}{2}, \\ \bar{n}_0 [1 - m_0 \cos(\omega t + \bar{\varphi})], & \frac{T}{2} \leqslant t \leqslant T, \end{cases}$$

where $\bar{n}_0 = \bar{n}_c(0{,}5 + q^{-1})$, $q = \bar{n}_c/\bar{n}_m$, $m_0 = \dfrac{m}{1 + 2q^{-1}}$;

m -- modulation depth coefficient.

Coherent reception of RPT-IM signals. In the assumption that the phase of the subcarrier oscillation signal is precisely known (henceforth we shall assume ϕ=0), coherent methods of receiving RPT-IM signals can be employed. A structural diagram of a receiver for this case is shown in Figure 1. Its noise stability, which for a binary channel is determined by the mean probability of error in receiving an elementary sympol $P_{ош}$, can be calculated as the probability of an event that in receiving a signal corresponding to hypothesis Γ_1, relation $x_{11} > x_{00}$ will not be fulfilled. We shall determine quantity $P_{ош}$ for a binary channel and equality of a priori data on hypotheses Γ_1 and Γ_0.

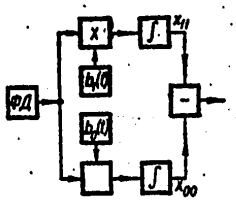

Figure 1.

With our assumption on Poisson transient flux statistics, the mathematical expectation and variance of random quantities at the integrator outputs will be determined by the following formulas:

$$m_{11} = \int_0^T \overline{n_1(t)}\, b_1(t)\, dt, \quad \sigma_{11}^2 = \int_0^T \overline{n_1(t)}\, b_1^2(t)\, dt,$$
$$m_{00} = \int_0^T \overline{n_1(t)}\, b_0(t)\, dt, \quad \sigma_{00}^2 = \int_0^T \overline{n_1(t)}\, b_0^2(t)\, dt. \qquad (1)$$

Distribution of random quantities x_{11}, x_{00}, due to the central limit theorem, is close to normal, while the random quantities themselves are uncorrelated [5]. Considering that quantity T is fairly large (in comparison with the subcarrier oscillation period), it is not difficult to obtain accurate solutions to the above integrals:

$$m_{11} = \frac{\bar{n}_s m_s T}{2}; \quad m_{00} = 0; \quad \sigma_{11}^2 = \sigma_{00}^2 = \sigma^2 = \frac{\bar{n}_s T}{2}.$$

In conformity with the above-selected mean probability of error criterion, its value can be determined from the expression

$$P_{\text{ош}} = \int_{-\infty}^{\infty} p(x_{11}) \int_{x_n}^{\infty} p(x_{00})\, dx_{00} dx_{11}$$

or taking into account assumptions on the character of distributions x_{11} and x_{00}

$$P_{\text{ош}} = \int_{-\infty}^{\infty} \frac{1}{\sqrt{2\pi}\sigma} e^{-\frac{(x_{11}-m_{11})^2}{2\sigma^2}} \int_{x_n}^{\infty} \frac{1}{\sqrt{2\pi}\sigma} e^{-\frac{x_{00}}{2\sigma^2}} dx_{00} dx_{11}.$$

The latter relation can be transformed to the form

$$P_{\text{ош}} = \frac{1}{2\sqrt{\pi}} \int_{-\infty}^{\infty} \exp(-z^2)\, \operatorname{erfc}\left(z + \frac{m_{11}}{\sqrt{2}\sigma}\right) dz, \qquad (2)$$

where

$$\operatorname{erfc}(y) = \frac{2}{\sqrt{\pi}} \int_y^{\infty} e^{-t^2} dt.$$

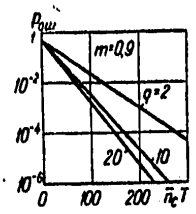

Figure 2

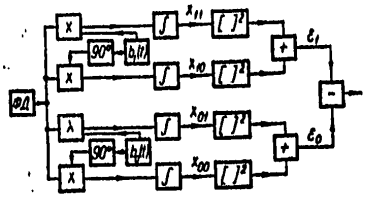

Figure 3.

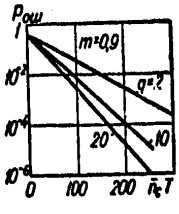

Figure 4.

Considering equality [6] to be correct,

$$\frac{1}{\sqrt{\pi}}\int_{-\infty}^{\infty}\exp(-y^2)\operatorname{erfc}(\alpha y+\beta)\,dy=\operatorname{erfc}\left(\frac{\beta}{\sqrt{1+\alpha^2}}\right),$$

the value of integral (2) can be determined precisely:

$$P_{ош}=\frac{1}{2}\operatorname{erfc}\left(\frac{m_0\sqrt{\bar{n}_0 T}}{2\sqrt{2}}\right). \qquad (3)$$

The obtained formula reflects the potential noise stability of reception of RPT-IM signals with coherent reception. Figure 2 contains a graphic illustration of relation (3).

In practice there are a number of factors which decrease the noise stability of coherent reception. One of them is the random nature of signal phase ϕ. Therefore in a number of instances it is advisable to transition to reception methods which are insensitive to phase instability.

Noncoherent reception of RPT-IM signals. Figure 3 contains a structural diagram of the receiver. Its noise stability can be calculated as the probability of the event that in receiving a signal corresponding to hypothesis Γ_1, relation $\varepsilon_1>\varepsilon_0$ will not be fulfilled.

Just as in the preceding case, it is easy to determine mathematical expectation and variance of quantities x_{11}, x_{10}, x_{01}, x_{00} at the integrator outputs:

$$m_{11}=\frac{\bar{n}_0 m_0 T}{2},\quad m_{10}=m_{01}=m_{00}=0,$$

$$\sigma_{11}^2=\sigma_{10}^2=\sigma_{01}^2=\sigma^2=\frac{\bar{n}_0 T}{2}.$$

Distribution parameters of quantities x_{11}, x_{10}, x_{01}, x_{00} unambiguously define the distribution parameters of output quantities ε_1 and ε_0, which have Rayleigh distribution [7] with the following densities:

$$p(\varepsilon_1) = \frac{\varepsilon_1}{\sigma^2} \exp\left(\frac{\varepsilon_1^2 + m_{11}^2}{2\sigma^2}\right) I_0\left(\frac{m_{11}\varepsilon_1}{\sigma^2}\right),$$
$$p(\varepsilon_0) = \frac{\varepsilon_0}{\sigma^2} \exp\left(-\frac{\varepsilon_0^2}{2\sigma^2}\right), \qquad (4)$$

where $I_0(z)$ -- zero-order Bessel function.

The probability of error in conformity with the above assumptions can be determined from the expression

$$P_{\text{ош}} = \int_0^\infty p(\varepsilon_1) \int_{\varepsilon_1}^\infty p(\varepsilon_0)\, d\varepsilon_0 d\varepsilon_1. \qquad (5)$$

After substituting (4) in (5) and integrating [8], we finally obtain

$$P_{\text{ош}} = \frac{1}{2} \exp\left(-\frac{\bar{n}_\text{э} T m_\text{э}^2}{8}\right). \qquad (6)$$

Formulas (3) and (6) enable us to estimate the potential noise stability of reception of RPT-IM signals with coherent and noncoherent methods of reception respectively. Figure 4 contains graphs of relationship of mean probability of error, calculated on the basis of formula (6).

Noise stability decreases when signals are transmitted through a turbulent medium. The effect of fluctuations in amplitude of optical radiation will be substantial for noncoherent reception. Determination of mean probability of error in this case reduces to calculation of the averaged value of expression (6)

$$\overline{P_{\text{ош}}} = \int_0^\infty P_{\text{ош}} p(v)\, dv, \qquad (7)$$

where $p(v) = [2\pi\sigma_v^2 v^2]^{-\frac{1}{2}} \exp\left[-\frac{(\ln v + \sigma_v^2)^2}{2\sigma_0^2}\right]$ -- normal density of distribution of the logarithm of relative amplitude of radiation v; σ_v^2 -- variance of amplitude logarithm ($\sigma_v < 0.8$).

Considering that expression (6) can be presented in the form

$$P_{\text{ош}} = \frac{1}{2} \exp\left(-\frac{\bar{n}_c T m^2}{32\left(0{,}5 + \frac{1}{q}\right)}\right),$$

formula (7) can be transformed

$$\bar{P}_{ош} = \frac{1}{2}\int_0^\infty \exp\left(-\frac{\bar{n}_c T m^2 v^2}{32\left(0{,}5+\frac{1}{qv^2}\right)}\right) p(v)\,dv. \qquad (8)$$

We shall note that when $P_{ош}<10^{-3}$ (this corresponds to practical instances), relation $q<<1$ is fulfilled, which makes it possible further to utilize a simplified expression for $P_{ош}$:

$$\bar{P}_{ош} = \frac{1}{2}\int_0^\infty \exp(-av^2)\, p(v)\,dv, \qquad (9)$$

where $a=\bar{n}_c Tm^2/16$.

Then, proceeding to a new integration variable

$$z = \frac{\ln v + \sigma_0^2}{\sqrt{2}\sigma_0},$$

formula (9) can be presented in the form

$$P_{ош} = \frac{1}{2\sqrt{\pi}}\int_{-\infty}^\infty \exp\{-a\exp[2\sigma_0(\sqrt{2}z-\sigma_0)]-z^2\}\,dz. \qquad (10)$$

We shall note that function e^{-z^2} decreases rapidly when $z^2>2.3$. This makes it possible with a sufficient degree of accuracy to limit oneself to the first three terms when expanding an exponential function in a subintegral expression into a power series. With these assumptions relation (10) can be rewritten:

$$\bar{P}_{ош} = \frac{1}{2\sqrt{\pi}}\int_{-\infty}^\infty \exp\left[-k-knz-\left(1+\frac{kn^2}{2}\right)z^2\right]dz, \qquad (11)$$

where $k = a\exp(2\sigma_0^2)$, $n = 2\sqrt{2}\sigma_0$.

Allowing that [8]

$$\int_{-\infty}^\infty \exp(-p^2x^2 \pm qx) = \exp\left(\frac{q^2}{2p^2}\right)\frac{\sqrt{\pi}}{p},$$

we shall reduce expression (11) to final form and obtain a mean probability of error with noncoherent reception of RPT-IM signals under conditions of fluctuations of intensity of optical radiation

$$\bar{P}_{\text{ош}} = \frac{1}{2c} \exp\left[-k + \left(\frac{kn}{2c}\right)^2\right], \qquad (12)$$

where

$$c = \sqrt{1 + \frac{kn^2}{2}}.$$

Analysis of the obtained relation indicates that the degree of decrease in noise stability increases both with an increase in the level of turbulence (growth of σ_V) and with an increase in intensity of radiation. Formula (12) makes it possible to perform corresponding engineer estimates.

One more factor diminishing the noise stability of reception of RPT-IM signals is the instability of the frequency of the reference generators relative to the frequency of the subcarrier oscillations of the signal radiation. We shall estimate this influence for an arrangement with noncoherent reception.

Let us assume that the frequencies of these fluctuations are not great and are characterized by relative deviation $\Delta\omega/\omega << 1$. Then the values of the mathematical expectations of random quantities at the integrator outputs in the diagram in Figure 3 will be equal to:

$$m_{11} = \frac{\bar{n}_0 m_0^2 T}{2} \frac{\sin\alpha}{\alpha}, \quad m_{10} = \frac{\bar{n}_0 m_0^2 T}{2} \frac{1-\cos\alpha}{\alpha}, \quad m_{01} = m_{00} = 0,$$

where $\alpha = \Delta\omega T$.

We shall note that the values of variances of these quantities will remain practically unchanged. Then the conditional probability of error can be obtained in the form

$$P_{\text{ош}} = \frac{1}{2} \exp\left[-a\left(\frac{\sin\frac{\alpha}{2}}{\frac{\alpha}{2}}\right)^2\right],$$

where $a = \frac{\bar{n}_0 T m_0^2}{8}$.

With fluctuations of α according to the normal law with parameters $(0, \sigma_\alpha)$, the averaged error value can be determined from the relation

$$\bar{P}_{\text{ош}} = \frac{1}{2\sqrt{\pi}} \int_{-\infty}^{\infty} \exp\left[-a \frac{\sin^2\left(\frac{x\sigma_\alpha}{\sqrt{2}}\right)}{\frac{x^2\sigma_\alpha^2}{2}} - x^2\right] dx.$$

Expanding function sin x by powers x taking into account the smallness of the arguement and integrating, we finally obtain a formula for determining mean probability of error with noncoherent reception of RPT-IM signals and reference generator frequency instability

$$P_{ош} = \frac{1}{2}\frac{\exp(-a)}{\sqrt{1-\frac{a\sigma_a^2}{6}}} = \frac{P_{ош}(\alpha = 0)}{\sqrt{1-\frac{a\sigma_a^2}{6}}}.$$

Utilizing the last formula, demands on stability of reference generators can be determined on the basis of allowable deterioration of noise stability.

Thus the analysis we have performed makes it possible to calculate mean probability of error in receiving RPT-IM signals and to estimate the influence of fluctuations in intensity of radiation and frequency of subcarrier oscillation on the reliability of transmission of binary information.

BIBLIOGRAPHY

1. Barbanel', I. S. "Calculating Noise Stability of Optical Communication Links With Discrete Modulation of Subcarrier Oscillations," RADIOTEKHNIKA, 29, No 10, 1974, page 5.

2. Borisov, E. V. and Kiselev, A. K. "Noise Stability of Reception of Optical Signals With Unknown Phase," IZV. VUZOV -- RADIOELEKTRONIKA, 21, No 4, 1978, page 123.

3. Gal'yardi, R. M., and Karp, Sh. "Opticheskaya svyaz'" [Optical Communications], Moscow, Svyaz', 1978.

4. Fink, L. M. "Teoriya peredachi diskretnykh soobshcheniy" [Theory of Transmission of Discrete Messages], Moscow, Sovetskoye radio, 1970.

5. Shchelkunov, K. N., and Kazovskiy, L. G. "Noise Stability of Optical Communication Links With Frequency-Division Multiplexing of Discrete Information Channels," RADIOTEKHNIKA, 27, No 3, 1972, page 1.

6. Chebyshev, P. L. "Teoriya veroyatnostey" [Probability Theory], Izd. AN SSSR, 1936.

7. Levin, B. R. "Teoreticheskiye osnovy statisticheskoy radiotekhniki" [Theoretical Principles of Statistical Radio Engineering], Moscow, Sovetskoye radio, 1966.

8. Gradshteyn, I. S., and Ryzhik, I, M. "Tablitsy integralov, summ, ryadov i proizvedeniy" [Tables of Integrals, Sums, Series and Products], Moscow, Fizmatgiz, 1962.

Submitted 7 July 1978

3024
CSO: 1870

PHOTOELECTRIC EFFECT

UDC: 621.391.519.25

EVALUATION OF THE QUALITY OF DETECTION OF A WEAK OPTICAL SIGNAL

Kiev IVUZ RADIOELEKTRONIKA in Russian No 4, Apr 79 pp 61-67

[Article by P. S. Akimov, A. N. Kubasov, and A. V. Minacheva]

[Text] This article examines a method and results of calculation of the performance characteristics of a weak optical signal detector operating according to the Neumann-Pearson criterion by observation sequence. The article presents detection characteristics with nonparametric (rank) processing.

Problems of detecting signals in the optical band have been less elaborated than in the radio-frequency band. For example, several articles have dealt with the characteristics of quality of optical signal detection, in which the authors examine particular instances of noise and signal distributions of a number of photoelectrons at the output of a photoenergy detector [1]. Some results are presented in monographs [2, 3]. Problems of evaluating the interference resistance of optical signal detectors are most fully examined in monograph [4]. But it too presents characteristics for an extremely limited number of cases. In addition, these characteristics are incorrect for small values of probability of spurious detection (10^{-3}–10^{-13}), since the normal approximation employed by the author of [4] for statistical distribution is highly approximate.

In this article we shall examine the method and results of calculation of the performance characteristics of a weak optical signal detector for the more general case of noise and signal distributions, operating according to the Neumann-Pearson criterion in count sequence. We shall also examine detection characteristics with nonparametric (rank) processing.

We shall examine an energy detector based on a photoelectron count. When a weak signal is being received, the detector output signal is characterized by distribution of probabilities P(k, T) of appearance of a fixed number of photoelectrons k during observation interval T.

Solution of the problem of evaluation of quality of detection requires knowledge of statistical distributions of the photoelectron flux at the

photodetector output when affected by noise and superposition of signal and noise. One observes in the optical band a diversity of types of distributions of the number of photoelectrons, depending on the type and properties of the signal, noise and reflecting surface. We include below a brief summary of the principal, most typical types of distributions of photoelectrons emitted by a signal $P_C(k, T)$, noise $P_П(k, T)$, and a mixture of signal with noise $P_{C+П}(k, T)$ [4], as well as explanations of the conditions of applicability of these laws.

Coherent Signal on a Background of Gaussian Noise

$$P_c(k, T) = \frac{S_c'^k}{k!} \exp(-S_c'), \tag{1}$$

$$P_n(k, T) = \frac{(T\Delta\omega_n - 1 + k)!}{(T\Delta\omega_n - 1)!\,k!} \frac{S_n'^k}{(1+S_n')^{k+T\Delta\omega_n}}. \tag{2}$$

Slow noise fluctuations $T\Delta\omega_n \ll 1$

а) $T|\omega_c - \omega_n| \ll 1$,

$$P_{c+n}(k, T) = \frac{S_n'^k}{(1+S_n')^{k+1}} \exp\left\{-\frac{S_c'}{1+S_n'}\right\} Lk\left[-\frac{S_c'}{S_n'(1+S_n')}\right]; \tag{3}$$

б) $T|\omega_c - \omega_n| \gg 1$,

$$P_{c+n}(k, T) = \frac{S_n'^k}{(1+S_n')^{k+1}} \exp(-S_c') \sum_{m=0}^{k} \frac{1}{m!}\left[\frac{S_c'(1+S_n')}{S_n'}\right]^m. \tag{4}$$

Rapid noise fluctuations $T\Delta\omega_n \gg 1$

а) $T|\omega_c - \omega_n| \ll 1$,

$$P_{c+n}(k, T) = \frac{S_n'^k}{(1+S_n')^{k+T\Delta\omega_n}} \exp\left\{-\frac{S_c'}{1+S_n'}\right\} L_k^{T\Delta\omega_n - 1}\left[-\frac{S_c'}{S_n(1+S_n)}\right]; \tag{5}$$

б) $T|\omega_c-\omega_n|\gg 1$

$$P_{c+n}(k,T)=\frac{S_n^k}{(1+S_n)^{k+T\Delta\omega_n}}\exp(-S_c')\times$$

$$\times\sum_{m=0}^{k}\frac{(T\Delta\omega_n-1+k-m)!}{(T\Delta\omega_n-1)!\,(k-m)!\,m!}\left[\frac{S_c'(1+S_n)}{S_n}\right]^m. \qquad (6)$$

Noncoherent Signal on Background of Gaussian Noise

$$P_c(k,T)=\left(\frac{S_c'}{1+S_c'}\right)^k\frac{1}{1+S_c'}. \qquad (7)$$

Slow noise fluctuations $T\Delta\omega_n\ll 1$

а) $T|\omega_c-\omega_n|\ll 1$,

$$P_{c+n}(k,T)=\frac{1}{1+S_n'+S_c'}\left(\frac{S_n'+S_c'}{1+S_n'+S_c'}\right)^k; \qquad (8)$$

б) $T|\omega_c-\omega_n|\gg 1$,

$$P_{c+n}(k,T)=\left(\frac{S_n'}{1+S_n'}\right)^k\frac{1}{(1+S_n')(1+S_c')}\frac{1-z^{k+1}}{1-z},\quad z=\frac{S_c'(1+S_n')}{S_n'(1+S_c')}. \qquad (9)$$

Rapid noise fluctuations $T\Delta\omega_n\gg 1$

а) $T|\omega_c-\omega_n|\ll 1$;

$$P_{c+n}(k,T)=\frac{1}{(1+S_n)^{T\Delta\omega_n-1}}\frac{(S_n+S_c')^k}{(1+S_n+S_c')^{k+1}}\times$$

$$\times F\left(-k;\ T\Delta\omega_n-1;\ -k;\ \frac{S_n(1+S_n+S_c')}{(1+S_n)(S_n+S_c')}\right); \qquad (10)$$

$$6)\ T|\omega_c-\omega_n|\gg 1,$$

$$P_{c+n}(k,T)=\frac{1}{(1+S_n)^{T\Delta\omega_n}}\frac{1}{(1+S_n')^{k+1}}\times$$

$$\times F\left(-k;\ T\Delta\omega_n;\ -k;\ \frac{S_n(1+S_c')}{S_c'(1+S_n)}\right). \qquad (11)$$

In formulas (1)-(11) F(·) is a hypergeometric series; L[·] are Laguerre polynomials; S' -- average number of photoelectrons during observation interval T; Δω -- signal (noise) frequency band; TΔω -- number of degrees of signal (noise) freedom; S=S'/TΔω.

The problem of detecting a coherent signal can arise, for example, when a laser in single-frequency mode is utilized as an emitting device. In this case distribution of photoelectrons emitted by such a signal at the detector output is governed by Poisson's law (1). A Poisson distribution is also characteristic of a weak signal of any coherence for which S_c' is small. We shall note that in the detection problem a constant-amplitude signal in the radio-frequency region is an analog to an optical coherent signal.

The problem of detection of a noncoherent signal arises in the case of employing as a source a laser operating in multiple mode. The amplitude of such a source is distributed according to the normal law, while distribution of the number of photoelectrons at detector output is described by the Bose-Einstein law [7]. In addition, this law can describe coherent laser radiation after passage of an inhomogeneous turbulent atmosphere, as well as a coherent signal reflected from an optically rough surface. A signal with Gaussian distribution of amplitudes is an analog of a noncoherent optical signal in the radio-frequency region.

Poisson and Bose-Einstein distributions are extreme cases of negative-binomial distribution (2) (taking into account corresponding index "c" or "п") when TΔω>>1 and TΔω=1 respectively.

During the effect of external interference, statistics of photoelectrons are described by negative-binomial distribution (2). For rapidly-fluctuating noise (that is, when TΔω>>1), distribution (2) transitions to Poisson (1). Thermal radiation of heated bodies, the Sun, Moon, and stars is a source of rapidly-fluctuating noise. With slow noise field fluctuations ($T\Delta\omega_п<<1$) distribution (2) transitions to (7). The source of such noise is thermal radiation, sky radiation, reflection from an optically "rough" surface, and scattering of sunlight by the atmosphere.

Distribution of photoelectrons caused by internal interference is described by the Poisson law [1].

The result of the effect of superposition of signal and noise on a detector is described by more complex laws of distribution $P_{c+п}(k, T)$ of photoelectrons and is determined in substantial measure by the degree of spacing of central frequencies of signal ω_c and noise $\omega_п$.

If the signal and noise frequencies are spaced in such a manner that $T|\omega_c-\omega_п|>>1$, distribution is described by a convolution of partial distributions, that is,

$$P_{c+n}(k, T)=\sum_{i=0}^{k} P_c(i, T) P_n(k-i, T).$$

For example, superposition of a coherent signal and slowly fluctuating noise gives a photoelectron distribution described by expression (4). With influence of superposition of a noncoherent signal and rapidly fluctuating noise radiation, distribution is described by expression (11), which is a convolution of (7) and (2).

Photoelectron distributions under condition $T|\omega_c-\omega_п|<<1$ (3), (5), (8), (9) were obtained on the basis of quantum analysis [4].

Since the problem of evaluating quality of detection under condition $T|\omega_c-\omega_п|\gg 1$ is partially solved in [1, 4] etc, we shall focus principal attention on the case $T|\omega_c-\omega_п|\ll 1$.

A plausibility ratio, which is written as follows with independent observations, is usually utilized as basis of optimal processing algorithms:

$$\lambda=\prod_{i=1}^{n}\frac{P_{c+n}(k_i)}{P_n(k_i)}, \qquad (12)$$

where $P(k_i)$ -- probability of obtaining k_i photoelectrons in i observation.

Analysis of the plausibility ratio for the case of detection of a coherent signal in Poisson noise indicates that the optimal algorithm boils down to accumulation of values k_i for n observations and comparison of the accumulated value with threshold C.

In the general case, however, the photoelectron accumulator proves nonoptimal. One can easily see this if one substitutes in (12) distributions which correspond, for example, to detection of a coherent signal on the background of rapidly fluctuating noise (2) and (5), or distributions corresponding to detection of a noncoherent signal on the background of rapidly fluctuating noise (7) and (10). When $T\Delta\omega_п=1$ (5) and (10) transition to superposition distributions of the corresponding signal and slowly fluctuating noise (3) and (8).

Since realization of algorithms of optimal processing involves considerable difficulties and proves to be different for different conditions of detection, it is of interest to examine the characteristics of the energy detector usually employed in practice and utilizing as determining statistics accumulated sum of readings

$$K=\sum_{i=1}^{n} k_i.$$

Utilizing the edifice of the generating function, one can show that distributions of determining statistics K corresponding to (2), (5) and (10), are equal to

$$P_{\text{п}}(K)=\frac{(nT\Delta\omega_{\text{п}}-1+K)!}{(nT\Delta\omega_{\text{п}}-1)!\,K!}\left(\frac{S_{\text{п}}}{1+S_{\text{п}}}\right)^{K}\left(\frac{1}{1+S_{\text{п}}}\right)^{nT\Delta\omega_{\text{п}}}, \tag{13}$$

$$P_{\text{с+п}}(K)=\frac{S_{\text{п}}}{(1+S_{\text{п}})^{K+nT\Delta\omega_{\text{п}}}}\exp\left\{-\frac{nS_{\text{с}}'}{1+S_{\text{п}}}\right\}L_{K}^{nT\Delta\omega_{\text{п}}-1}\left[-\frac{nS_{\text{с}}'}{S_{\text{п}}+S_{\text{п}}^{2}}\right], \tag{14}$$

$$P_{\text{с+п}}(K)=\frac{(S_{\text{п}}+S_{\text{с}}')^{K}}{(1+S_{\text{п}})^{n(T\Delta\omega_{\text{п}}-1)}(1+S_{\text{п}}+S_{\text{с}}')^{K+n}}\times$$

$$\times\sum_{m=0}^{K}\frac{[n(T\Delta\omega_{\text{п}}-1)-1+m]!\,[n+K-m-1]!}{[n(T\Delta\omega_{\text{п}}-1)-1]!\,m!\,(n-1)!\,[K-m]!}. \tag{15}$$

Specifying probability of spurious detections α and utilizing expressions for $P_{\text{п}}(K)$ and $P_{\text{с+п}}(K)$, we can calculate the values of detection threshold C and probability of detection D in conformity with the Neumann-Pearson criterion from relations

$$\alpha=\sum_{K=C}^{\infty}P_{\text{п}}(K),\quad D=\sum_{K=C}^{\infty}P_{\text{с+п}}(K). \tag{16}$$

Employing this method, with utilization of expressions (13), (14) and (15), we calculated detection characteristics with the aid of a computer -- dependences of detection probability D on the signal/noise ratio $a=10\lg S_{\text{с}}'/S_{\text{п}}'$ for various values α, $S_{\text{п}}'$, $T\Delta\omega_{\text{п}}$. Figure 1 contains photoelectron accumulator detection characteristic curves for coherent (solid lines) and noncoherent (dashed lines) $T\Delta\omega_{\text{п}}=1, 5, 100$, $\alpha=10^{-7}$ and $S_{\text{п}}'=4$, $n=10$. The path of the curves is in general of a traditional nature and does not differ from classic curves of characteristics for the

radio-frequency region, with the exception of the fact that there is a dependence of probability D not only on the signal/noise ratio but also on the value $S_п'$, which characterizes noise energy. The curves of characteristics for a noncoherent signal (dashed line) are somewhat flatter than the coherent signal curves (solid lines), due to greater dispersion of distribution of the noncoherent signal. At a level D=0.5 characteristics for noncoherent and coherent signals coincide.

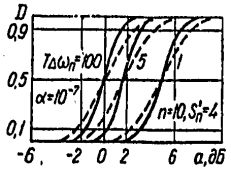

Figure 1.

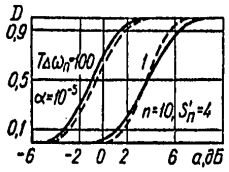

Figure 2.

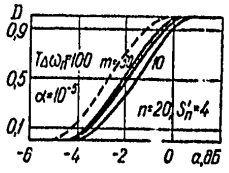

Figure 3.

Figure 2 contains examples of photoelectron accumulator detection characteristics for a noncoherent signal when $T|\omega_с-\omega_п|\gg1$ [5] (dashed lines) and $T|\omega_с-\omega_п|\ll1$ (solid lines) $T\Delta\omega_п$=1, 100, n=10, $S_п'$=4. A comparative analysis of the curves indicates their full agreement during signal detection in Poisson noise ($T\Delta\omega_п$=100) and a slight difference in Gaussian noise when $T\Delta\omega_п$=1 (Bose-Einstein distribution).

A characteristic feature of the problem of detecting a signal in the optical band is the fact that detection is performed under conditions of a priori uncertainty in a case where there is a lack of information on signal and noise statistics and there is a strong dependence of corresponding distributions on various factors (atmospheric turbulence, weather conditions, time of day, year, etc), precise consideration of which is impossible. In addition, actual statistical distributions may differ from the theoretical models examined above. Under these conditions the quality of detection may differ substantially from the calculated figure.

Employment of nonparametric processing [6] should be considered promising as a means of combatting a priori uncertainty. Nonparametric detection is characterized by the property of invariance of probability of spurious detection in relation to the type and parameters of noise distribution. At the same time such detectors are insignificantly inferior in detection probability to optimal detectors, and with a change in type of distribution, as a rule they are superior to the latter, which lose their optimalness thereby.

In [5] the authors examine a nonparametric procedure of optical signal detection. To solve the problem of detection in any channel (resolution element) they employ rank values $r_i(i=\overline{1,n})$, that is, the number of

instances of exceeding photoelectron counts x_i in this channel relative to noise sample count y_{ij} $(j=\overline{1,m})$ in m adjacent independent resolution channels (time, angle, velocity) for n periods of observation. The test statistics are based on the sum of ranks

$$R=\sum_{i=1}^{n} r_i=\sum_{i=1}^{n}\sum_{j=1}^{m} h(x_i-y_{ij}),\quad h(x_i-y_{ij})=\begin{cases}1, & x_i>y_{ij}\\ 0, & x_i<y_{ij}\end{cases}, \tag{17}$$

and for reaching a decision are tested for threshold C. Detection threshold C is selected taking into account statistics distribution function $P_{\Pi}(R\leq l)$ in the presence of noise alone which, due to nonparametricity, is independent of the noise characteristics

$$P_n(S\leqslant l)=\frac{1}{(m+1)^n}\sum_{i=0}^{l}\sum_{j=0}^{\left[\frac{i}{m+1}\right]}(-1)^j\binom{n}{j}\binom{n+i-j(m+1)-1}{n-1}, \tag{18}$$

where $[\cdot]$ is a whole part, and $\binom{a}{b}$ is a number of combinations from a with b.

From relation $P_n(R\leqslant C)=1-\alpha$ and (18) we calculate threshold C.

To determine detection probability D for the obtained threshold, we utilize a normal approximation of statistics distribution (correct when $m+n\geqslant 20,\ n\geqslant 4$) for superposition of signal and noise, that is,

$$D=1-\Phi\left(\frac{C-M}{\sigma}\right), \tag{19}$$

where $\Phi(\cdot)$ -- Laplace interval; M and σ^2 -- mathematical expectation and statistic dispersion.

Parameters M and σ are determined from relations [7]:

$$\begin{gathered}M=mnp,\quad \sigma=mn[p-mp^2+(m-1)q],\\ p=P(x>y)=\int G(t)\,dF(t),\quad q=\int G^2(t)\,dF(t),\end{gathered} \tag{20}$$

where G(t), F(t) are functions of noise distribution and a mixture of signal and noise respectively.

Utilizing in place of G(t) and F(t) discrete distribution $P_{\Pi}(k)$ and $P_{C+\Pi}(k)$ and replacing in (20) integration by addition, one can calculate parameters M and σ and further, with (19), probability D.

In Figure 3 the solid lines are coherent signal detection characteristic curves for various values of $T\Delta\omega_{\Pi}$, while the dashed lines are photoelectron accumulator

characteristics. Figure 4 contains curves of noncoherent signal detection with a rank detector (solid lines) and accumulator (dashed line).

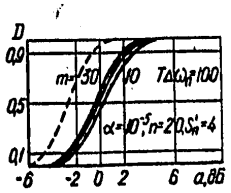

Figure 4.

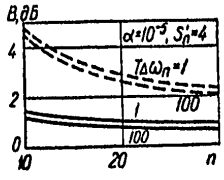

Figure 5.

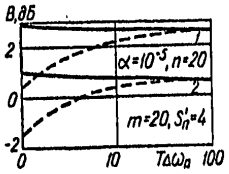

Figure 6.

Figure 5 contains gain relations in threshold signal / noise ratio B of an accumulator in comparison with rank detector from n. In the case of a noncoherent signal (dashed lines), the magnitude of ranked detector losses in comparison with the accumulator is greater by 2 db than with a coherent signal (solid lines). Figure 6 shows dependencies of gain on number of degrees of freedom of noise $T\Delta\omega_п$, while the dashed lines show the relations of gain for the case $T|\dot{\omega}_0-\omega_п|\gg 1$, obtained in [5].

Due to a priori uncertainty relative to distributions of noise and the mixture of signal with noise, and the transient nature of the conditions of detection, in designing optical systems one must substantially overestimate system power. Employment of nonparametric (rank) processing guarantees a constancy of level of false alarms independent of noise and consequently eliminates the necessity of overestimating the threshold level to the detriment of probability of detection, to which one must resort with traditional processing. Thus the slight loss of a rank detector to the traditional detector is compensated for by the property invariance of the rank statistic, whereby such a large power "safety factor" is not needed.

BIBLIOGRAPHY

1. Momsik, V. P. "Characteristics of Detection of Optical Signals for One Class of Distributions of Photoelectron Flux," VOPROSY RADIOELEKTRONIKI, General Technical Series, Issue 12, 1973, page 40.

2. Volokhatyuk, V. A.; Kochetkov, V. M.; and Krasovskiy, R. R. "Voprosy opticheskoy lokatsii" [Problems of Optical Detection and Ranging], Moscow, Sovetskoye radio, 1971.

3. Kuriksha, A. A. "Kvantovaya optika i opticheskaya lokatsiya" [Quantum Optics and Optical Detection and Ranging], Moscow, Sovetskoye radio, 1973.

4. Sheremet'yev, A. G. "Statisticheskaya teoriya lazernoy svyazi" [Statistical Theory of Laser Communications], Moscow, Svyaz', 1971.

5. Akimov, P. S., and Kubasov, A. N. "Rank Detection of an Optical Signal," IZV. VUZOV -- RADIOELEKTRONIKA, 20, No 7, 1977, page 29.

6. Akimov, P. S. "Nonparametric Signal Detection," RADIOTEKHNIKA, 32, No 11, 1977, page 17.

7. Akimov, P. S., and Yefremov, V. S. "Characteristics of Detection of a Rank Radar Detector," RADIOTEKHNIKA I ELEKTRONIKA, 19, No 7, 1974, page 1527.

Submitted 11 July 1978

3024
CSO: 1870

PULSE TECHNIQUE

UDC 621.372.852+621.377.22

THE CASCADE CONNECTION OF SURFACE ACOUSTIC WAVE FILTERS

Kiev IZVESTIYA VUZ RADIOELEKTRONIKA in Russian Vol 22 No 1, 1979 pp 105-107

[Article by V.I. Valov, manuscript received 21 Nov 77]

[Text] It is well known that Rayleigh surface acoustic waves (PAV)* have no dispersion, and for this reason, one (or two) transducers with a variable step are employed to obtain the dispersion characteristic of a matched filter (SF) for a linear FM signal using PAV's. The amount of the dispersion delay does not depend on the frequency and is determined only by the length of the transducers and the parameters of the piezoelectric crystal, on the surface of which these transducers are applied [1]. With the finite dimensions of the piezoelectric crystals existing at the present time, the delay time in a single channel line does not exceed 100 μsec [2]. An increase in the maximum delay in a PAV matched filter can be achieved, for example, by the cascade (series) connection of the sections (of the filters). Each section has a pulse response width of $T_1 = T/N$ and a bandwidth of $\Delta f_1 = \Delta f$ (T and Δf are the requisite pulse response width and bandwidth of the matched filter on the whole respectively). There are no breaks in the resulting dispersion characteristic of the cascaded system. The requisite transfer function of the matched filter on the whole, $K_{sf}(j\omega)$ should coincide with the resulting transfer function $K_p(j\omega)$ of the cascaded sections:

$$K_p(j\omega) = K_1(j\omega) K_2(j\omega) \ldots K_N(j\omega) = |K_1(j\omega)|^N.$$

These requirements are met if the transfer functions of each section have a rectangular envelope in the passband Δf, while the phase-frequency responses are in the form of second order parabolas. The transfer functions of the actual sections do not satisfy these requirements.

In fact, according to optimal signal processing theory [3], the overall amplitude-frequency response (AChKh) of a matched filter for a linear

*We will speak only of Rayleigh PAV's in the following.

FM signal with a width T and a bandwidth Δf is determined by the following expression:

$$|K_{cb}(j\omega)| = B\left(\frac{T}{2\Delta f}\right)^{\frac{1}{2}} \{[C(x_1)+C(x_2)]^2+[S(x_1)+S(x_2)]^2\}^{\frac{1}{2}}, \quad (1)$$

while its phase-frequency response is determined by:

$$\varphi_{k\,cb}(\omega) = \frac{(\omega_0-\omega)^2}{2\Delta\omega}T - \text{arc tg}\,\frac{S(x_1)+S(x_2)}{C(x_1)+C(x_2)} - \omega t_0, \quad (2)$$

where B is a normalizing factor, $C(x) = \int_0^x \cos\frac{\pi}{2}y^2dy$, $S(x) = \int_0^x \sin\frac{\pi}{2}y^2dy$ are Fresnel integrals:

$$x_1 = \sqrt{\frac{\Delta f T}{2}}\left(1-\frac{\omega_0-\omega}{\Delta\omega}\right), \quad x_2 = \sqrt{\frac{\Delta f T}{2}}\left(1+\frac{\omega_0-\omega}{\Delta\omega}\right), \quad (3)$$

ω_0 is the instantaneous angular frequency; ω_0 is the average angular frequency [sic, typographical error in original]; $\Delta\omega = 2\pi\Delta f$ is the frequency deviation; t_0 is the delay constant.

The Fresnel integrals are quasi-oscillating ones, and for this reason, the transfer function of a matched filter for a linear FM signal containes pulsations, the number of periods and the amplitude of which depend on the compression factor $D = T\Delta f$.

Substituting $T_1 = T/N$ in (1), (2) and (3), instead of T, we obtain the following expressions for the transfer functions of a single section, $|K_1(j\omega)|$, $\phi_{k_1}(\omega)$ and a cascaded system $|K_p(j\omega)|$, $\phi_{kp}(\omega)$:

$$|K_1(j\omega)| = B\left(\frac{T_1}{2\Delta f}\right)^{\frac{1}{2}} \{[C(x_1)+C(x_2)]^2+[S(x_1)+S(x_2)]^2\}^{\frac{1}{2}}, \quad (4)$$

$$\varphi_{k1}(\omega) = \frac{(\omega_0-\omega)^2}{2\Delta\omega}T_1 - \text{arc tg}\,\frac{S(x_1)+S(x_2)}{C(x_1)+C(x_2)} - \omega t_0, \quad (5)$$

$$|K_p(j\omega)| = B\left(\frac{T_1}{2\Delta f}\right)^{\frac{N}{2}} \{[C(x_1)+C(x_2)]^2+[S(x_1)+S(x_2)]^2\}^{\frac{N}{2}}, \quad (6)$$

$$\varphi_{kp}(\omega) = \frac{(\omega_0-\omega)^2}{2\Delta\omega}NT_1 - N\,\text{arc tg}\,\frac{S(x_1)+S(x_2)}{C(x_1)+C(x_2)} - \omega N t_0. \quad (7)$$

Expressions (1), (2) and (4), (5) show that as a result of the difference in the compression factors of N times, the Fresnel pulsations of the

requisite transfer function of the matched filter on the whole and the Fresnelpulsations of the transfer function for one section have a different form (the number of pulsations and their amplitude), and the amplitude-frequency response of a single section falls off more slowly at the boundaries of the passband than the requisite amplitude-frequency response of the matched filter as a whole. It can be seen from a comparison of expressions (4), (5) and (6), (7) that the amplitude of the Fresnel pulsations in the resulting transfer function of the cascaded system increases over their amplitude in the transfer of a single section, and does so more significantly the greater the number of sections, N, while the number of pulsations remains unchanged. It is apparent that the bandwidth of the cascaded system is reduced as compared to the bandwidth of a single section. Thus, in a strict analysis, the resulting transfer function of the cascaded system does not coincide with the requisite transfer function of the matched filter as a whole.

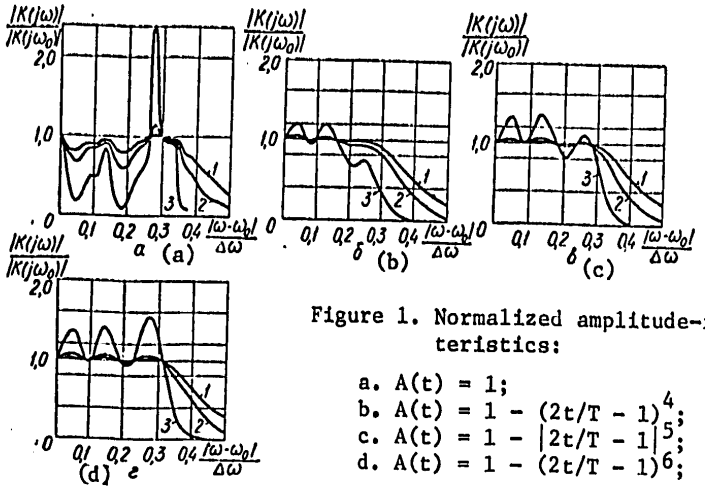

Figure 1. Normalized amplitude-frequency characteristics:

a. $A(t) = 1$;
b. $A(t) = 1 - (2t/T - 1)^4$;
c. $A(t) = 1 - |2t/T - 1|^5$;
d. $A(t) = 1 - (2t/T - 1)^6$;

1. One VShP;
2. Two VShP's (one section);
3. Five sections.

An increase in the Fresnel pulsations in the matched filter transfer function leads to a rise in the level of the side lobes of the compressed signal at the output of this filter [4]. The amplitude of the Fresnel pulsations in the resulting transfer function of the cascaded system can be reduced while maintaining the structures of the TAV sections identical by using sections, the pulse characteristics of which have smooth envelopes. For example, this can be achieved by varying the overlap of the electrodes of one (or both) of the opposing pin transducers (VShP) of each section.

The normalized amplitude-frequency characteristics of one nonequidistant VShP, one section with two nonequidistant VShP's and a cascaded system consisting of five identical sections were computed for various laws governing the envelopes A(t) of the pulse response using the method of δ analysis [5], for the case of $\Delta fT = 20$, $\Delta fT = 40$ and $\Delta fT = 200$ respectively, using the formula:

$$\frac{|K(j\omega)|}{|K(j\omega_0)|} = \left\{\frac{[C_1(\omega)]^2 + [C_2(\omega)]^2}{[C_1(\omega_0)]^2 + [C_2(\omega_0)]^2}\right\}^{\frac{1}{2}},$$

where

$$C_1(\omega) = \sum_{n=0}^{N} (-1)^n \frac{A(t_n)}{f_n} \cos \omega t_n, \quad C_2(\omega) = \sum_{n=0}^{N} (-1)^n \frac{A(t_n)}{f_n} \sin \omega t_n,$$

$n = 0, 1, 2, \ldots, N = 2f_0T$ is the number of electrodes of the nonequidistant VShP; t_n is the delay interval between the first and subsequent electrodes; f_n is the frequency of the VShP at the readout point t_n.

Graphs of the normalized amplitude-frequency characteristics for various laws governing the envelope A(t) of the pulse response are shown in Figure 1. These graphs show that amplitude-frequency characteristics having a large amplitude of the Fresnel pulsations correspond to a pulse response with a rectangular envelope. The use of pulse responses with smoothly changing envelopes permits a significant reduction in the amplitude of the amplitude-frequency characteristic pulsations, especially at the edges of the passband, and the bandwidth of a cascaded system is reduced in this case.

Thus, the cascade connection of N identical sections (filters) with a pulse response width of T/N and a bandwidth of Δf in the general case is not a matched filter for the processing of a linear FM signal of width T and bandwidth Δf. However, this is not a substantial drawback where it is necessary to obtain a compressed signal, the sidelobe level of which is less than 13 dB [4]. The maximum effectiveness of sidelobe level reduction will occur when using the smallest possible number of sections, which have the greatest possible compression factor D, for the corresponding shape of the pulse response envelope of the identical sections.

BIBLIOGRAPHY

1. White R., "Poverkhnostnyye uprugiye volny" ["Elastic Surface Waves"], TIIER, 1970, 58, No 8, p 68.

2. Holland M., Clayborn L, "Ustroystva na poverkhnostnykh akusticheskikh volnakh" ["Acoustic Surface Wave Devices"], TIIER, 1974, 62, No 5, p 45.

3. Lezin Yu. S., "Optimal'nyye fil'try i nakopiteli impul'snykh signalov" ["Optimal Filters and Storage Devices for Pulse Signals"], Moscow, Sovetskoye Radio Publishers, 1969.

4. Kuk Ch., Bernfel'd M., "Radiolokatsionnyye signaly" ["Radar Signals"], Moscow, Sovetskoye Radio Publishers, 1971.

5. Kadyshev Sh.K., Zibarov V.V., Ivanova I.A., "Chastotnyye kharakteristiki p'yezokvartsevykh ustroystv formirovaniya i obrabotki LChM impul'sov s apodizirovannymi preobrazovatelyami" ["The Frequency Characteristics of Quartz Piezoelectric Devices for the Generation and Processing of Linear FM Pulses with Apodized Transducers"], TR. LIAP [PROCEEDINGS OF THE LENINGRAD INSTITUTE OF AVIATION INSTRUMENT CONSTRUCTION], No 93, Leningrad, 1975, p 3.

8225
CSO:8144/1367

PULSE TECHNIQUE

UDC: 621.396

OPTIMIZATION OF PARAMETERS OF A MULTICHANNEL PULSE SIGNAL SCAN DEVICE

Kiev IVUZ RADIOELEKTRONIKA in Russian No 4, Apr 79 pp 80-82

[Article by Ye. A. Sherstnev]

[Text] There arises in various pulse radio systems the need to determine the location of a short pulse signal in a fairly long signal scan time interval. With periodic signal repetition and the occurrence of various kinds of radio interference this task as a rule is accomplished by accumulating data on the signal and interference during a certain number of repetition periods. Digital methods and devices for signal processing and accumulating the required information are the most promising to achieve this goal [1, 2, et al]. These devices perform amplitude binary quantization of the signal-noise mixture by comparing it with a certain threshold U_0 and formation at points where the threshold is exceeded of pulses which are standardized in amplitude and duration, fed to the scanning device. Of course there arises thereby the problem of optimizing quantity U_0, which is resolved taking into account concrete device operation algorithms, such as [3, 4]. In addition, in digital devices the entire time interval T_m of possible positions of the sought signal breaks down (is quantized in time) into a finite number N of individual regions, with an accuracy to the duration of which $\Delta T=T_m/N$ and the position of the signal is determined during scan. In this instance signal scan reduces to the well-known problem of isolating one signal channel from N channels, among which the remaining N-1 channels contain only noise. There exist a number of technical solutions to this problem. The simplest are scanning devices with one storage circuit, which is connected to one of N channels, and if on the basis of the results of accumulation of a number of binary-quantized pulses appearing in this channel during accumulation the decision is made that there is no signal in this channel, the storage circuit switches to the next channel, etc, until a signal detection decision is made. With high noise levels, however, the speed of such a device may prove to be unacceptably small. In order to increase speed one must employ more complex systems with several storage circuits, as many as N storage units operating simultaneously.

We evaluate below the influence of the magnitude of amplitude threshold of quantization U_0 and the duration of individual time segments Δt on the speed of a digital device for parallel signal scanning in all N regions with the aid of N storage devices during reception of a periodic signal mixed with

noise and random pulse interference (RPI). On the basis of this evaluation we obtained recommendations on optimal selection of parameters for such a scanning device.

We shall characterize the speed of operation of this scanning device with the number M signal repetition periods, which must be isolated for storing in the storage circuits information sufficient to indicate the signal channel (region ΔT in which it is located) with a specified probability of correct decision P. For certainty we shall also assume that in each k storage circuit a number is stored which is equal to the number of periods of signal repetition in which in k segment of interval T_m threshold U_0 was exceeded at least once by a mixture of signal and noise. Since in the signal segment there is present a sum of signal and noise, while in all other N-1 segments there is only noise, the probability of at least one time exceeding of threshold U_0 in a segment with signal p_s is always greater than probability p_n that the same threshold will be exceeded by noise alone in any of N-1 nonsignal segments. Then the probability of correct completion of scanning, that is, the probability that after M periods of storage the greatest number will be contained in the signal segment storage circuit is equal to

$$P = \sum_{l=1}^{M} [C_M^l p_s^l (1-p_s)^{M-l}] \left[\sum_{j=0}^{l-1} C_M^j p_n^j (1-p_n)^{M-j} \right]^{N-1}.$$

The given expression unambiguously links scanning device characteristics P and M with its parameters (ΔT, N, U_0) and the signal and noise parameters, which enter the expression for p_s and p_n. With independent action of noise and RPI exceeding threshold U_0, we have:

$$p_s = p_{s\delta} + p_p - p_{s\delta} p_p,$$
$$p_n = p_{n\delta} + p_p - p_{n\delta} p_p.$$

Here $p_p = 1-\exp(-\delta R_p/N)$ -- probability that at least one RPI pulse will fall in time segment $\Delta T = \delta\tau$; R_p -- average number of RPI pulses in interval T_m; τ -- signal pulse duration; $p_{s\delta}$ and $p_{n\delta}$ -- probabilities that threshold U_0 will be exceeded at least once in segment ΔT by a mixture of signal and noise and by noise alone respectively.

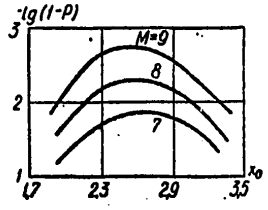

Figure 1.

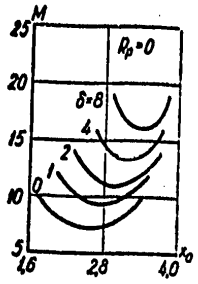

Figure 2.

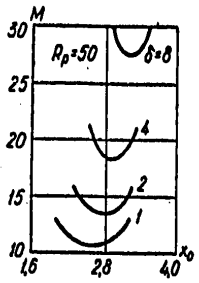

Figure 3.

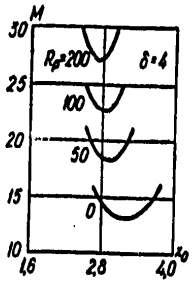

Figure 4.

Assuming that when the signal-from-noise filtration system band agrees with signal duration the noise output values taken in intervals exceeding signal pulse duration τ slowly varying, for $\delta>1$ we can assume [5] that:

$$p_{s\delta} = 1 - (1 - p_{s1})(1 - p_{n1})^{\delta-1},$$
$$p_{n\delta} = 1 - (1 - p_{n1})^{\delta},$$

where p_{s1} and p_{n1} -- probabilities that threshold U_0 will be exceeded by a signal-noise mixture and by noise alone respectively in time interval $\Delta T=\tau$. As we know from the literature [6, 7], probabilities that the threshold will be exceeded in a finite time interval can be written as functions of the duration of this time interval and of the probabilities that a given threshhold will be exceeded "at the point," calculated from univariate distributions of instantaneous values of a signal-noise mixture and noise alone. If we utilize the first approximations of these functions, obtained from the combined distribution of instantaneous values of a random process at a certain point and its derivative at the same point, and if we consider that this approximation is correct only in the correlation interval of the given process, which in this case may be placed close to 0.5 τ, then according to [6, 7] one can write:

$$p_{s1} = p_{s0} + (1 - p_{s0})[1 - \exp(-0{,}5\tau R_n)],$$
$$p_{n1} = p_{n0} + (1 - p_{n0})[1 - \exp(-0{,}5\tau R_n)].$$

Here, according to [8], $R_n = [x_0 \exp(-0{,}5x_0^2)]/\tau$ -- mean number of noise spikes per second, exceeding relative threshold $x_0=U_0\sigma$ (0.8 σ -- effective noise value at amplitude binary quantizer input), and

$$p_{s0} = \int_{x_0}^{\infty} r I_0(ra) \exp[-0,5(r^2 + a^2)]\, dr,$$

$$p_{n0} = \exp(-0,5x_0^2),$$

where a -- signal/noise ratio; $I_0(r)$ -- first-type zero-order Bessel function of imaginary argument.

The noted expressions make it possible to obtain qualitative relationships between scanning device characteristics, its parameters, signal and noise levels. Examples of these relationships, obtained with the aid of computer and tables [9] for a signal/noise ratio of a=3.5 and correct detection probability P=0.99, are contained in figures 1-5. Figure 1, for example, shows the relationships between spurious scan probability 1-P, scanning duration and the relative amplitude quantization threshold for the case of absence of RPI and N=2000, obtained with utilization of probabilities of surpassing "at the point" (p_{s0} and p_{n0}). It is evident from the path of the curves that for each prior-specified value of probability of correct completion of scan P there exists an optimal value of relative threshold x_0, which minimizes the duration of scan in the number of signal repetition periods M. This conclusion also remains valid when $\delta \geq 1$ and $R_p > 0$.

Figure 2 contains a family of dependences on threshold x_0 of the minimum number of repetition periods M requisite for ensuring the specified probability of correct detection with differing relative duration of analyzed segments and in the absence of RPI. Figure 4 illustrates relationship M with varying RPI for the case δ=4. Figure 5 shows the relationship between the smallest storage period numbers taken in the curve minima of figures 2-4 on the relative duration of the analyzed segments.

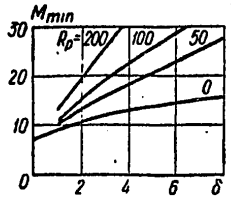

Figure 5.

Thus the above expressions make it possible to determine in each concrete case the requisite minimum storage time (expressed in number of signal repetition periods) and the corresponding optimal relative quantization threshold value.

The following conclusions can be drawn on the basis of the above.

There exists for any RPI value and relative duration of analyzed segments δ an optimal relative quantization threshold value x_0, minimizing storage time with a specified probability of correct detection. With an increase in the relative duration of analyzed segments the optimal quantization threshold value increases somewhat, while it decreases with an increase in RPI intensity. In view of this fact, with a specified signal/noise ratio and a sufficiently broad range of variation in RPI value and duration of analyzed segments, one can recommend establishing a "compromise" quantization threshold with a slight worsening of scanning device characteristics.

A decrease in the relative duration of analyzed segments δ at the same time leads to an increase in both accuracy and signal scan rate. The influence of δ thereby on the minimally requisite storage time proves to be more substantial with the existence of RPI than with noise alone. It follows from this that in order to obtain precise and rapid signal scanning systems one should reduce the relative duration of analyzed segments to $\delta=1$, although this also results in increased complexity of the scanning device by increasing the number of required storage circuits.

BIBLIOGRAPHY

1. Kuz'min, S. Z. "Osnovy teorii tsifrovoy obrabotki radiolokatsionnoy informatsii" [Principles of Theory of Digital Processing of Radar Information], Moscow, Sovetskoye radio, 1974.

2. Rabiner, L., and Gould, B. "Teoriya i primeneniye tsifrovoy obrabotki signalov" [Theory and Application of Digital Processing of Signals], Moscow, Mir, 1978.

3. Beloshitskiy, A. P., and Kravchenko, V. I. "Influence of Fluctuations of Computing Device Threshold on Detector Characteristics," RADIOTEKHNIKA, 30, No 11, 1975, page 87.

4. Ozerskiy, Yu. P. "Optimization of Clipping Threshold in a Rapid Signal Scan System," IZV. VUZOV -- RADIOELEKTRONIKA, 20, No 9, 1977, page 27.

5. Pavlov, V. D. "Refining the Efficiency of Two Modes of Storage," IZV. VUZOV -- RADIOELEKTRONIKA, 12, No 5, 1969, page 535.

6. Kuz'min, S. Z. "Tsifrovaya obrabotka radiolokatsionnoy informatsii" [Digital Processing of Radar Information], Moscow, Sovetskoye radio, 1967.

7. Fedosova, A. I. "Detecting Weak Repeating Signals in Noise With Binary Storage," RADIOTEKHNIKA, 32, No 12, 1977, page 39.

8. Bunimovich, V. I. "Flyuktuatsionnyye protsessy v radiopriyemnykh ustroystvakh" [Fluctuation Processes in Radio Receiving Devices], Moscow, Sovetskoye radio, 1951.

9. Bark, L. S., et al. "Tablitsy raspredeleniya Releya-Raysa" [Rayleigh-Rice Distribution Tables], USSR Academy of Sciences Computer Center, 1957.

Submitted 23 October 1978

3024
CSO: 1870

PULSE TECHNIQUES

UDC: 621.391.1:621.394.512

RECEPTION NOISE RESISTANCE IN A SYSTEM WITH QAM AND COMPLEX SIGNALS UNDER PULSE INTERFERENCE CONDITIONS

Kiev IVUZ RADIOELEKTRONIKA in Russian No 4, Apr 79 pp 87-90

[Article by G. Grigor'yev]

[Text] One of the possible ways to construct modems for data transmission at a rate of 9600 bit/s by tone frequency channels is employment of quadrature amplitude double-sideband two-level modulation (QAM).

As we know [1, 2], up to 20% of errors in transmitting data by wire channels are due to the influence of pulse interference. In transmission systems with a high rate of transmission and reduced protection against interference, the influence of pulse interference increases, since the quantity of low-amplitude noise is considerably greater than the quantity of high-amplitude noise. Elimination of errors during transmission by coding involves loss of transmission speed.

Employment of complex signals of increased duration makes it possible to reduce the influence of pulse interference on reliability of information transmission. As is shown in [3], a signal with linear frequency modulation (LFM) is optimal under conditions of pulse interference.

In view of the optimal nature of QAM, it is of interest to evaluate the influence of pulse interference on reliability of information transmission during utilization of signals with LFM as information carriers.

Construction of such a system is possible, for example, with the method described in [4]. In conformity with [4], conventional QAM signals are stretched during transmission by a first dispersion delay line (DDL). During reception the stretched signals are compressed by a second DDL, at the output of which the normal QAM signals are again obtained.

Figure 1 contains an aggregate of signals for a system with QAM. In Figure 1 the ends of the signal vectors are marked with dots, while the dashed lines indicate the boundaries of the correct reception zones. The coordinate axes also constitute boundaries of the correct reception zones.

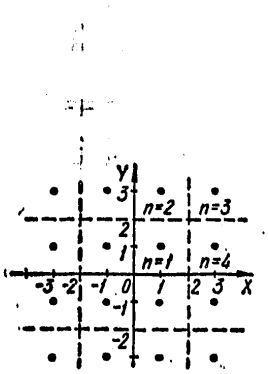

Figure 1.

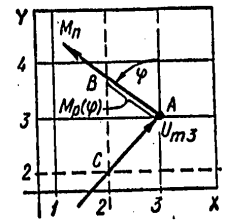

Figure 2.

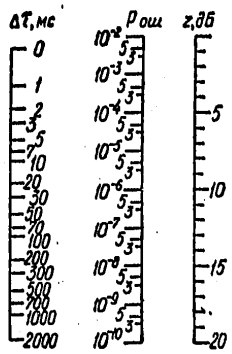

Figure 3.

It is easy to demonstrate that the probability of error for such a system can be determined with the formula

$$P_{ош} = \frac{1}{4}\sum_{n=1}^{N} P_{ошn}, \qquad (1)$$

where $P_{ош\ n}$ -- probability of incorrect signal registering, designated by subscript n in Figure 1; N=4.

In determining probability of error we shall assume that signals are fed to the receiver resolver input from the DDL output. We shall assume that transmission factor $K_д(j\omega)$ of this DDL is equal to

$$K_д(j\omega) = \exp[jk\omega^2]. \qquad (2)$$

Assuming that the interference spectrum at the DDL input has a modulus $S_п$ independent of frequency and a zero phase, we shall find interference spectrum $S_п(j\omega)$ at delay line output

$$S_п(j\omega) = S_п \exp[jk\omega^2], \quad \text{with} \quad -\frac{\pi}{T} \leqslant \omega \leqslant \frac{\pi}{T}. \qquad (3)$$

The interference time function $s_п(t)$ will be determined by a Fourier transform from (3). Utilizing the methodology from [5], we obtain

$$s_п(t) \cong \frac{S_п}{2\sqrt{\pi k}} \exp\left[-j\left(\frac{t^2}{4k} - \frac{\pi}{4}\right)\right], \quad \text{with} \quad |t| \leqslant 2\pi k/T. \qquad (4)$$

Expression (4) enables us to conclude that interference at the DDL output can be viewed as an LFM signal with modulus

$$M_п \cong S_п/2\sqrt{\pi k}. \qquad (5)$$

Possible deviations of the modulus value from the value determined by (5) do not exceed 34% with a small signal base and 17% with a large base.

We shall determine coefficient k by difference $\Delta\tau$ of DDL group delay time at the frequency range boundaries

$$k = \frac{\Delta\tau T}{4\pi}. \qquad (6)$$

Substituting (6) in (5), we obtain the mean interference modulus value at DDL output in relation to its length $\Delta\tau$

$$M_п = S_п/\sqrt{\Delta\tau T}. \qquad (7)$$

We shall compare the obtained interference signal with the interference signal at the DDL input $s'_П(t)$. It is obvious that

$$s'_п(t) = \frac{S_п}{T}\frac{\sin\frac{\pi}{T}t}{\frac{\pi}{T}t}. \qquad (8)$$

Expression (8) can be approximated by a rectangle of duration T and height $M'_П=S_П/T$.

Taking (7) into consideration, we shall determine the interference modulus attenuation factor $\Phi_Д$ of the dispersion delay line

$$\Phi_д = M'_п/M_п = \sqrt{\Delta\tau/T}. \qquad (9)$$

It is obvious that $\Phi_Д \geq 1$, while when $\Phi_Д=1$ the duration of interference is equal to ~$T=1/\Delta f$.

A decrease in the interference amplitude in the DDL changes by the increase in duration of interference to quantity $\Delta\tau$, that is, each interference pulse will act on L transmitted signals of the number L_0, where

$$L = \Delta\tau/T_п, \qquad (10)$$

while

$$L_0 = t_0/T_п \qquad (11)$$

In (10) $T_П$ is a value inverse to modulation rate B, while in (11) quantity t_0 determines the mean value of the interval between two pulse interferences. Taking into consideration (10) and (11), we determine $P_{ош}$ n

$$P_{ошп} = P_{сбп}L/L_0 = P_{сбп}\Delta\tau/t_0, \qquad (12)$$

APPROVED FOR RELEASE: 2007/02/09: CIA-RDP82-00850R000100070023-8

where $P_{сбn}$ -- conditional probability of failure of a single n alphabet element when affected by a single pulse interference.

We shall determine quantity $P_{сбn}$ in conformity with the method in [6], assuming that reception is performed by the single sample method.

As an illustration we shall find $P_{сбэ}$. Figure 2 shows the following:
a) signal vector $U_{mэ}=3\sqrt{2}U_1$, where U_1 -- single relative amplitude;
b) interference vector of length $M_п$ and phase ϕ. It is obvious that failure will always occur when $M_п$ is greater than quantity $M_п(\phi)$. Probability $P_{сбэ}$ will be determined by formula

$$P_{сбэ}=\int_{\varphi_0}^{\varphi_0}w(\varphi)\int_{M_p(\varphi)}^{\infty}w(M_п)\,d\varphi dM_п. \qquad (13)$$

We shall assume interference phase distribution $\omega(\phi)$ uniform:

$$w(\varphi)=1/2\pi, \quad \text{with} \quad -\pi<\varphi<\pi. \qquad (14)$$

We take interference amplitude distribution $\omega(M_п)$ from [7]:

$$w(M_п)=2\alpha M_{п0}^{2\alpha}/M_п^{2\alpha+1}, \qquad (15)$$

where $M_{п0}$ -- lower boundary of determination region of distribution $\omega(M_п)$, equal to 50 mV at tone frequency channel point with a measuring level equal to +4.34 db; α -- coefficient characterizing communications channel quality as regards pulse interference. $1<\alpha<3$.

From triangle ABC, utilizing the law of sines, we find

$$M_p(\varphi)=U_1/\sin\varphi. \qquad (16)$$

We shall perform a calculation for a channel of average quality (α=2). Substituting (14), (15), and (16) in (13) and integrating by $M_п$ within the indicated limits and by ϕ in limits from 0 to $3\pi/2$, we obtain

$$P_{сбэ}=A_3(M_{п0}/U_1)^4, \qquad \text{where } A_3=0.362.$$

By analogous calculations we obtain

$$P_{сбn}=A_n(M_{п0}/U_1)^4, \qquad (17)$$

where $A_1=0.727$; $A_2=A_4=0.555$.

Substituting (17) in (12) and (12) in (1), and considering that interference attenuates $\Phi_д$ times in the DDL, we find $P_{ош}$

$$P_{ош}=\frac{A\Delta\tau}{4f_0z_1^4\Phi_д^4}, \qquad (18)$$

where $z_1=U_1/M_{п0}$; $A=\sum_{n=1}^{4}A_n=2.2$.

For practical application it is convenient to establish dependence $P_{ош}$ on delay line length $\Delta\tau$ and mean statistical effective voltage of a random sequence of signals from a specified aggregate $U_{ср}$. Substituting (9) in (18) and considering that $T=1/\Delta f$, while $U_{ср} = \sqrt{2}U_{д}$, we obtain

$$P_{ош} = \frac{13{,}7}{\Delta f^3 t_0 \Delta\tau z^6}, \qquad (19)$$

where $z=U_{ср}/M_{ш0}$ (during transmission of signals with a mean power of 32 microwatts at a point with zero tone-frequency channel measurement level, z comprises ~13 db).

The graphic dependence of $P_{ош}$ on z with a logarithmic scale is represented with various $\Delta\tau$ by parallel straight lines with a slope factor of -1.588 times/db (-1 order of magnitude for every 5 db).

In selecting a delay line with specified $P_{ош}$ and z, it is more convenient to utilize a nomogram (Figure 3), which also makes it possible to find $P_{ош}$ with certain $\Delta\tau$ and z, etc, in conformity with (19). The nomogram is constructed for $t_0=0.625$ s and $\Delta f=3100$ Hz. The value of any of the indicated variables is read on the corresponding scale at the point of intersection of this scale with a straight line which intersects the other scales at points determined by the specified values of the two other variables.

Utilizing the nomogram, it is easy to see that an increase in reliability of transmission by two orders of magnitude is secured with utilization of a DDL with $\Delta\tau=30$ ms, and that an equal increase in reliability can be achieved by raising the signal level by 10 db. A nomogram can also be employed to determine allowable decrease in signal level when the effect of pulse interference increases substantially.

In addition, by employing a nomogram one can establish that an increase in reliability by three orders of magnitude requires a very substantial increase in length of the DDL (to 300m, s), which evidently is not always feasible.

As a result of our investigations we have demonstrated that employment of complex signals as carriers in a wire channel information transmission system with QAM makes it possible substantially to increase reliability of transmission; in developing and utilizing such systems an evaluation of the effect of pulse interference can be easily performed with the aid of nomograms with parallel scales.

BIBLIOGRAPHY

1. "Kanaly peredachi dannykh" [Data Transmission Channels], Moscow, Svyaz', 1970.

2. Bomshteyn, B. D.; Kiselev, L. K.; and Morgachev, Ye. T. "Metody bor'by s pomekhami v kanalakh provodnoy svyazi" [Methods of Combatting Interference in Wire Communication Channels], Moscow, 1975, Svyaz'.

3. Klyuyev, V. F. "Selection of an Optimal Signal Waveform Under Conditions of Pulse Interference," IZV. VUZOV -- RADIOELEKTRONIKA, 18, No 4, 1975, page 118.

4. Kiselev, L. K., and Meshkov, A. A. "Method of Increasing the Noise Immunity of Data Transmission Channels With Pulse Interference and Interruptions in the Line," ELEKTROSVYAZ', No 5, 1966, page 28.

5. Varakin, L. Ye. "Teoriya slozhnykh signalov" [Theory of Complex Signals], Moscow, Sovetskoye radio.

6. Kuritsyn, S. A. "Noise Stability of Reception of FM Signals With Obliteration Under Conditions of Pulse Interference," Moscow, TUIS, No 47, 1979.

7. Brusilovskiy, K. A., and Bleykhman, V. S. "Univariate Density of Probability of Pulse Interference in a Low-Frequency Communication Channel," VOPROSY RADIOELEKTRONIKI, Series 11, 1964, Issue 6.

Submitted 6 January 1978;
Revised and resubmitted 19 June 1978

3024
CSO: 1870

RADAR

UDC 621.371.(211.6)

DISTINGUISHING AGE CATEGORIES OF SEA ICE IN RADAR AND RADIOTHERMAL OBSERVATIONS IN THE MICROWAVE BAND

Moscow RADIOTEKHNIKA in Russian No 4, Apr 79 pp 31-35

[Article by A. Ye. Basharinov (deceased) and A. A. Kurskaya]

[Text] Numerous experimental studies on radioprobing of sea ice of various ages [Ref. 1-10] have shown changes in the intensity of radiation and scattering of radio waves, which has enabled remote evaluations of the condition of ice fields. Successful work has been done on using pulsed SHF waves to determine the thickness of ice [Ref. 6]. In this paper experimental materials on radiothermal emission and scattering of radio waves in ice covers are compared with the data of model calculations, and it is shown how structural changes influence the radiative indices of ice covers. Development of models for sea ice with strong and moderate absorption and porous structures enables description of the peculiarities of the radiative indices of young ice, ice with low salinity and pack ice. The analysis shows the possibilities of remote differentiation of age gradations of ice.

Sea ice is a complex system that contains crystals of fresh-water ice and cells of brine. The growth process of young sea ice is accompanied by displacement of brine from capillaries and a reduction in the amount of liquid phase due to freezing out.

The salinity of the ice depends on the salinity of the water and the conditions of ice formation. Correlations have been found between the salinity of the surface layer and the thickness of the ice, varying from 20‰ (for thin ice up to 5-10 cm) to 3-5‰ (for ice 1-1.8 m thick). The relative amount of liquid phase W_i is related to the salinity of the ice:

$$W_i = S_i \Psi(T), \qquad (1)$$

where $\Psi(T) = \frac{\Gamma}{S_B(T)}$, $S_B(T)$ is the temperature-dependent salinity of the brine.

Infrared research data show that the temperature of the upper layer of ice differs from the air temperature; this difference decreases with an increase in the thickness of the ice.

The permittivity of specimens of sea ice consisting of crystals of fresh-water ice and brine is a function of the volumetric moisture content, and is approximated by the linear expression

$$\varepsilon_l = \varepsilon_{l0} + W_l(\varepsilon_W - \varepsilon_{l0}), \tag{2}$$

where ε_{l0} and ε_W are the permittivities of fresh-water ice and water. A change in the weight content of brine during growth of the ice causes considerable changes in the loss tangent in ice specimens, which has been experimentally confirmed [Ref. 5, 10].

The absorption of radio waves in young sea ice in the centimeter wave band is characterized by values of 100-500 dB/m (the thickness of the skin layer being a few centimeters). The moisture content in ice with low salinity under similar temperature conditions is noticeably lower than that in young sea ice. In virtue of this, the dielectric properties of ice with low salinity lie in a narrow range of values. The conditions of thawing during the warm season are conducive to creation of a porous structure of the upper layer of pack ice.

Let us examine typical electrodynamic models of ice covers:

saline sea ice with a thin skin layer;

ice covers with moderate absorption, modeled by multilayer structures;

pack ice of porous structure.

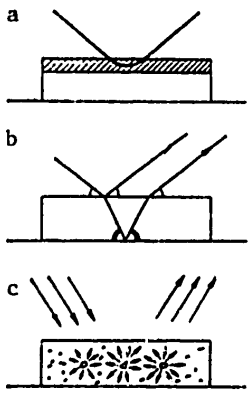

Fig. 1

A schematic representation of processes of reflection and scattering in the investigated models is shown in Fig. 1. The theoretical expressions that relate the indices of the state and the radiative properties of ice covers can be compared with the observed experimental relations.

For young sea ice with a thin skin layer the relations for emissivity as a function of the permittivity of the upper layer of ice under conditions of the Fresnel approximation for vertical and horizontal polarizations take the form

$$\varkappa_V(\theta) = 1 - \left[\frac{\varepsilon_l \cos\theta - \sqrt{\varepsilon_l - \sin^2\theta}}{\varepsilon_l \cos\theta + \sqrt{\varepsilon_l - \sin^2\theta}}\right]^2, \tag{3}$$

$$\varkappa_H(\theta) = 1 - \left[\frac{\cos\theta - \sqrt{\varepsilon_l - \sin^2\theta}}{\cos\theta + \sqrt{\varepsilon_l - \sin^2\theta}}\right]^2, \tag{4}$$

where θ is the angle of observation, ε_l is the permittivity of the upper layer of ice.

Surface roughness has a comparatively weak effect on the formation of the radiation flux, and in the first approximation can be disregarded. Relations

for emissivity as a function of thickness are calculated with consideration of (1)-(4) and data on the surface temperature of ice of different thicknesses. A comparison of calculated and experimental data on the emissivity of young sea ice on the Kara Sea and the Laptev Sea obtained during the spring in 1976 and 1977 can be seen in Fig. 2 and 3 for directions of vertical observation ($\theta = 0$). As we can see, in observations on wavelengths of 0.8 and

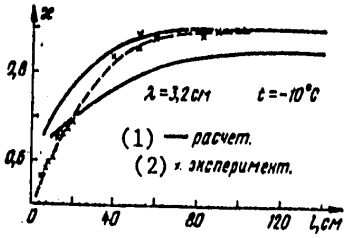

Fig. 2

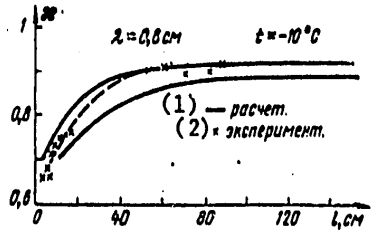

Fig. 3

KEY: 1--calculated
2--experimental

3.2 cm the experimental data agree well with the calculations. The slope of the curve $\kappa = f(l)$ remains nearly constant for ice thickness up to 70 cm; it declines noticeably at 70-150 cm. Data of microwave radiometric observations permit differentiation of 6-8 gradations of young ice up to 1.5 m thick.

The scattering properties of young sea ice as a rough surface are characterized by the backscattering pattern. For small-scale roughness with cylindrical surface relief the relations for the coefficient of backscattering take the form

$$\sigma_{HH} \equiv \frac{4}{\pi} k^4 \sigma_h^2 \cos^4\theta \left| \frac{\varepsilon_l - 1}{\left[\cos\theta + \sqrt{\varepsilon_l - \sin^2\theta}\right]^2} \right|^2 \Phi(\varkappa_0), \qquad (5)$$

$$\sigma_{VV} \equiv \frac{4}{\pi} k^4 \sigma_h^2 \cos^4\theta \left| \frac{(\varepsilon_l - 1)(\varepsilon_l - \sin^2\theta + \varepsilon_l \sin^2\theta)}{\left[\varepsilon_l \cos\theta + \sqrt{\varepsilon_l - \sin^2\theta}\right]^2} \right|^2 \Phi(\varkappa_0), \qquad (6)$$

where $\Phi(\kappa_0)$ is the spectral density of surface unevennesses at values of $\kappa_0 = 2k \sin 0$; σ_h is the effective value of the height of irregularities. Relations (5) and (6) can be used for comparison with experimental data. As shown by radar measurements made on a wavelength of about 2 cm by Parashar et al. [Ref. 7], when ice is up to 50-70 cm thick one observes a reduction in the coefficient of backscattering as ice thickness increases, which is caused by a reduction in the dielectric constant of the upper layer of ice in agreement with calculated data.

When the ice is more than 60 cm thick, the observed increase in the coefficient of backscattering is due to the influence of unevenness of the ice surface. The table summarizes the comparison of calculated $\Delta\sigma_c$ and experimental $\Delta\sigma_e$ indices of the change in the coefficient of backscattering for thin ice (the angles of observation were 20-30°).

l, cm	$\Delta\sigma_c$, dB	$\Delta\sigma_e$, dB
10-20	1.5-2.5	2.5-3
20-40	0.5-1.5	0.5-1
40-60	0.5-1	0.5-1

The range of distinguishable states of ice is extended by measuring the values of the coefficient of backscattering in the centimeter and decimeter bands, which enables remote evaluations of 5-6 age gradations of young ice.

The peculiarities of the radiative and scattering properties of ice covers with moderate absorption are determined by the influence of reflections from the lower edge and inhomogeneities in the intermediate layers of ice. Ice in this class is modeled by multilayer structures. For a two-layer isothermal model the dependence of the emissivity of ice on thickness (in the case of observation with a narrow field of view) is characterized by interference oscillations as the ice thickness changes:

$$\varkappa_\lambda(0) = \frac{(1-R_1)\left(1-R_2 e^{-\tau_\lambda}\right)}{1+R_1R_2e^{-2\tau_\lambda}+\sqrt{R_1R_2}e^{-2\tau_\lambda}\cos\left[2kl\cos\vartheta+\varphi_1+\varphi_2\right]}, \qquad (7)$$

where R_1, ϕ_1, R_2, ϕ_2 are the moduli and phases of the coefficients of reflection from the upper and lower edges of the ice; $\tau_\lambda = \gamma_\lambda l$ is the integral absorption of radio waves in an ice layer of thickness l; γ_λ is the linear coefficient of absorption.

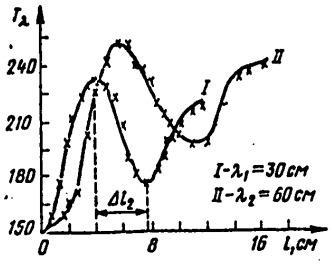

Fig. 4

Analysis of experimental data on radiothermal emission during ice growth in the Kara Sea in 1965 (Fig. 4) with the use of a two-layer model (7) enabled evaluation of the permittivity and coefficient of absorption of radio waves in the ice layer. For the example shown in Fig. 4, they were $\varepsilon_i \approx 4$, $\gamma \approx 10$ dB/m respectively on a wavelength of 50 cm. The influence of interference effects also shows up in observations of intensity dependences of scattering of sea ice in the decimeter band.

In observations of radiothermal emission of ice with a field of view of finite dimensions, the interference oscillations are "washed out" and the dependence of emission intensity on thickness becomes monotonic:

$$T_a = (1-R_1)\left[(1-R_2)T_0e^{-\tau_\lambda}+\int_0^l T(h)\gamma_\lambda(h)e^{-\int_0^h \gamma_\lambda(x)dx}dh\right], \qquad (8)$$

where T_0 is the temperature on the water-ice interface; T(h) is the vertical profile of temperature distribution through the ice thickness.

Observations of radiothermal emission for Baltic Sea ice up to 90 cm thick have demonstrated a monotonic relation between emission intensity on decimeter

waves and ice thickness [Ref. 4]. Such relations for ice with moderate absorption permit radiometric evaluation of the thickness of ice covers.

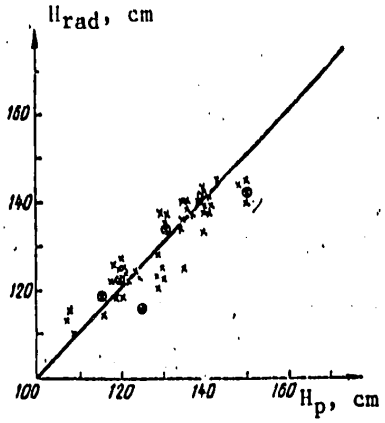

Fig. 5

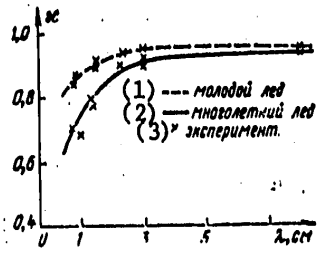

Fig. 6

KEY: 1--young ice
2--old ice
3--experiment

Fig. 5, comparing the values of radiometric estimates of the thickness of fresh-water ice at the mouth of the Ob' with thicknesses found by pulse probing, demonstrates the feasibility of distinguishing 6-8 gradations of ice thickness with low salinity up to a thickness of 1.5 m.

Pack ice has a porous structure that is formed during the summer thaw of the upper layer of ice. The degree of porosity of pack ice may reach several dozen percent. Air bubbles and structural inhomogeneities cause scattering of radio waves, which has an effect on the indices of radiothermal emission and backscattering of radio waves.

The emissivity and coefficient of backscattering of an ice layer are determined with consideration of internal scattering:

$$\varkappa_\lambda \approx (1 - R_1)(1 - \rho_\lambda) \quad (9), \qquad \sigma_\lambda = \sigma_{S\lambda} + \sigma_{V\lambda}, \quad (10)$$

where $\rho_\lambda = \Sigma\sigma_{\lambda i}$ is the index of volumetric scattering of inhomogeneities; $\sigma_{\lambda i}$ is the scattering cross section of the i-th inhomogeneity; $\sigma_{S\lambda}$ is the component of surface scattering; $\sigma_{V\lambda}$ is the component of volumetric scattering.

The spectral dependence of the index of volumetric scattering is determined by the ratio of the dimensions of inhomogeneities and wavelength, and is weakly selective in nature. For actual dimensions of inhomogeneities there is an increase in the coefficient of scattering and a reduction of emissivity as the wavelength decreases [Ref. 3, 9].

The calculated and experimental values of the spectrum of emissivity of old (pack) and young sea ice are shown in Fig. 6. The experimental data were obtained by analyzing the results of observations on board the Kosmos-243 spacecraft and the U. S. Convair-990 flying laboratory.

The spectral indices of scattering intensity enable use of radiometric and radar methods for distinguishing young ice and pack ice and for evaluating the degree of porosity of the structure of ice cover.

Conclusions. The radiation models of ice covers that have been developed provide a quantitative description of the governing principles in available experimental data.

The results characterize the effectiveness of the remote method of determining the state of sea-water and fresh-water ice by means of passive and active probing in the microwave band, which can be used on artificial satellites and aircraft.

REFERENCES

1. A. A. Kurskaya, A. V. Fedorova, G. D. Yakovleva, "Trudy Glavnoy geofizicheskoy observatorii" [Transactions of the Main Geophysics Observatory], No 222, Leningrad, Gidrometeoizdat, 1968.

2. W. Nordberg, J. Conaway, D. Ross, JOURN. ARM. SCI., Vol 28, No 3, 1971.

3. T. Wielheit, W. Nordberg et al., REM. SENS OF ENVIRONMENT, Vol 2, No 1, 1972.

4. M. Tuiri, M. Hallikainen, K. Kaski, "Proc. URSI Spec. Meet. on Microwave Scatter. and Emission from the Earth," Bern, 1974.

5. "Sovetsko-amerikanskiy eksperiment 'Bering'" [The U. S.-Soviet "Bering" Experiment], Leningrad, Gidrometeoizdat, 1975.

6. M. I. Finkel'shteyn, V. L. Mendel'son, V. A. Kutev, "Radiolokatsiya sloistykh zemnykh pokrovov" [Radar Detection of Layered Ground Covers], Moscow, Sovetskoye radio, 1977.

7. S. Parashar, A. Biggs, A. Fung, R. Moore, "Proc. of IX Internat. Symp. on Rem. Sens. of Environment," Ann Arbor, Michigan, 1974.

8. L. T. Tuchkov, A. Ye. Basharinov (deceased), M. A. Kolosov, A. A. Kurskaya, "Trudy Glavnoy geofizicheskoy observatorii," No 222, Leningrad, Gidrometeoizdat, 1968.

9. A. Ye. Basharinov (deceased), A. A. Kurskaya, in the book: "Issledovaniye prirodnoy sredy kosmicheskimi sredstvami" [Using Space Technology to Study the Natural Environment], Vol 3, Moscow, USSR Academy of Sciences, 1974.

10. M. Hallikainen, "Dielectric Properties of Sea Ice at Microwave Frequencies," Res. S. 94, Helsinki Univ. of Technol., 19`7.

6610
CSO: 1870

RADAR

UDC 621.369.967:621.391.82

OPTIMUM EVALUATION OF THE PARAMETERS OF TRAJECTORIES OF A GROUP OF MOVING OBJECTS

Moscow RADIOTEKHNIKA in Russian No 4, Apr 79 pp 74-76

[Article by V. V. Mkrtumov]

[Text] To suppress signals reflected from meteorological elements and nearby objects, circular-scan radars use methods based on the high degree of correlation of these signals from one scan to the next. Realization of such methods requires high precision in measuring the coordinates of the interference and the rate of its displacement. Moreover, 90% of the volume of instrument expenditures go for the main memory unit. To increase the effectiveness of interference suppression and reduce equipment expenditures, one can utilize the property of interference to move in space at a velocity that is the same for a group of several objects.

The signals at the input of the processing device are the coordinates of pips that arrive in certain time intervals equal to the period of rotation of the antenna with errors determined by the radar accuracy characteristics.

Considering that the displacement of meteorological interferences takes place as a rule under the action of wind with some constant velocity, the trajectories of the paths can be approximated with a small error by a polynomial of first degree. Since the measurement errors for three coordinates are independent, it is sufficient to find the solution for a single coordinate. The solutions for other coordinates are analogous. We represent the signals in the form

$$Y(A_1 t) = a_{01} + a_1 t,\ Y(A_2 t) = a_{02} + a_1(t), \ldots,\ Y(A_m t) = a_{0m} + a_1 t, \qquad (1)$$

where a_{0i} is the initial position of the object; a_1 is the velocity of displacement of the objects, which is the same for all paths. The realization for a fixed sample space is the set of coordinates

$$y_{ij} = a_{0i} + a_1 t_j + \xi_{ij}, \qquad (2)$$

where the ξ_{ij} are independent random quantities distributed according to a normal law; i is the number of the path of the object; j is the scan number.

To get an algorithm for evaluating the parameters a_{0i} and a_1, we use the method of maximum likelihood. The likelihood function is written as

$$L(Y_{11}Y_{12}Y_{13},\ldots,Y_{mn}/A_1A_2,\ldots,A_m)=\frac{1}{(\sqrt{2\pi}\sigma)^{mn}}\exp\left\{-\frac{1}{2\sigma^2}\sum_{i=1}^{m}\sum_{j=1}^{n}\xi_{ij}^2\right\}. \quad (3)$$

where σ^2 is the standard deviation of the random quantity.

By differentiating (3) with respect to the components a_{0i} and a_1 and setting the results equal to zero, we get a system of equations that can be solved to get an estimate of the parameters a_{0i}^* and a_1^*. Since the scan period is constant, instead of a_1 we can get a more convenient quantity -- the increment of a coordinate during the scan $u^*=a_1^*T_0$, where T_0 is the period of rotation of the antenna. With T_0 constant for each scan

$$a_{0i}^*=\frac{\sum_{j=1}^{n}y_{ij}}{n}-\sum_{i=1}^{m}\sum_{j=1}^{n}\frac{6j-3-3n}{n(n+1)}y_{ij},\quad u^*=\sum_{i=1}^{m}\sum_{j=1}^{n}\frac{12j-6-6n}{mn(n^2-1)}y_{ij}.$$

The estimate of the coordinate of the i-th path smoothed for the last scan

$$a_{ni}^*=\frac{1}{n}\sum_{j=1}^{n}y_{ij}+\sum_{i=1}^{m}\sum_{j=1}^{n}\frac{6j-3-3n}{mn(n-1)}y_{ij},$$

and the value of its coordinate extrapolated on the $n+1$-th scan

$$a_{n+1}^*=\frac{1}{n}\sum_{j=1}^{n}y_{ij}+\sum_{i=1}^{m}\sum_{j=1}^{n}\frac{6j-3-3n}{mn(n-1)}y_{ij}.$$

The standard deviation of measurement errors for the quantities u, a_η, $a_{\eta\vartheta}$ in evaluation by these rules is equal to

$$\sigma_u^2=\sigma_y^2\frac{12}{n(n^2-1)m};$$

$$\sigma_{a\eta}^2=\sigma_y^2\frac{\sum_{j=1}^{n}[(n+1)m+6j-3-3n]^2+(m-1)(6j-3-3n)^2}{n^2(n+1)^2m^2};$$

$$\sigma_{a\vartheta}^2=\sigma_y^2\frac{\sum_{i=1}^{m}[(n-1)m+6j-3-3n]^2+(m-1)(6j-3-3n)^2}{n^2(n+1)^2m^2},$$

where σ_y^2 is the standard deviation of the error of measurement of the y coordinate.

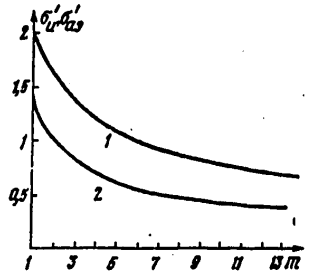

Fig. 1

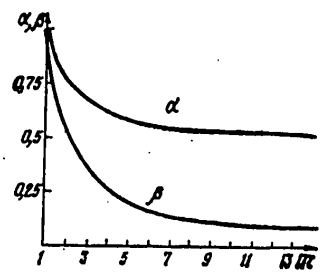

Fig. 2

Shown in Fig. 1 are relations for the normed value of the rms deviation $\sigma_u' = \sigma_u/\sigma_y$ (curve 1) and $\sigma_{a\ni}' = \sigma_{a\ni}/\sigma_y$ (curve 2) as a function of the number of paths in evaluation of the parameters of the paths on two scans (n = 2). As can be seen from the curves, even for n = 2 high accuracy can be obtained in evaluating the parameters of trajectories by processing a group of paths.

The memory volume required for storing information on the velocity increment is reduced by a factor of m. The memory volume required for storing information on the position of an object on n scans remains large. This volume is reduced by using the method of sequential smoothing of the parameters of the trajectory.

The essence of the method of sequential (iterative) smoothing consists in the fact that the smoothed value of the i-th estimate in the succeeding j-th scan is determined from preceding values obtained in the (j - 1)-th scan, and the results of observations in the (j - 1)-th scan. In evaluating each parameter, only two numbers are used -- the preceding estimate and the result of the k-th observation.

A technique described in Ref. 1 was used to get a recurrent algorithm for estimating the parameters of the trajectories. Algorithms of parameter evaluation for groups of objects turn out to be the same as for an isolated object:

$$u^*_{kn} = u_{k-1,\,n} + \beta\left[y_{kn} - a^*_{kn\ni}\right];\ a^*_{kn} = a^*_{kn\ni} + \alpha\left[y_{kn} - a^*_{kn\ni}\right],$$

where $\beta = \frac{6}{n(n-2)m + 3k}$ is the coefficient of smoothing of the estimate of the increment of the coordinate of the objects; $\alpha = \frac{3(n-1)}{n[(n-2)m + 3k]} + \frac{1}{n}$ is the coefficient of smoothing of the estimate of the position of the objects; $a^*_{kn\ni} = a^*_{k(n-1)} + u^*_{kn}$ is the extrapolated value of the y coordinate for path k as calculated on the n-th scan after evaluating the velocity increment from the preceding (k - 1)-th path.

Shown in Fig. 2 are the coefficients of smoothing α and β as functions of the number of paths m for evaluating the parameters of trajectories from two scans. It is clear from the graph that as m increases, α falls to 0.5, and β approaches zero. Moreover, the graph shows that it is possible to estimate the value of the extrapolation point of a path with high accuracy even on the second scan.

Conclusions. 1. Accounting for the mutual correlation of the velocity of displacement of objects enables improvement of the accuracy of measuring the parameters of the trajectories of the objects and reduces the memory volume for storing information on the velocity of their displacement.

2. The memory volume needed for storing information about the position of objects is reduced by the method of sequential smoothing.

3. In principle it is possible to evaluate the position of an extrapolation point as early as on the second scan.

REFERENCE

1. S. Z. Kuz'min, "Tsifrovaya obrabotka radiolokatsionnoy informatsii" [Digital Processing of Radar Information], Moscow, Sovetskoye radio, 1974.

6610
CSO: 1870

SIGNAL PROCESSING

UDC 621.396.96:621.391.26

A UNIFIED REPRESENTATION OF THE ORTHOGONAL MATRICES USED IN DIGITAL SIGNAL PROCESSING

Moscow RADIOTEKHNIKA I ELEKTRONIKA in Russian Vol 24 No 1, 1979 pp 66-71

[Article by L.P. Yaroslavskiy, manuscript received 26 Dec 77]

[Text] A representation is given for the matrices of the orthogonal transforms used in digital signal processing in the form of sums of Kronecker matrices, where this representation is convenient for the design of fast transform algorithms using the tools of matrix algebra.

Signal transforms with orthogonal matrices are widely employed in the digital processing of signals, and especially, images: the Haar transform, Walsh-Hadamar transforms, discrete Fourier transform, transforms using Wilenkin-Krestenson functions (VKF), the modified Hadamar transform, the hybrid Hadamar-Haar transform, and others [1 - 2]. All of these transforms are remarkable in that the matrices corresponding to them can be represented in the form of a product lightly filled matrices, because of which there exist so-called transform algorithms (the fast Fourier transform, fast Hadamar transform, fast Haar transform, and others). This is evidence of the deep kinship of these transforms. To further develop the family of such transforms, it would be desirable to ascertain the roots of this relationship: to formulate a unified representation for all of these matrices.

As is well known, the existence of fast Walsh-Hadamar transform algorithms, and in general, those using VKF's is based on the fact that the corresponding matrices are Kronecker matrices, i.e., they take the form of the direct (Kronecker) product of certain elementary matrices [2 - 4]. It was demonstrated in [5] how by means of a specified generalization of the concept of the Kronecker product of matrices, fast algorithms can be designed for both Kronecker matrices and for such a non-Kronecker matrix as the discrete Fourier transform matrix. This paper analyzes how by means of representing transform matrices in the form of sums of Kronecker matrices, one can obtain a unified description for all of the transforms enumerated above and a unified method of deriving the fast algorithms of these transforms.

We shall introduce the following elementary matrices:

$$
\begin{aligned}
&V_2^0 = \begin{bmatrix} 1 \\ 0 \end{bmatrix}; \quad V_2^1 = \begin{bmatrix} 0 \\ 1 \end{bmatrix};\\
&G_2^0 = [1\ 0]; \quad G_2^1 = [0\ 1]; \quad G_2^2 = [1\ 1]; \quad G_2^3 = [1\ -1];\\
&I_2 = \begin{bmatrix} 1 & 0 \\ 0 & 1 \end{bmatrix}; \quad J_2 = \begin{bmatrix} 0 & 1 \\ 1 & 0 \end{bmatrix}; \quad h_2 = \begin{bmatrix} 1 & 1 \\ 1 & -1 \end{bmatrix};\\
&d_4 = \begin{bmatrix} 1 & 0 \\ 0 & \exp(2\pi\sqrt{-1})(1/2^4) \end{bmatrix}.
\end{aligned} \tag{1}
$$

and the symbols

$$
\delta_i = \begin{cases} 0, & i=0; \\ 1, & i\neq 0; \end{cases} \tag{2}
$$

$M^{[n]}$ is the n-th Kronecker degree of the matrix; Пр is the Kronecker product of several matrices. Then the matrices of the following transforms: Haar HAR_{2^n}, Walsh-Hadamar HAD_{2^n}, Walsh-Pali PAL_{2^n}, Walsh WAL_{2^n}, the modified Hadamar transform $MHAD_{2^n}$, the mixed Hadamar-Haar transform $HDHR_{2^n}^{(F)}$, discrete Fourier transform $FOUR_{2n}$, and the VKF transforms G_{2n} can be represented in the form of Kronecker products or the sums of Kronecker products of these elementary matrices, as shown in Table 1. Also shown in the last four rows of this table is how such matrices as a binary inversion permutation matrix $M_{2n}^{инв}$, the transposition matrix from a Gray code to a direct binary code $M_{2^n}^{гр/пр}$, transition matrices from a Haar transform to a Pali transform M_{2n}^{H-P} and from a modified Hadamar transform to a discrete Fourier transform (DPF) M_{2n}^{MH-F} can be represented in the form of the sums of Kronecker products.

Such a representation creates a convenient basis for the comparison of all of the transforms with each other. Thus, by comparing the HAR_{2n} and the $MHAD_{2n}$ matrices, it is easy to note that they differ in the inverted order of the repetition of the G_2^2, G_2^3 and I_2 matrices in each term*, the $MHAD_{2n}$ matrix differs from the HAD_{2n} matrix in that it is not built on H_2, but rather I_2, etc. Moreover, this representation makes it possible to set up

*We will note that matrices of the V_2 and G_2 type can change places in the Kronecker product. Changing the order of the repetition of V_2 type matrices in their Kronecker product yields the corresponding transposition of the rows of the resulting matrix, while changing the order of repetition of type G_2 matrices in their Kronecker product yields a double inversion of the columns.

a factorized representation of the matrices, which is the basis for fast transform algorithms, by means of simple matrix algebra operations, employing the well-known properties of a direct sum and direct (Kronecker) product of the matrices and the following four theorems, the proof of which we shall leave out because of their simplicity.

Theorem 1. If the matrix M can be broken down into two submatrices with a horizontal line, each of which is the product of a certain two matrices:

$$M=\left[\frac{M^{(1)}_{r,s}\cdot M^{(2)}_{s,q}}{M^{(3)}_{u,v}\cdot M^{(4)}_{v,q}}\right],$$

Then

$$M=[M^{(1)}_{r,s}\oplus M^{(3)}_{u,v}]\left[\frac{M^{(2)}_{s,q}}{M^{(4)}_{v,q}}\right],$$

where $\oplus$ is the symbol for the direct sum of the matrices.

Theorem 2. If the matrix M can be broken down into two submatrices with a horizontal line, each of which is the direct (Kronecker) product of a particular matrix-row by a particular matrix:

$$M=\left[\frac{G^{(1)}_{1,s}\times M^{(1)}_{r,s}}{G^{(2)}_{1,b}\times M^{(2)}_{p,q}}\right],$$

Then

$$M=[M^{(1)}_{r,s}\oplus M^{(2)}_{p,q}]\left[\frac{G^{(1)}_{1,s}\times I_s}{G^{(2)}_{1,b}\times I_q}\right]$$

where $\times$ is the symbol for the Kronecker product of the matrices; I_s, I_q are unit matrices of dimensions s x s and q x q resp cively.

Theorem 3. The Kronecker matrix

$$M=M^{(1)}_{r,s}\times M^{(2)}_{q,p}$$

can be represented in the form of the product of two lightly filled matrices*:

$$M=(M^{(1)}_{r,s}\times I_q)\,(I_s\times M^{(2)}_{q,p}).$$

*This theorem for square matrices was formulated and proved in [3].

Theorem 4:

$$\left[\frac{M^{(1)}_{r,s} \times G^{(a)}_{1,2}}{M^{(2)}_{p,s} \times G^{(b)}_{1,2}}\right] = \left[\frac{G^{(a)}_{1,2} \times M^{(1)}_{r,s}}{G^{(b)}_{1,2} \times M_{p,s}}\right]\left[\frac{I_s \times G^0_2}{I_s \times G^1_2}\right].$$

TABLE 1

Transform Преобразование	Representation in Terms of Elementary Matrices Представление через элементарные матрицы
Преобразование Хаара (ХП)	$HAR_{2^n} = \frac{1}{2^{n/2}} \sum_{i=0}^{n} \left(2^{\frac{i-1}{2}}\right)^{\delta_i} (V^0_2)^{[n-i]} \times \times [V^1_2 \times (I_2)^{[i-1]} \times G^1_2]^{\delta_i} \times (G^0_2)^{[n-i]}$ Haar Transform (KhP)
Преобразование Уолша – Адамара (У – АП)	$HAD_{2^n} = \frac{1}{2^{n/2}} \sum_{i=0}^{n} (V^0_2)^{[n-i]} \times (G^0_2)^{[n-i]} \times \times [V^1_2 \times G^0_2 \times (h_2)^{[i-1]}]^{\delta_i} = \frac{1}{2^{n/2}} (h_2)^{[n]}$ Walsh-Hadamar Transform (U-AP)
Преобразование Уолша – Пэли, (У – ПП)	$PAL_{2^n} = \frac{1}{2^{n/2}} \sum_{i=0}^{n} (V^0_2)^{[n-i]} \times \left[V^1_2 \times \left(2^{\frac{i-1}{2}} PAL_{2^{i-1}}\right) \times G^0_2\right]^{\delta_i} \times \times (G^0_2)^{[n-i]}$ Walsh-Pali Transform (U-PP)
Преобразование Уолша (УП)	$WAL_{2^n} = \frac{1}{2^{n/2}} \sum_{i=0}^{n} (V^0_2)^{[n-i]} \times [V^1_2 \times ((I_2)^{[i-2]} \times \left(2^{\frac{i-1}{2}} WAL_{2^{i-1}}\right)) \times G^0_2]^{\delta_i} \times (G^0_2)^{[n-i]}$ Walsh Transform (UP)
Модифицированное преобразование Адамара (МПА)	$MHAD_{2^n} = \frac{1}{2^{n/2}} \sum_{i=0}^{n} 2^{\frac{i-1}{2}\delta_i} (V^0_2 \times G^0_2)^{[n-i]} \times \times [V^1_2 \times G^0_2 \times (I_2)^{[i-1]}]^{\delta_i}$ Modified Hadamar Transform (MPA)
Преобразование Адамара – Хаара (А – ХП)	$HDHR^{(r)}_{2^n} = \frac{1}{2^{n/2}} \sum_{i=0}^{n-r} 2^{\frac{i-1}{2}\delta_i} (h_2)^{[r]} \times (V^0_2)^{[n-r-i]} \times \times [V^1_2 \times (I_2)^{[i-1]} \times G^0_2]^{\delta_i} \times (G^0_2)^{[n-r-i]}$ Hadamar-Haar Transform (A-KhP)
Дискретное преобразование Фурье (ДПФ)	$FOUR_{2^n} = \frac{1}{2^{n/2}} M^{\text{инв}}_{2^n} \left(\sum_{i=0}^{n} (V^0_2 \times G^0_2)^{[n-i]}\right) \times \times \left[V^1_2 \times G^0_2 \times \left(2^{\frac{i-1}{2}} M^{\text{инв}}_{2^n} FOUR_{2^{i-1}}\right)\left(\prod_{j=0}^{i-2} pd_{j+2}\right)\right]^{\delta_i}$ Discrete Fourier Transform (DPF)

TABLE 1 [continued]:

Обобщенное преобразование (преобразование по ВКФ)	$G^{(r)}_{2^n r} = (\mathrm{FOUR}_{2^n})^{(r)}$ Generalized Transform (VKF Transform)
(1) Преобразование перестановки по двоичной инверсии	$M^{\text{инв}}_{2^n} = \sum_{i=1}^{n} (V^0_2)^{[n-i]} \times (V^1_2 \times M^{\text{инв}}_{2^{i-1}} \times G^1_2)^{\bar{\delta}_i} \times (G^0_2)^{[n-i]}$
Преобразование перестановки из кода Грея в прямой	$M^{\text{гр/пр}}_{2^n} = \sum_{i=0}^{n} (V^0_2)^{[n-i]} \times (G^0_2)^{[n-i]} \times [V^1_2 \times G^1_2 \times (I_2)^{(i-1)} M^{\text{гр/пр}}_{2^{i-1}}]^{\bar{\delta}_i}$

Gray code to direct code transposition transform

Transform Преобразование	Representation in Terms of Elementary Matrices Представление через элементарные матрицы
(2) Преобразование перехода от ХП к У – ПП	$M^{\text{НЯ-Р}}_{2^n} = \sum_{i=0}^{n} (V^0_2)^{[n-i]} \times (G^0_2)^{[n-i]} \times [V^1_2 \times G^1_2 \times M^{\text{НЯ-Р}}_{2^{i-1}} \times \times 2^{\frac{i-1}{2}} \mathrm{HAR}_{2^{i-1}}]^{\bar{\delta}_i}$
(3) Преобразование перехода от МПА к ДПФ	$M^{\text{МН-Ф}}_{2^n} = \sum_{i=0}^{n} (V^0_2)^{[n-i]} \times (G^0_2)^{[n-i]} \times [V^1_2 \times G^1_2 \times 2^{\frac{i-1}{2}} \times \times M^{\text{МН-Ф}}_{2^{i-1}} \mathrm{MHAD}^{i-1}_2 \prod_{j=0}^{i-1} p d_{j+2}]^{\bar{\delta}_i}$

Key: 1. Binary inversion transposition transform;
2. Transition transform from a Haar transform to a Walsh-Pali transform;
3. Transition transform from a modified Hadamar transform to a discrete Fourier transform.

* * *

TABLE 2

	Transform Преобразование	Factored Representation Факторизованное представление
(1)	Преобразование Хаара (ПХ)	$\mathrm{HAR}_{2^n} = \frac{1}{2^{n/2}} D_{2^n}^{\mathrm{HAR}} \prod_{i=0}^{n-1} \left[\left[\frac{I_{2^i} \times G_{2^i}^0}{I_{2^i} \times G_{2^i}^1} \right] \oplus I_{2^{n-i+1}} \right]$
(2)	Преобразование Уолша – Адамара (У – АП)	$\mathrm{HAD}_{2^n} = \frac{1}{2^{n/2}} \prod_{i=0}^{n-1} (I_{2^{n-i-1}} \times h_2 \times I_{2^i})$
(3)	Преобразование Уолша – Пэли (У – ПП)	$\mathrm{PAL}_{2^n} = \frac{1}{2^{n/2}} \prod_{i=0}^{n-1} \left(I_{2^{n-i-1}} \times \left[\frac{I_{2^i} \times G_{2^i}^0}{I_{2^i} \times G_{2^i}^1} \right] \right)$
(4)	Преобразование Уолша (УП)	$\mathrm{WAL}_{2^n} = \frac{1}{2^{n/2}} \prod_{i=0}^{n-2} \left(I_{2^{n-2-i}} \times \left(\left[\frac{I_{2^i} \times G_{2^i}^0}{I_{2^i} (I_{2^i} \times G_{2^i}^1)} \right] \oplus \right. \right.$ $\left. \left. \oplus [I_{2^{i+1}} \left[\frac{I_{2^i} + U_{2^i}^0}{I_{2^i} (I_{2^i} \times U_{2^i}^1)} \right] I_{2^{i+1}} \right) \right) \left[\frac{I_{2^{n-1}} \times G_{2^{n-1}}^0}{I_{2^{n-1}} (I_{2^{n-1}} \times G_{2^{n-1}}^1)} \right]$
(5)	Модифицированное преобразование Адамара (МПА)	$\mathrm{MHAD}_{2^n} = \frac{1}{2^{n/2}} D_{2^n}^{\mathrm{HAR}} \prod_{i=0}^{n-1} [(h_{2^i} \times I_{2^i}) \oplus I_{2^{n-i+1}}]$
(6)	Преобразование Адамара – Хаара (А – ХП)	$\mathrm{HDHR}_{2^n}^{(r)} = \frac{1}{2^{n/2}} (I_{2^n} \times D_{2^{n-r}}^{\mathrm{HAR}}) \prod_{i=0}^{r-1} (I_{2^{r-i}} \times h_2 \times I_{2^{n-r+i}}) \cdot$ $\cdot \prod_{i=r}^{n-1} \left(I_{2^{r-i}} \times \left[\left[\frac{I_{2^{i-r}} \times U_{2^i}^0}{I_{2^{i-r}} \times U_{2^i}^1} \right] \oplus I_{2^{n-i-2+1}} \right] \right)$
(7)	Дискретное преобразование Фурье (ДПФ)	$\mathrm{FOUR}_{2^n} = \frac{1}{2^{n/2}} M_{2^n}^{\text{инв}} \prod_{i=0}^{n-1} (I_{2^{n-i-1}} \times [I_{2^i} \oplus \prod_{j=0}^{i-1} d_{j+2}]) \times$ $\times (I_{2^{n-i-1}} \times h_2 \times I_{2^i})$
(8)	Обобщенное преобразование (преобразование по ВКФ)	$G_{2^n r_s}^{(r)} = \prod_{i=0}^{r-1} (I_{2^{r-i-1}} \times \mathrm{FOUR}_{2^n} \times I_{2^i})$

Key: 1. Haar transform (TKh);
2. Walsh-Hadamar transform (U-AP);
3. Walsh-Pali transform (U-TP);
4. Walsh transform (UP);
5. Modified Hadamar transform (MPA);
6. Hadamar-Haar transform (A-KhP);
7. Discrete Fourier transform (DPF);
8. Generalized transform (VKF transform);

TABLE 2 [continued]:

(9) Преобразование перестановки по двоичной инверсии	$M_{2^n}^{\text{инв}} = \prod_{i=0}^{n-1} \left(I_{2^{n-i-1}} \times \left[\frac{I_{2^i} \times G_{2^0}}{I_{2^i} \times G_{2^1}} \right] \right)$
(10) Преобразование перестановки из кода Грея в прямой	$M_{2^n}^{\text{с.р/пр}} = \prod_{i=0}^{n-1} (I_{2^i} \times [I_{2^{n-i-1}} \oplus I_{2^{n-i-i}}])$
(11) Преобразование перехода от ХП к У – ПП	$M_{2^n}^{\text{НВ-Р}} = \prod_{i=1}^{n-1} \prod_{k=0}^{i-1} \left(I_{2^{n-i-1}} \times \left[I_{2^i} \oplus \left[\frac{I_{2^k} \times U_{2^2}}{I_{2^k} \times G_{2^2}} \right] \oplus I_{2^{i-2k+1}} \right] \right)$
(12) Преобразование перехода от МПА к ДПФ	$M_{2^n}^{\text{МН-Р}} = \prod_{i=1}^{n-1} \left(\prod_{k=0}^{i-1} (I_{2^{n-i-1}} \times [I_{2^i} \oplus (h_2 \times I_k) \oplus I_{2^{i-2k+1}}]) (I_{2^{n-i-1}} \times [I_{2^i} \oplus \prod_{j=0}^{i-1} d_{j+2}]) \right)$

[Key to TABLE 2 continued]:
9. Binary inversion transposition transform;
10. Gray code to direct code transposition transform;
11. Transition transform from a Haar transform to a Walsh-Pali transform;
12. Transition transform from a modified Hadamar to a discrete Fourier transform.

The factored representations of the matrices from Table 1 which are obtained with this approach are given in Table 2 in the form of the product of lightly filled matrices.

BIBLIOGRAPHY

1. N. Ahmed, K.R. Rao, "Orthogonal Transforms for Digital Processing," Springer Verlag, 1975.

2. A.M. Trakhtman, V.A. Trakhtman, "Osnovy teorii diskretnykh signalov na konechnykh intervalakh" ["The Fundamentals of the Theory of Discrete Signals in Finite Ranges"], Sovetskoye Radio Publishers, 1975.

3. I.J. Good, J.ROY. STATIST. SOC., SER. B, 1958, 20, 361.

4. H.C. Andrews, J. Kane, J. ACM, 1970, 17, 2, 260.

5. L.P. Yaroslavskiy, N.S. Merslyakov, "Metody tsifrovoy golografii" ["Methods of Digital Holography"], Nauka Publishers, 1977.

8225
CSO:8144/1369

END